DISSERTATION

Submitted to the
COMBINED FACULTIES FOR THE
NATURAL SCIENCES AND FOR MATHEMATICS
of the
RUPERTO-CAROLA UNIVERSITY
OF HEIDELBERG, GERMANY

for the degree of
DOCTOR OF NATURAL SCIENCES

presented by
Master of Science, Andrés Flórez
born in: Cúcuta, Colombia

Oral-examination: January 23rd, 2017

MYCN modulates the restriction point and ferroptosis in Neuroblastoma

Referees: Prof. Dr. Thomas Höfer
Prof. Dr. Frank Westermann

Acknowledgments

First I would like to thank God for supporting me during the difficult times of my PhD.

I would like to thank Prof. Thomas Höfer for giving the opportunity to perform my PhD under his mentorship. I appreciate his scientific input, his constructive criticism and the flexibility that I had to pursue experiments motivated by my scientific instinct.

Special thanks to PD Dr. Frank Westermann for his openness to this fruitful collaboration between our Systems Biology group and his Neuroblastoma group. I am greatful for opening the doors of his lab and for the experimental support to accomplish the results of this thesis. To all the members of his group, special thanks as well for the openness in discussing results and design new experiments.

Special thanks as well to Tatjana Ryl, smart and talented colleague for her support in discussing and generating new ideas for our projects. As well for her moral support in the moments of crisis.

I would like to express my gratefulness to a number of people, specially Dr. Qin Zhang for outstanding experimental support, Diana Haendly for her great help in facilitating administrative matters. To all the friends I met through the PhD, a list that is gigantic and that I wouldn't like to list here for fear of missing someone.

To all salsa friends, which helped me as well as supportive group outside the scientific environment. To my girlfriend Veronika Chevyreva for her help and support.

Finally, I would like to thank my mother for always being there for me.

Table of contents

Abstract

Neuroblastoma is the most common extracranial solid tumor in childhood. It constitutes an interesting model for tumor progression since the mutation rate is relatively low as compared to other tumors, allowing to investigate specific tumor drivers in a relatively homogeneous genetic background. One of the important drivers of tumor formation in neuroblastoma is the oncogene MYCN. This transcription factor is responsible for the activation of a cascade of genes involved in cell proliferation and metabolism The study of MYCN's role in these processes is highly relevant because a deep understanding of the regulation could lead to more effective therapies for MYC-driven tumors. In this PhD thesis, an approach was developed to study cell cycle and metabolism on MYCN-driven neuroblastomas. One of the caveats of cell cycle studies is the lack of markers to study cell cycle transition, and the artifacts caused by cell synchronization. By combining the E2F1-d2GFP and Cdt1-degron markers it was possible to identify a G0-like state, which is more prominent upon reduction of MYCN. This state is transient and it was not possible to detect it before in this cell system. The cells under high MYCN expression avoid passing through the G0-like state. This decision happens early in the cell cycle and it is not influenced by p21, contrary to what was found in other studies. Gene expression profiling of sorted cells using the cell cycle markers demonstrated that the transcriptional program of G0-like state caused by MYCN reduction is different from mitogen starvation and contact inhibition, suggesting that the G0-like state might be a spectrum of states with similar phenotypes but distinct expression profiles. As an outlook, the network analysis of the expression data suggests RABL6 as a potential marker of MYCN that controls the commitment to cell cycle by inhibiting p16, however further experiments are required to confirm this finding. From the metabolic perspective, we found that MYCN-high cells are strongly addicted to the amino acid cystine, which serves as a source for the glutathione pathway. Inhibition of enzymes from this pathway shows a dramatic lethal effect exclusively on MYCN-high cells. We found that the mechanism of cell death under cystine starvation in MYCN-amplified cells is ferroptosis, a recently described pathway that involves lipid peroxidation enhanced by iron. To our knowledge, this is the first time that MYCN is associated with ferroptosis which opens an avenue for developing new drugs targeting MYC-driven tumors via induction of ferroptosis.

Zusammenfassung

Das Neuroblastom ist der häufigste während der Kindheit auftretende extracraniale solide Tumor. Da es verglichen mit anderen Tumoren eine relativ niedrige Mutationsrate hat, stellt es ein interessantes Modell zur Erforschung der Tumorentwicklung dar und ermöglicht die Untersuchung spezifischer Tumortreiber vor einem relativ homogenen genetischen Hintergrund. Einer der wichtigsten Faktoren der Tumorbildung im Neuroblastom ist das Onkogen MYCN. Dieser Transkriptionsfaktor reguliert die Aktivierung einer Kaskade von Genen, die an Zellproliferation und Metabolismus beteiligt sind. Ein tiefes Verständnis der Funktionen und Regulierung des Onkogens MYCN in diesen Prozessen ist unabdingbar, um daraus effektivere Therapien für MYC-getriebene Tumore ableiten zu können. Im Rahmen dieser Doktorarbeit wurde ein Verfahren entwickelt, um den Zellzyklus und Metabolismus von MYCN-getriebenen Neuroblastomen zu untersuchen. Fehlende Marker für die einzelnen Zellzyklusphasen und Artefakte aufgrund von Zellsynchronisation schränken Zellzyklusstudien stark ein. Durch Kombination von E2F1-d2GFP und Cdt1-degron-Marker war es möglich, einen G0-ähnlichen Zustand zu identifizieren, der insbesondere nach MYCN-Reduzierung aufgetreten ist. Es handelt sich hierbei um einen vorübergehenden Zustand, der zuvor noch nicht in diesem Zellsystem detektiert/beschrieben werden konnte. Zellen mit einer hohen MYCN Expression vermeiden den G0 ähnlichen Zustand. Diese Entscheidung wird bereits sehr früh im Zellzyklus getroffen und nicht, wie in früheren Arbeiten beschrieben, durch p21 beeinflusst. Genexpressionsanalysen von durch die oben genannten Zellmarker sortierten Zellen, zeigten, dass das Transkriptionsprogramm des durch MYCN- Reduzierung induzierten G0-ähnlichen Zustandes sich von den durch Mitogenmangel und Kontaktinhibition verursachten Zuständen unterscheidet. Dies lässt vermuten, dass es sich bei dem G0-ähnlichen Zustand um ein Spektrum von Zuständen mit ähnlichem Phänotyp, aber unterschiedlichen Expressionsprofilen handelt. Netzwerkanalysen der Expressionsdaten legen nahe, dass RABL6 ein potentieller MYCN-Marker ist, der die Einhaltung des Zellzyklus durch Hemmung von p16, kontrolliert. Allerdings sind weitere Experimente erforderlich, um dies eindeutig zu belegen. Des Weiteren haben wir festgestellt, dass Zellen mit einer hohen MYCN Expression eine starke Abhängigkeit von der Aminosäure Cystein zeigen, die als Quelle für den Glutathion Signalweg dient.

Eine Hemmung der Enzyme dieses Signalwegs ist mit einer äußerst hohen Letalität ausschließlich von Zellen mit hoher MYCN Expression verbunden. Des Weiteren konnten wir zeigen, dass es sich bei dem Mechanismus des Zelltods unter Cystein-Mangel bei Zellen mit erhöhter MYCN Expression um Ferroptose, einen kürzlich beschriebenen Signalweg, bei dem Peroxidation durch Eisen verstärkt wird, handelt. Nach unseren Kenntnissen wird MYCN an dieser Stelle zum ersten Mal mit Ferroptose assoziiert. Dies eröffnet völlig neue Wege für die Entwicklung neuer Medikamente für MYCN-getriebene Tumore durch Induzierung von Ferroptose.

1. Introduction

2. Definition of the problem

2.1. Challenges of cancer therapy

Cancer is a complex disease with almost all tumors sharing similar characteristics such as: unlimited division, protection against cellular stresses, evasion from apoptosis, sustained angiogenesis, and metastasis in the advanced cases. Diverse therapeutic approaches have been developed through the years to target the hallmarks of cancer, but a complete cure is still elusive, and perhaps in only very early diagnosed cases, stressing the importance of early detection (Pavet, Portal et al. 2011). Drug development in cancer has low success rate as compared to other diseases such as cardiovascular diseases. Recent data shows that the probability in developing a successful drug for treating cardiovascular diseases is 3 times higher than for anti-cancer drugs (Kamb, Wee et al. 2007). Cancer therapy started with initial use of DNA damaging agents that could kill high proliferating cells. This came with a cost since cytotoxic agents induced serious collateral effects due to destruction of normal cells in the surrounding tissues of the tumor. More recently, targeted-therapy has shown a few successful cases. One of them is Imatinib, kinase inhibitor used to treat leukemia and Pembrolizumab (Robert, Ribas et al. 2014), a recently developed monoclonal antibody used to treat advanced melanoma cases. This drug has gained popularity as it was successfully used to cure melanoma of United states ex-president Jimmy Carter. The drug now called the Carter's drug, seems promising for patients with Melanoma and BRAF mutation and even a lung cancer clinical trial was stopped as it was found that this drug worked exceptionally good in lung cancer patients. http://www.nbcnews.com/health/cancer/lung-cancer-trial-stopped-after-jimmy-carter-drug-stops-tumors-n593726. However the spectacular cases obtained with the new target-therapy are still limited since cancer resistance originates relatively fast rendering some tumors impossible to treat (Kamb, Wee et al. 2007)

2.2. Neuroblastoma as a model to study cancer proliferation

Embryonic tumors are exceptional on its nature as they occur in the early ages as compared to regular cancer types that appear in adulthood. According to frequency, Neuroblastoma is the most frequent embryonal tumor and it appears in children usually

less than 1 year (Brodeur 2003). Neuroblastoma is an special and interesting model of cancer as it has the highest rate of spontaneous regression (Figure 1), with around 20% of cases suffering remission without any therapeutic regime (Everson 1964, Gatta, Ferrari et al. 2012). This surprising fact makes Neuroblastoma an interesting cancer model to study the mechanisms that control cell proliferation. The Neuroblastoma cell of origin has been hypothesized to be the neural crest. This cell type originates at the dorsal neural tube and migrate to give rise to neurons and glia of the peripheral nervous system (PNS) and mesenchymal cells like craniofacial cartilage and smooth muscle (Green and Bronner 2013).

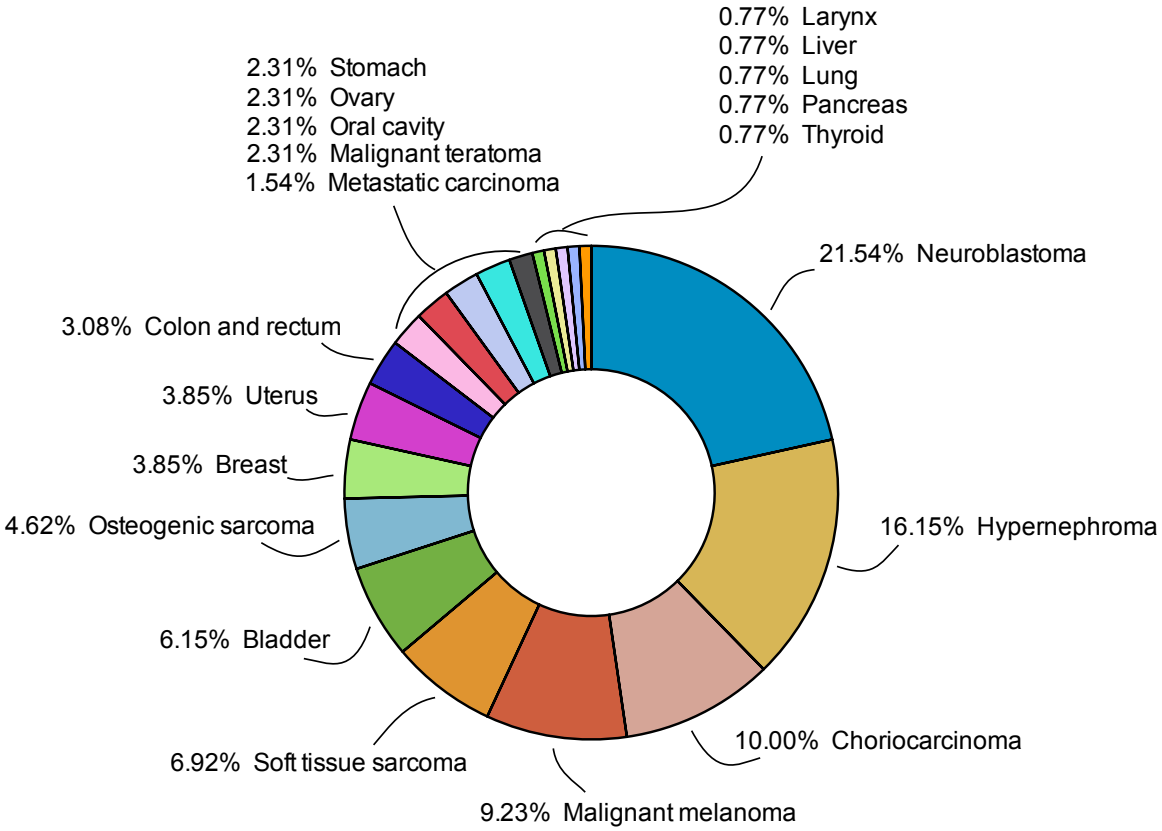

Figure 1. Incidence of spontaneous regression cases among different tumor types. Percentages were calculated based on the data from (Everson 1964).

Due to its cell of origin, Neuroblastoma arises from the sympathetic nervous system and localizes often in the adrenal medulla or paraspinal ganglia. Metastatic neuroblastoma usually has poor prognosis and usually the therapeutic approaches include a multimodal approach with immunotherapy, surgical resection, and treatment with differentiation

agents such as retinoic acid (Matthay, Villablanca et al. 1999, Berthold, Boos et al. 2005). Interestingly the mutational load of neuroblastoma is much lower than other tumor types (Alexandrov, Nik-Zainal et al. 2013) this “simplifies” the process of mechanistically understand the networks driving tumor progression. Of the few genetic alterations in neuroblastoma is the amplification of the oncogene MYCN. This was the first biomarker described with actual clinically utility. Amplification of this oncogene is found in 20% of neuroblastoma cases and it correlates with poor prognosis(Brodeur, Seeger et al. 1984). *In vivo* confirmation of the effects of MYCN showed that it can generate tumors upon its overexpression in the sympathetic ganglia (Cheung, Murray et al. 2013). MYC oncoproteins are deregulated not only in neuroblastoma but in approximately 50% of human tumors (Horiuchi, Anderton et al. 2014). MYC acts as global regulator of transcription and it has been found to bind to about 10 to 15% loci of the entire human genome (Nie, Hu et al. 2012). Therapeutic approaches in high-risk MYCN-amplified neuroblastomas has yielded relatively low success rates (Maris 2010), stressing the need for alternative and more effective therapies.

Other genetic modifications have been found relevant in predicting neuroblastoma outcome. Additional genetic markers such as ALK and LMO1 mutations have been found to increase disease susceptibility (Mosse, Laudenslager et al. 2008, Wang, Diskin et al. 2011). More recently, studies carried out at the collaboration lab found that TERT rearrangements are prevalent in approximately 31% of high-risk neuroblastomas with MYCN single copy, identifying a new subtype of aggressive tumors with elevated expression of telomerase (Peifer, Hertwig et al. 2015). (See Figure)

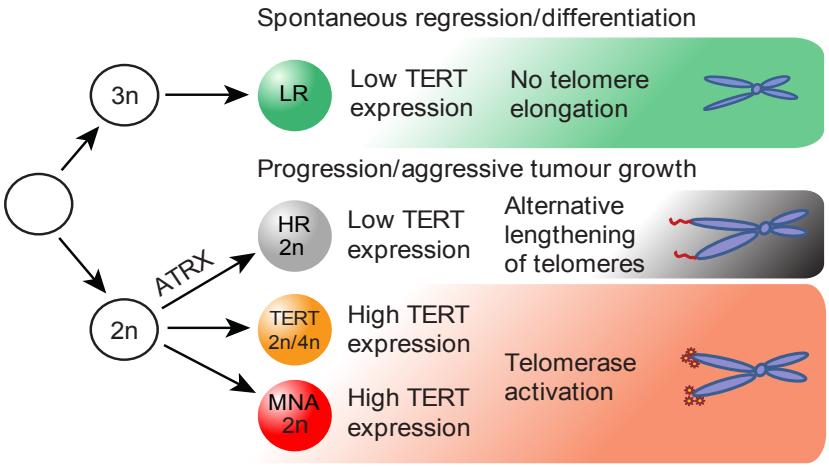

Figure 2. Neuroblastoma stratification based on TERT expression. Adapted from (Peifer, Hertwig et al. 2015). 3n – near triploid, 2n – near diploid, LR – low risk, HR – high risk, MNA – MYCN-amplified. (Reproduced with permission from Tatjana Ryl)

3. MYCN influence in neuroblastoma cell cycle

MYC has been proposed to be a global regulator of gene expression with around 1000 target genes and confirmed binding of 15% of genome loci. MYC targets are generally activated but a significant set of genes are also repressed by MYC. It was suggested that MYC could act as RNA amplifier but more recent evidence did not find this regulatory property when comparing quiescent and proliferating cells. This suggests that MYC might alter the cellular state which results in increase RNA production (Sabo, Kress et al. 2014). The pleiotropic effects complicate the understanding of the different mechanisms employed by MYC to surpass growth control. In the context of neuroblastoma and MYCN, it is recognized the importance of the genes involved in cell cycle and apoptosis. The guardian of the genome, p53, has been involved in repressing MYCN expression in neuroblastoma cells, (Torres, Regan et al. 2010), but it could be possibly counteracted by the repressive functions of MYCN on p21 promoter. (Gartel, Ye et al. 2001). This has important consequences specially when cells are challenged by DNA damage agents, as MYCN overrides the DNA damage checkpoint cells are more likely to survive and acquire mutations.

From the cell cycle perspective, there are some well known targets regulated by MYCN. CDK4, a cyclin-dependent kinase is involved in Rb inactivation via phosphorylation and MYCN has been shown to directly act on its the promoter increasing the expression (Gogolin, Ehemann et al. 2013). More recently, it was found that MYCN regulates SKP2 expression (Evans, Chen et al. 2015), another important protein involved in cell cycle regulation. SKP2 is as well an oncogene and it is frequently overexpressed in human tumors. SKP2 encodes the F-box protein of the ubiquitin ligase SCF-SKP2 complex that is comprised of three core proteins RBX1, CUL1, and SKP1. The substrate is bound to SKP2 and CSK1 and more than 20 substrates have been found and most of them are regulators of G1/S transition. Among them, p27 stands up as the most important regulator of the G0-G1 transition. Previous animal models have shown that loss of p27 and increased expression of c-MYC cooperates in the formation of aggressive tumors. Therefore one of the mechanisms of MYC to foster cell cycle entry is the increase of pRb (phospho-Rb) and the downregulation p27 via SKP2 upregulation. (Bretones, Acosta et al. 2011)

However, another study challenged this hypothesis in Neuroblastoma. By using different SKP2 promoter constructs to screen for importance of transcriptional sites, Westermann's group found that SKP2 expression is mostly regulated by derepression and hyperactivation in MYCN amplified cels. This means that active clearance of Rb-E2F repressive complex and hyperactivation of SKP2 promoter via E2F is responsible for the high levels of SKP2 mRNA observed in MYCN amplified cells.T his mechanism is supported by the findings of high CDK4 expression that correlates with the higher levels of pRb found in the presence of MYCN. This is supported also by the idea that low mutational rate on RB1 gene is compensated by enhaced inactivation at the protein level. (Muth, Ghazaryan et al. 2010)

Despite its clear influence on cell proliferation, the mechanisms by which MYC and similarly MYCN exert the effects on the cell cycle machinery are not well understood. MYC overall promotes the expression of cyclins (E and A) and potentially E2F1, with E2F1 as well acting on the MYC promoter. MYC has been implicated in preventing growth arrest induced by p27 through sustained activation of CDK2. So it seems that MYC favors G0 scape but the molecular regulator is still unidentified. In addition, it is not

entirely clear where do MYC exerts its strongest effect, if G1 early or G1 late (Mateyak, Obaya et al. 1999, Huang and Weiss 2013). In Figure 3 it is summarized the potential effects of MYC in cell cycle.

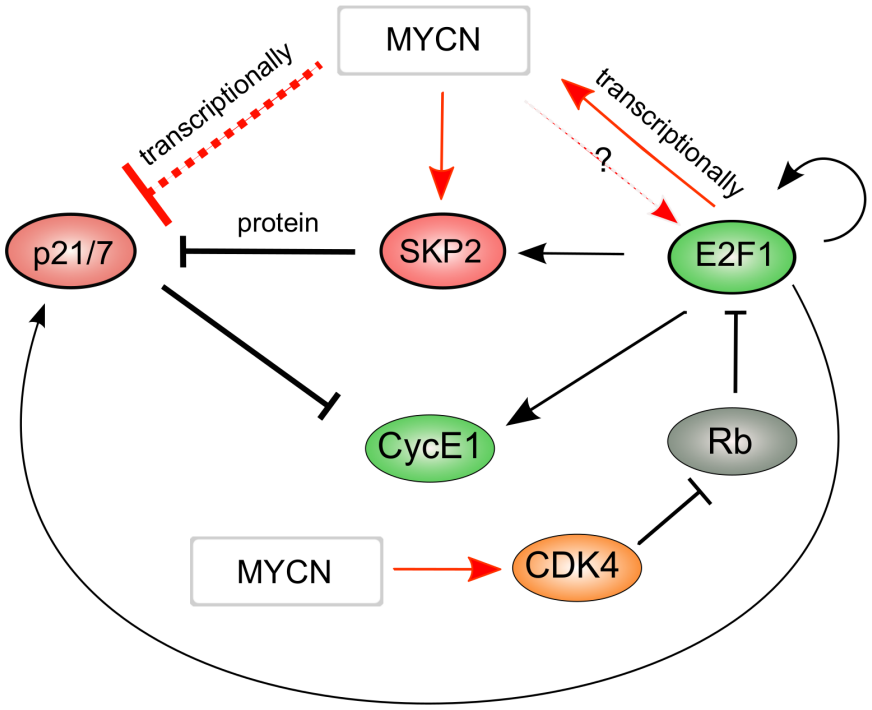

Figure 3. Network representation of MYCN actions on important cell cycle regulators

4. Regulation of cell cycle entry at restriction point

CDK4 and SKP2, main targets of MYCN that affect proliferation are specifically involved in the regulation of the restriction point in normal cells. The restriction point (RP) is defined as the mitogen-sensitve window before cells are committed to cell cycle (Figure 4A). During this period many different events are occurring to ensure correct passage of restriction point, prevention of replicating errors and supplying cells of replicatory demands. Many oncogenes in different tumor types exert their effects at the RP in G1, but the mechanisms are still unclear (Yao, Tan et al. 2011)

G1 phase is sensitive to stimulation by mitogens, however when conditions are not fulfilled cells enter into another state called quiescence or G0. It is hypothesized that cancer cells avoid these controls to remain in the proliferative state, so understanding

the mechanisms of restriction point control is central to our understanding of how cancer cells proliferate continuously (Sherr 1996).

The classical mechanism of how RP was described as a sequential inactivation of Rb with the boost of E2F1 target genes transcription. In quiescent cells or recently born cells E2F1 is bound to Rb and binds the promoters of several genes. Rb-E2F binding represses genes involved in DNA replication. Upon certain mitogen threshold which is cell type dependent, the MAPK kinase pathway is activated and c-MYC activity is increased inducing the expression of Cyclin D1. CDK4/6 are then activated by Cyclin D1 binding and starts the phosphorylation of Rb. Inactivation of Rb leads to the release of E2F and then the transcription of Cyclin E1. E2F1 itself is activated increasing the expression of more Cyclin E1, this constitutes the classical positive feedback that results in Cyclin E1/CDK2 binding and final inactivation of Rb by phosphorylation (Figure 4B). However binding of polypeptide inhibitors to CDK4 and CDK6, the so-called INK4 proteins, can also actively stop Rb inactivation ultimately causing G1 arrest. The four known 15- to 19-kD INK4 proteins (p16, p15, p18, and p19) bind and inhibit CDK4 and CDK6, but not other CDKs. INK4 genes are expressed in different tissues suggesting they are not redundant. (Sherr 1996).

Positive feedbacks are the hallmark of bistable switches. To understand the mechanism of how the Rb-E2F works on the single cell level, Yao et al developed rat fibroblasts with E2F and Cyclin D1 promoter constructs driving GFP expression. Single cell studies help to uncover dynamics that might be hidden by average measurements. Serum titration of the fibroblasts with and without serum pulse showed that cells on the E2F promoter exhibit bimodal behavior. And the transition between the two states (ON and OFF) depend on a particular serum threshold that was conserved by repeating the experiments about 6 times. (with some variability). On the other hand the Cyclin D1 reporter only exhibited a unimodal response with levels proportional to the serum dose. (Yao, Lee et al. 2008).This results showed for the first time that the restriction point works as a bistable switch.

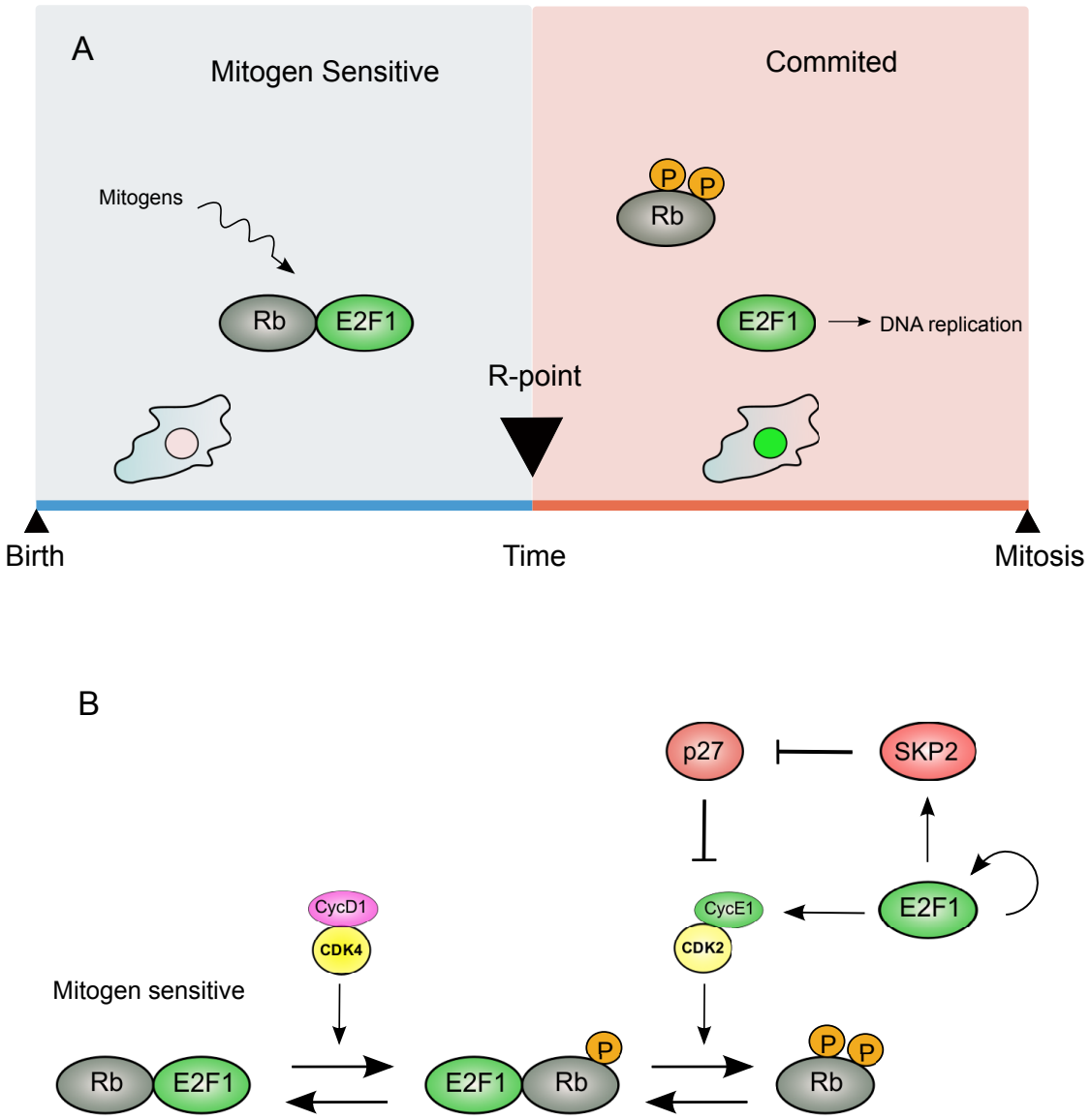

Figure 4. The restriction point switch. A) The cell with green nucleus illustrates the reporter used in (Yao, Lee et al. 2008) to measure the transition into S phase. Commited cells exhibit full activation of E2F1. B) Molecular network that controls passage through restriction point. (See text for details)

The classical model revealed that it was necessary continuous mitogen stimulation to obtain the passage through the restriction point. However an early study observed that stimulation with 2 pulses separated by 9 hrs was enough to induce S phase entry (Jones and Kazlauskas 2001). This points to the idea that different transcriptional programs are required in different parts of G1 for passage through RP. (Pulses EGF) went further to described the transcriptional programs and the main finding points towards a phase where lipid biosynthesis is started and followed by second phase that leads to fully

acitavtion of ERK on the first pulse and finally on the second pulse the activation of PI3K that suppresses p53 target genes (Zwang, Sas-Chen et al. 2011). Therefore a clear understanding how growth factor signals are transduced to activate Cdk4 and Cdk6 are critical medical importance.

However there are some limitations to the classical RP model. As new experiments are being carried out, new functions are uncovered for known cell cycle regulators and in some cases those functions are cell type depdent. One interesting example is Cyclin D1. It has been always considered as the starting step on the activation of Rb-E2F network. However its role still remains controversial. A recent study found that Cyclin D1 might play an important role in the machinery of DNA repair (Jirawatnotai, Hu et al. 2011). Depletion of Cyclin D1 could sensitize cells to radiation by impairing DNA repair when Rb is not present. Interestingly depletion of Cyclin D1 did not affect cell proliferation in vivo, only when cells were treated with radiation, growth was retarded, highlighting its role in DNA repair. The mechanism described in the study points to a recruitment of Cyclin D1 by BRCA2 to the site of damage helping the recruitment of RAD51. Even though cyclin D1 is not essential for DNA repair it plays a role in increasing affinity of repair machinery to damage sites.

Rb phosphorylation also brings complexity to the regulation of RP. Rb has 15 phosphorylation sites that depend on CDKs (Narasimha, Kaulich et al. 2014). The biological function of the different sites still remains unknown, although some sites are specifically phosphorylated by certain kinases. CDK4, for example, phosphorylates S807/S811 in vitro, and deletion of the Cdk4 docking site in RbC abrogates S807/S811 phosphorylation. Mutation of this site abrogates phosphorylation in additional sites, suggesting that S807/S811 is important for overall Rb phosphorylation (Rubin 2013). More interestingly, it was observed that Rb is mostly mono-phosphorylated by CDK4/6 in G1 early in any of the different 14 sites before quantum hyper-phosphorylation by CDK2 at G1 late takes at RP, discarding the idea of progressive phosphorylation from the classical RP model. However, of how meaningful are the different sites in terms of gene regulation remains to be found (Narasimha, Kaulich et al. 2014)

Another part of the puzzle not yet defined is the role of by CAK (CDK activating kinase). Cyclin D1 binding is a requirement for CDK4 and CDK6 activity. However for full activation the phosphorylation by CAKs is required. CDK7 can activate CDK4 and CDK6 *in vitro* and deletion of CDK7 leads to reduced activity of CDK4 in mouse fibroblasts. However it is not yet defined the role of CDK7 *in vivo.* More recent results showed that CDK7 can activate both CDK6 and CDK6 under physiological conditions. Interestingly CDK2 activation remained after CDK7 was normally turned off but CDK4 activation was rapidly lost. Experiments in human cells showed that CDK7 activity increased together with CDK4 activity after cells re-enter cell cycle from quiescence, suggesting that CDK7 and perhaps not much Cyclin D1 are responsible for passage through RP via activation of CDK4 (Schachter, Merrick et al. 2013). Even though CDK7 has been involved in regulating RP, it has additional functions. It can bind to the transcription factor TFIIH, which is involved in transcription initiation therefore regulating global mRNA transcription. Interestingly, MYCN has seen to transcriptionally up-regulate genes through the usage of super-enhancers, clusters of enhancers that are densely occupied by transcription factors, cofactors, and chromatin regulators. When using a covalent CDK7 inhibitor (THZ1) the authors found a strong selective cell death on MYCN/c-MYC amplified cells. The effect might be mediated to an active suppression of essentially all active transcripts, especially those required for uncontrolled proliferation leading to potent and selective cytotoxicity while sparing normal cells (Chipumuro, Marco et al. 2014).

The RP machinery also presents connection with the p53 axis. E2F1 activation leads to a increase expression of Sirt1 which in turns inactivates p53 allowing cells to scape p21 arrest via p53 induction. However as shown before with the two –pulse regulation of RP, this might be time dependent (Wong, Dong et al. 2011). Altogether, the evidence suggests that the classical model of RP might need some refinement, including the new functions of the cell cycle players involved in RP regulation.

4.1.1. Dynamical studies on mechanism of restriction point

The initial studies of Yao gave insight into RP mechanism by describing it as a bistable switch. However questions such as if cell cycle entry depends on the previous cell cycle, the duration of the quiescence state, can only be answered by dynamical measurements such as live cell imaging. Modifications of initial Yao's reporter for live cell imaging revealed that commitment depends on the amplitude of the E2F1 promoter activity. This means that only when E2F1 reaches certain threshold, cells can commit to the cell cycle. (Dong, Maddali et al. 2014)

An elegant study (Spencer, Cappell et al. 2013) measured CDK2 activity in single cells and found a bifurcation at the end of the previous cell cycle. The fluorescent sensor consists of a segment of human DNA helicase B that contains CDK phosphorylation sites and nuclear localization and export signals fused to the yellow fluorescent protein mVenus (DHB-Ven). Upon CDK2 phosphorylation the nuclear signal is hidden and the fluorescent protein is shuttled to the cytoplasm. The cytoplasmic to nuclear ratio of fluorescence intensity can be then used as a readout of CDK2 activity, as validated in individual cells emerging from mitogen starvation. The measurements showed that 2 groups of cells exhibited either low or high CDK2 activity at the moment of birth. The bifurcation of CDK2 levels was reported to be dependent on mitogenic signaling in G2 of the previous cell cycle. Interestingly the major driver of the bifurcation was p21 in the cell lines tested in the study. In principle cells that are born with high p21 levels and low CDK2 activity experience a second restriction window in which mitogens are needed to re-enter cell cycle and build up CDK2 activity (Figure 5). On the other hand cells with CDK2inc (CDK2 high) enter S phase without the need of mitogens as shown by inhibition of MEK (Spencer, Cappell et al. 2013). An interesting prediction from the study is if cancer cells would mimic the CDK2inc state by changing the proportion of CDK2low cells. This question motivated the further experiments carried out in this thesis to find out how the RP is regulated in cancer cells.

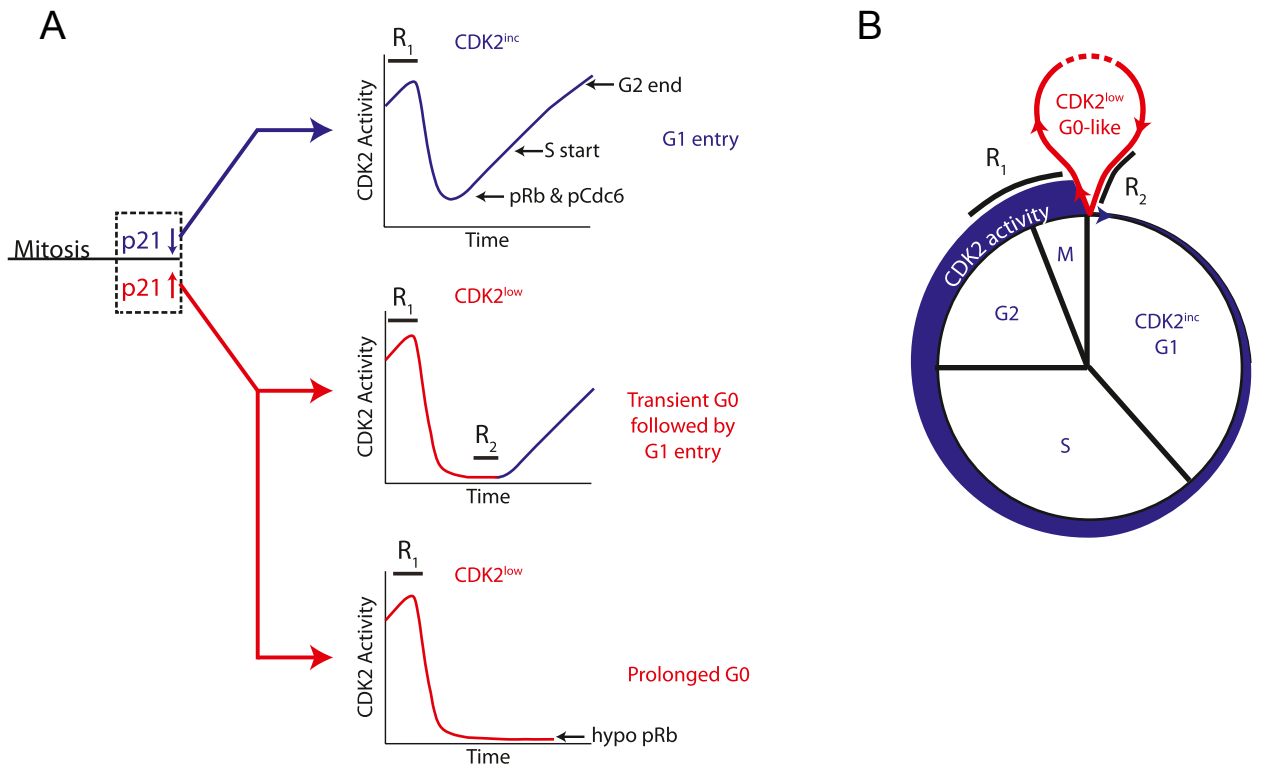

Figure 5. p21 drives bifurcation at mitotic exit. A) The model proposed by (Spencer, Cappell et al. 2013) indicates that p21 levels in mitosis which is sensitive to mitogens (First restriction point or R1) dictate the future fate of cells in the next cell cycle. 1) Low p21 in mitosis allows rapid entry in S phase in the next cell cycle without the need of mitogens 2) high p21 can drive a transient state in G0 where cells are sensitive to mitogens leading to a second restriction point (R2) or remain in G0 for longer times (senescence?). B) Summary of the finds in the proposed model of the restriction point. Adaptated from (Spencer, Cappell et al. 2013)

A follow up study from the CDK2 activity paper explained a more defined mechanism of RP regulation. It turns out that irreversibility in RP, meaning the point of commitment and start of DNA synthesis independent of a mitogen signal, it is not Rb phosphorylation but APC-Cdh1 inactivation driven by Emi1, and this happens long after Rb phosphorylation. This suggests that the actual bistable irreversible switch occurs at the boundary of G1/S transition and not at the RP as thought before. Another interesting finding is that cellular stresses can act upon the period before cells inactivate APC-Cdh1, this leads to cells enter quiescence meaning switching off E2F but still remaining sensitive to mitogens. However once cells pass the point of no return (or RP) by inactivating APC-Cdh1 with Emi1, only damage checkpoints are activated independent of mitogen signaling. (Cappell, Chung et al. 2016). The results allow a more precise definition of RP, including

the period where cells are sensitive to mitogens up to Rb phosphorylation plus the time that leads to final APC-Cdh1 inactivation.

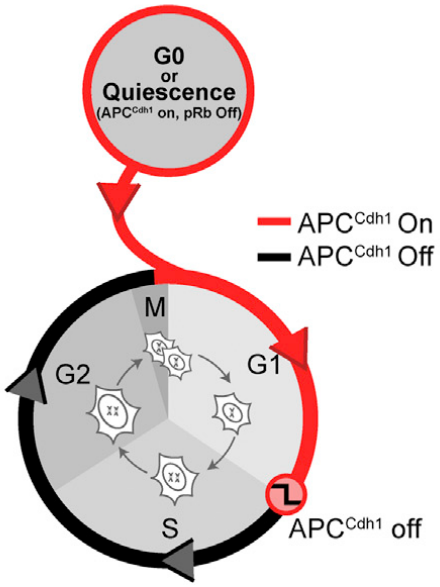

Figure 6. Restriction point model involving APC-Cdh1 regulation. The scheme illustrates the proposed biochemical RP defined by the inactivation of APC-Cdh1. Adapated from (Cappell, Chung et al. 2016)

4.1.2. Molecular definition of G0 phase

Quiescence or G0 are defined as a state where cells exit the cell cycle and become nonproliferative. A practical definition of G0 state has been elusive and sometimes confusing among cell cycle literature. One of the reasons is that the molecular characteristics of G0 can be variable and there is no consensus in the specific transcriptional programs controlling G0 that allow a practical distinction from normal cell stress or senescence However it is of medical relevance to molecularly define the G0 phenotype since chemotherapy selection could potentially enrich for G0 cells. As for the case of leukemia, following chemotherapy many patients exhibit minimal residual disease, with a subpopulation of leukemia cells that seem under cell cycle arrest, this could be caused by chemotherapy itself. However the surviving cells constitute a threat since re-awakening of cells might re-populate the tumor or even spread it more

aggressively due to random mutations during the G0 state, although this process might take long time. (Merlo, Pepper et al. 2006)

As expected, E2F1 its one of the main negative regulators of G0. Cells that exit G0 and enter in S phases start the synthesis of E2F1, passing from being undetectable in G0 to high levels equivalent to those in S phase. On the other hand, E2F4 seems to function in the opposite role. Unlike E2F1, E2F4 lacks cyclin A binding sites and it is present in growth arrested cells. Interestingly, localization of E2F4 is nuclear in G1 early and G0, suggesting that it might function as repressive transcription factor. When cells were entering S phase, E2F4 was shuttled to the cytoplasm. Whether nuclear E2F-4 acts as a transcriptional activator or as part of a repressor complex in different stages of the cell cycle remains to be determined (Lindeman, Gaubatz et al. 1997). However, experiment in mice showed that E2F1–3 function as transcriptional activators, but are dispensable for cell division and instead are necessary for cell survival. However simulatenous loss of Rb prevented cells to enter in differentiation state (Chong, Wenzel et al. 2009). Together this shows that E2F4 might promote entrance in G0 and E2F1 foster the exit from it. To increase the expression of E2F1 and therefore favor the exit from G0 there is need of previous Rb inactivation. Interestingly it was found that phosphorylation by cyclin C/Cdk3 on S807/S811 phoshphorylation site is necessary for an efficient G0-G1 transition, but still cells with the mutated site could enter G1 at a lower rate. Even more suprising is that Rb phosphorylated in vitro by Cdk3 and microinjected into cells cannot inactivate E2F, suggesting cyclin C/Cdk3 phosphorylation of S807/S811 specifically mediates G0 exit. (Macdonald and Dick 2012).

G0 is usually induced by withdrawal of mitogens, or when mitogens do not reach a certain threshold. However other mechanisms could induce quiescence in presence of mitogens. When cells in G1 are treated with doxorubicin, drug that induces DNA damage, Rb is recruited to the classic repressive pRB-E2F-HDAC complex inducing G0. This prevents cell-cycle entry and thus acts indirectly to protect cells from apoptosis. On the other hand, in proliferating cells, DNA damage favors formation of the transcriptionally active pRB-E2F1-P/CAF complexes because Rb phoshpohorylation prevents the formation of repressive complexes. In this setting, pRB favors the activation of genes involved in apoptosis. This goes in line with the APC-Cdh1 study, showing that

quiescence can only happen in G1. Additionally, reduction of Rb levels impairs Rb's proapoptotic function without altering proliferation (Ianari, Natale et al. 2009).

4.1.3. The transcriptional program of G0

Previous studies have intended to measure expression profiles in G0 cells versus actively cycling cells (Iyer, Eisen et al. 1999, Venezia, Merchant et al. 2004). However, as discussed before, quiescence can be induced by different stressors and the distinction among them is important to define a global transcription program of G0. These kind of analysis will lead to answer questions such as 1) Is it G0 one particular state or different states with similar phenotypic characteristics?, 2) is G0 actively maintained? 3) Is there such a thing as G0 transcription program?.

A more recent study (Coller, Sang et al. 2006) tried to address this problem by measuring expression profiles in three independent growth arrest signals, and for various periods of time. Interestingly, at least for fibroblasts, G0 seems to be a collection of states rather than a unique state but it appears there is a global signature common to all different states. Mitogen withdrawal upregulated the expression of G-protein molecules, MAPK and inositol-triphosphate– signaling pathways as well as IGFBP3, perhaps as a compensatory mechanism to stabilize IGFs and promote growth. Interestingly, contact inhibition induced downregulation of PCNA, lamin B, CENPA, enzymes from nucleotide metabolism and splicing factors, genes mostly involved in DNA replication and mitosis. Loss of adhesion, on the other hand, induced downregulation of cyclin E1, Cul-1, and FGF4, genes driving G1/S transition. Together this shows that different regulators of G0 might exist with specific regulatory programs. Interesting at later time points (4 days) the genes became uniformly regulated and a stable transcriptional program unique for each growth arrest signal became more evident. Mitogen withdrawal led to a persistent downregulation of POLD2, and POLR2I, genes involved in nucleic acid synthesis together with EIF3S9 and HARS involved in protein synthesis. TGF-b pathway was also involved to a lesser degree. E2F4, described before as a potential regulator of G0, was predominantly and uniquely upr-

egulated in the contact-inhibition condition. Lastly, loss of adhesion affected the expression of phosphatases involved in the MAPK pathway. Thus, the events that drive G0 seem to be more complex, so that might explain why certain signals do not favor cells to exit G0. Another important point will be to understand the role of oncogenes fostering cells to scape G0 since this can become relevant to eradicate cancerous G0 cells. Perhaps the G0 states might be as well different in the in vivo case, which deserves further investigation.

Other genes found to be downregulated are ones related to APC and SCF. This goes in line with the APC-Cdh1 study stressing the role of APC in controlling the G0 state. Other genes to be unspecifically regulated are TP53, FAT, PTK7 and CDH11. Those genes may help to maintain the G0 state by promoting cell cycle arrest. Importantly, G0 unlike senescence, apoptosis or differentiation is not a permanent state but a transitory one, therefore it is very likely that oncogenes might help to suppress genes that lead into those irreversible states (Coller, Sang et al. 2006). The location of G0 is another point of discussion. Experiments in hESCs showed that in early G1 phase differentiation is triggered into endoderm, whereas in late G1 were limited to neuroectoderm differentiation. Connecting to previous evidence, there seems to be G0-like behavior in early G1 (Pauklin and Vallier 2013).

Together, the evidence shows that understanding precisely where G0 is located, its molecular signature and regulation of exit are necessary to understand processes such as tumorigenesis, which fundamentally becomes in some cases an active scape from G0 states.

5. Molecular events beyond the restriction point

Exit from G0 is followed by commitment to DNA replication. Once cells cross the restriction point, Cdc6 and Cdt1 proteins load the MCM helicase onto the ORC to form the pre-RC. To initiate DNA replication CDK and DDK (Dbf4-dependent kinase) activate the helicase and load the replisome. “Replication licensing” refers to the process of forming the pre-RC. An important safety check during DNA replication is to prevent re-replication by blocking MCM loading during S, G2 and M phases (Sclafani and Holzen

2007). One of the mechanisms of preventing re-replication is the degradation of Cdt1 via SCF–Skp2 E3 ubiquitin ligase complex, in which Cdt1 proteolysis is regulated by CDK4 and CDK2 through phosphorylation favoring the recognition by SCF-SKP2 (Truong and Wu 2011). This step also coincides with the inactivation of APC, which has brought more recent relevance since it marks the actual point of no return in cell cycle. Cdt1 is therefore an interesting marker for the RP as it will be shown in the experiments performed in this thesis.

6. Experimental tools used to interrogate cell cycle behavior

6.1. Cell cycle synchronization methods

To understand how the molecular machinery that controls cell cycle commitment works it is necessary to perform synchronization. That means, arresting cells in a particular phase of the cell cycle via physical or chemical methods, and then observe cell cycle progression in terms of protein or gene expression levels. This approach has been successfully applied to obtain the current understanding of cell cycle regulation in different organisms, and in some cases has lead to the discovery of biomarkers for cancer prognosis. Of note, synchronization by serum starvation lead to the discovery of the restriction point (Pardee 1974). Other synchronization methods such as thymidine block, inhibit DNA synthesis and other such as nocodazole inhibit microtubule formation arresting cells in mitosis. However, it has been shown that current synchronization methods induce serious artifacts that hamper the reliability of certain cell cycle studies. Serum starvation has been shown to cause DNA fragmentation and to reduce survival of cells. Methods altering DNA replication usually trigger DNA damage response, perturb RNA synthesis and induce apoptosis. On top of those artifacts, aligning cells in a particular phase does not mean that the molecular machinery remains intact, translation and transcription continues in cells that are arrested first so heterogeneity is artificially induced in the cells and the levels might not reflect the correct physiological levels (Shaw, Payer et al. 2012). This limits the validity of the results. It has been found that protein levels of synchronized cells do not correlate with that of unperturbed cells (Gong, Traganos et al. 1995)

6.2. Genetic reporters for labeling cell cycle phases

To address this issue, efforts in developing genetic reporters that facilitates cell cycle staging are being developed. The idea in principle is to distinguish cell cycle stages in single cells by fluorescence; this allows classifying cells rather than synchronizing them, which in addition, gives the power of observing single cell behavior. The most successful example were the FUCCI reporters (Sakaue-Sawano, Kurokawa et al. 2008). The technique is based on constant expression of Cdt1 (G1 phase) and geminin (S/G2) peptides that contain cell cycle dependent degradation signals but lack the active domains that could perturb cell cycle in the host cell (Figure 7). The fragments are fused to fluorescence proteins (diverse set of panels exist) and the intensity of the signal is generally proportional to the length of the cell cycle phase. Interestingly a recent study found that the Cdt1 reporter could distinguish G0 cells, those exhibiting the highest Cdt1 signal exhibited as well Ki-67 negative staining (Tomura, Sakaue-Sawano et al. 2013). Given that FUCCI mice exist, the reporter could be a promising alternative to better understand the regulation of RP in vivo In the same direction, another reporter was develop using a p27-rrdegron (Oki, Nishimura et al. 2014). The probe contained the fluorescent protein mVenus and a p27K2 mutant fragment lacking CDK inhibitory activity (mVenus-p27K2), which was introduced in NIH3T3 cells. The reporter successfully identified the G0 cells and the G0-G1 transition could be observed by combination with the other FUCCI reporters. Interestingly, the reporter was active in G1 early and G0 cells, confirming the findings observed by E2F4 activation in G1 early and low CDK2 activity reported by Spencer et all. CDK2 activity sensor described above, suggested that for cells emerging from a starvation (G0 state), the CDK2low state could be defined as a continued G0 state that persists for at least 8 hr after mitogen addition, and the initial activation of CDK2 could be interpreted as the beginning of the G1 phase (Spencer, Cappell et al. 2013) In addition G1 early cells that had CDK2low remained in G0 in normally cycling cells confirming again what was observed using the p27 degron reporter.

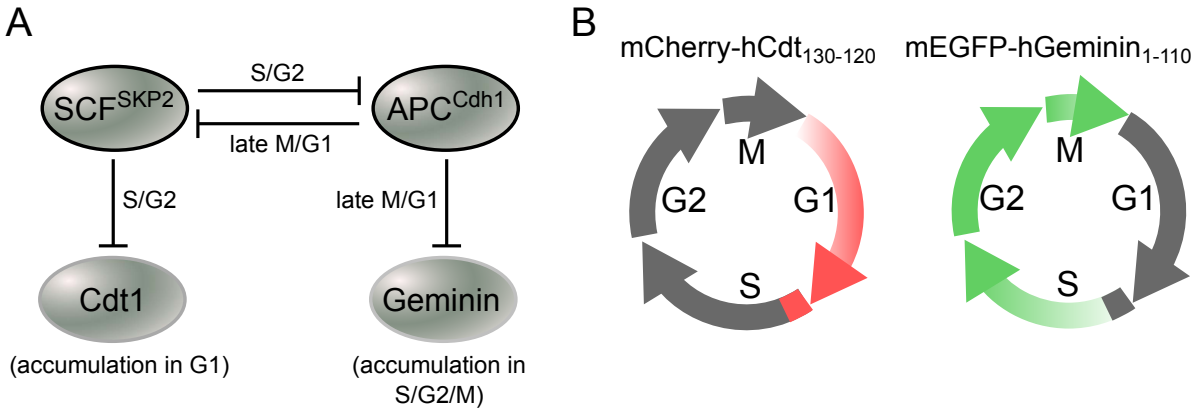

Figure 7. FUCCI reporters used for cell cycle staging. A) Cdt1 and Geminin levels are cell cycle dependent and controlled by degradation via SCF or APC complex. B) Diagram of activation of the different reporters, Cdt1 predominantly in G1 and early S and Geminin S through Mitosis. (Reproduced with the permission of Tatjana Ryl)

6.3. Methods to extracting cell cycle dynamics from snapshot data.

The described reporters are useful specially when cells are suitable for live cell imaging. But in some cases, some cell lines tend to form clusters or morphology makes difficult any attempt of microscopy examination. Cell size is also another factor that hampers proper data analysis, specially when the reporters are localized in the nucleus. Another interesting approach that is gaining popularity especially in the field of single RNA sequencing and Mass cytometry is to be able to extract dynamic data from a static picture of a steady state population. Since cell cycle is also a dynamic process with a series of defined steps, it becomes a suitable process to be studied using this methodology. Usually it involves computing a segmentation of the data, and organization of the stages by looking at the intensity of additional markers. Once the progression line is established the other markers can be analyzed. However the limitations are that cells need to be in steady state and the markers should provide sufficient information of all possible transitions. (Kafri, Levy et al. 2013) applied this method to determine growth regulation in a population of cells labeled with geminin degron and DNA staining. The authors used a mathematical framework called Ergodic rate equation (ERA) to extract dynamic information from snapshot data. Using ERA they showed that cell-to-cell size variation is regulated by a negative feedback at the G1/S transition. The authors also claimed that the dynamics of other processes, such as the

temporal changes in phosphoproteins during the cell cycle could be extracted with relatively high accuracy . However, in some situations as in the case of cell cycle, the snapshot data will exhibit all possible fates taken by the cells, for example, some cells will enter S phase and others will arrest in G0 temporarily. These bifurcations are evident in the snapshot data since cells are not synchronized. Another method called Wishbone went further to address that problem.

Based on a previously published algorithm from the same group called Wanderlust (Bendall, Davis et al. 2014), the authors used nearest-neighbor graphs to capture developmental path using using shortest paths. Each node in the graph represents a cell, and edges connect each cell to its most similar cells based on expression of the markers. Distances between cells can be computed using shortest paths, that is, a series of short steps through the neighbors in the graph, where each step between closely related cells is likely to represent similarity in degree of maturity. The ordering of the cells is refined by using a selected set of cells, called waypoints. The inconsistencies in distances between waypoints are used to identify the branch point and branch associations for all cells. The algorithm was able to recover the known stages of T-cell development in the mouse thymus, including the bifurcation point (Setty, Tadmor et al. 2016). One last algorithm and the one used here for data analysis is the Difussion maps calculation called Diffusion Pseudotime (DPT). The measure is a random-walk-based distance that is computed based on simple Euclidian distances in the 'diffusion map space'. The diffusion map is a nonlinear method for recovering the low-dimensional structure underlying high-dimensional data mid-dimensional data such as FACS. The branching is also calculated by comparing pseudotime sequences and measuring the correlation, at the point where correlation breaks the branching point is detected (Figure 8A). The main advantage of DPT with respect to Wishbone is its computationally efficiency which comes from using less processing steps which are more susceptible to parameter selection, leading to a more robust detection of branching points (Haghverdi, Buttner et al. 2016).

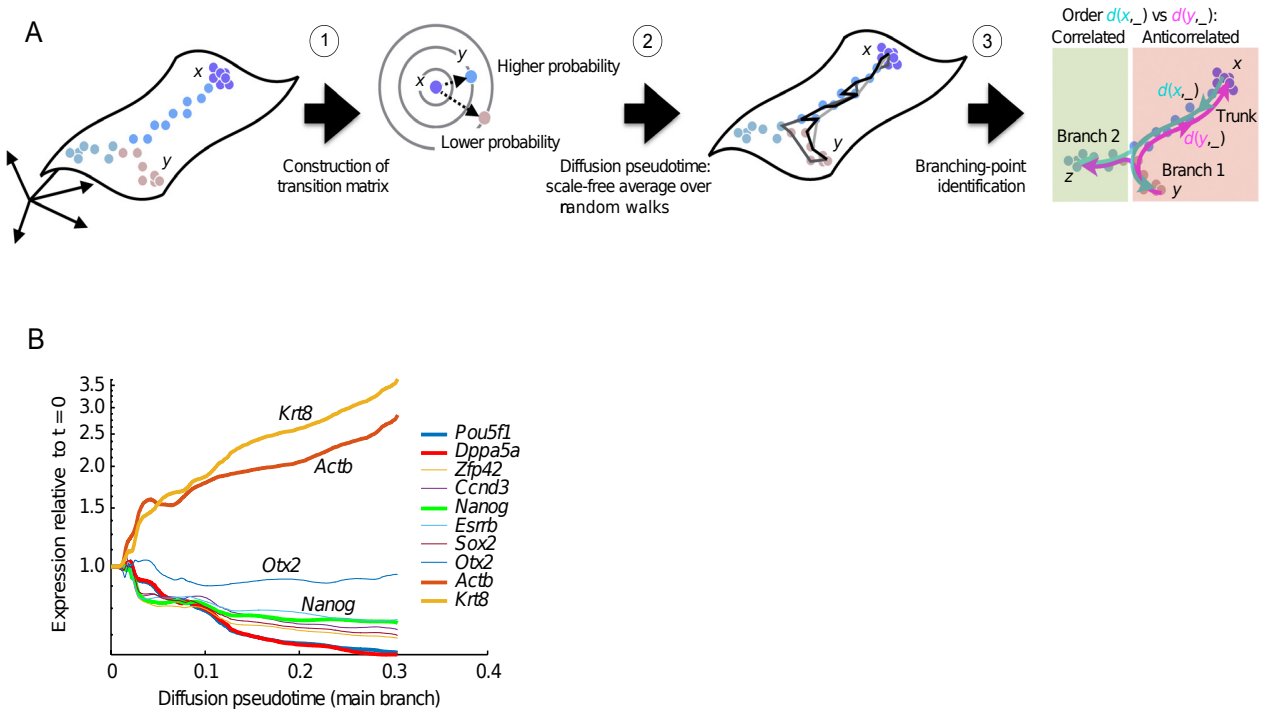

Figure 8. Diffusion maps method to extract dynamic data from snapshot data. A) The diffusion transition matrix is computed as transition probability from once cell to another (1). Diffusion pseudotime dpt(x,y) approximates the distance between cells (2). Branching points are identified as points where anticorrelated distances from branch ends become correlated (3) B) Example of dynamics extracted from snapshot single cell RNA-seq data. Adapted from (Haghverdi, Buttner et al. 2016)

7. MYCN effects on cell metabolism.

As stated previously, MYCN influences predomintantly proliferation, however another important process required for cell division is metabolism, and previous studies have shown that MYC regulates glucose and glutamine utilization through the increased expression of key glycolytic and glutaminolytic enzymes. Increased overall metabolism supports cell growth. MYC-high cells use glutamine as carbon source for the tricarboxylic acid (TCA) cycle, and deprivation of glutamine was shown to kill cells expressing high levels of c-MYC and MYCN (Yuneva, Zamboni et al. 2007, Wise, DeBerardinis et al. 2008, Qing, Li et al. 2012) Several pieces of evidence have shown that MYC up-regulates enzymes involved in oxidative phosphorylation and similarly to RAS it appears to use respiration rather the glycolysis alone for ATP production(Morrish, Neretti et al. 2008, Dang 2011, Zirath, Frenzel et al. 2013). Another aspect in close connection with cell metabolism is the redox balance which is required for normal

cellular functioning (Gorrini, Harris et al. 2013). Oxidative phosphorylation in the mitochondria is considered the major intracellular source for ROS, however the final cellular response to oxidative ROS depends largely on ROS type, location, and level. MYC was previously reported to impact various aspects of redox homeostasis. Despite the fact that MYC increases mitochondrial activity and subsequently enhance endogenous source of ROS, various antioxidant pathways are also regulated by MYC, enabling cells to prevent oxidative damage (DeNicola, Karreth et al. 2011) Recently Lien and colleagues found that inhibition of GSH biosynthesis and cotreatment with cisplatin can enhance DNA damage therapeutic effect in cells carrying PI(3)K mutation (Lien, Lyssiotis et al. 2016). MYC seems to stabilize *NRF2* transcription factor, which regulates glutamate-cysteine ligase modifier (GCLM) and heme oxygenase 1 (HMOX1) eliminating the lethal effects of oxidative stresses (Alam, Stewart et al. 1999, Gorrini, Harris et al. 2013). It also has been indicated that c-MYC suppresses ferritin, making the stored iron metabolically available for cells, that might sensitize the cells to ferroptosis (Wu, Polack et al. 1999, O'Donnell, Yu et al. 2006).

Ferroptosis is non-apoptotic form of regulated cell death dependent from the accumulation of lipid ROS and intracellular iron levels (Dixon, Lemberg et al. 2012). Previous work has shown that the activation of ferroptosis is mainly controlled by enzymes of GSH pathway, such as SLC7A11and GPX4 (Dixon, Lemberg et al. 2012, Yang, SriRamaratnam et al. 2014). Other positive regulators of ferroptosis are p53, CARS and NOX (Xie, Hou et al. 2016). Small molecule screen found erastin as potent inducer of ferroptosis (Yagoda, von Rechenberg et al. 2007, Dixon, Lemberg et al. 2012). This molecule was found previously to inhibit oncogenic RAS and GSH biosynthesis (Dolma, Lessnick et al. 2003). In vivo experiments using a HT-1080 fibrosarcoma cells xenograft mourse model showed reduction of tumor growth under piperazine-erastin treatment injected subcutaneously (Yang, SriRamaratnam et al. 2014). Although MYC regulates GSH synthesis at multiple points, to our knowledge there are no reports indicating an association between MYC and ferroptosis.

8. Aims of the study

From previous data was concluded that MYCN influences the cell cycle machinery leading to uncontrolled proliferation. Reducing MYCN levels promotes G1 phase lengthening and it appears to be the same case for other tumor types involving the homologous c-MYC. However the mechanism of how MYCN regulates the cell cycle machinery to promote proliferation is still not well understood. Regular cell cycle studies using chemical synchronization might contain artifacts, which could obscure the real dynamics, so we used here cell cycle genetic reporters to study the effects in single cells. Metabolic deregulation is another hallmark of oncogenic MYCN and one approach to find new potential therapeutical strategies is to explore synthetic lethal combinations of metabolic genes with MYCN.

The aim of the project was to understand how MYCN promotes cell cycle commitment in neuroblastoma cells via modulation of the restriction point of the cell cycle. In addition, aminoacid metabolism was investigated to find vulnerable points that can be used for therapeutic purposes in MYCN-driven tumors. The questions that were addressed in this project are the following:

1. How does MYCN modulate the restriction point in neuroblastoma cells?

   To prevent synchronization artifacts, genetic reporters for cell cycle staging were stably integrated in MYCN-amplified cells with tunable MYCN levels. Measurements of cell cycle players by FACS and microscopy were performed under different perturbations to tease out the role of MYCN in the restriction point.

2. What are the transcriptional programs driven by MYCN controlling the passage through the restriction point?

   Given the advantage of genetic reporters, cell sorting and transcriptomics can be performed in unperturbed cells. This data can give a clearer picture of the effects of MYCN on transcriptional program controlling the restriction point.

3. Which are the metabolic requirements of MYCN amplified cells?

   Using metabolomics measurements of MYCN amplified cells we intended to detect metabolic dependencies specific for high MYCN cells.

9. Materials and Methods

9.1. Materials

Research equipment

Microscope Olympus, CKX41	Olympus
Microscope Olympus, Cell^R	Olympus
Miltenyi MACSQuant Analyser	Miltenyi
LSRII	BD Biosciences
Steri-cult CO_2 incubator	Thermo Scientific
Tecan Infinite M 200	Tecan
NanoDrop ND-1000 spectrophotometer	NanoDrop
Vortex Genie	NeoLab
Thermo water bads	GFL, Hans Byaer, Julabo
Bioanalyzer	Agilent
Cell culture hood HERA	Heraeus
Centrifuges	Eppendorf, Beckman Coulter
Qbit	Qubit
Light Cycler 480	Roche
FACS sorter Aria II	BD Biosciences
GC/MS-QP2010 Plus (metabolomics)	Shimadzu®

Molecular biology reagents

ABSOLUTE qPCR ROX mix	Thermo Scientific
Agencourt AMPure XP beads	Beckton Dickinson
Bovine serum albumin (BSA)	Roche Diagnistics

Cell Titer Blue	Promega
ERCC Spike-in control	Life Technologies
QBit RNA assay	Life TechnologiesMethylene
PBS	Santa Cruz
Spike-In	Life technologies
Real-Time Cell Analyzer (RTCA)	Roche

Kits for molecular biology

Click-iT EdU Flow Cytometry Assay Kit	Life Technologies
Effectene Transfection Ragent	Qiagen
ScriptSeq Complete Gold Kit (Human/Mouse/Rat)	Epicenter
First Strand cDNA Synthesis Kit	Thermo Scientific
RiboGold Kit	Epicenter
RNeasy mini Kit	Qiagen

Chemicals and Reagents

DMSO	AppliChem
EDTA	Sigma
Ethanol	Sigma
Formaldehyde 4%	BioLegend
FxCycle Violet Stain	Life Technologies
Vybrant Dye Cycle Violet Stain	Life Technologies
Isopropanol	Greiner Bio One
Methanol	Greiner Bio One
Nuclease-free water	Ambion

Triton X-100	Sigma
RNAse A	Thermo Fischer
RNAse inhibitor	Clontech
Monobromobimane	Calbiochem
Chloroform	Sigma
Methoxyamine hydrochloride	Sigma 226904
Pyridine	Sigma
MSTFA	Sigma

Table 1 Antibodies and Isotypes for FACS

Specificity	**Host**	**Supplier/Catalog number**
p-Rb (S807/811) XP Alexa 647 Conjugate	Rabbit	Cell Signaling/ 8974
SKP2 (D3G5) XP	Rabbit	Cell Signaling/ 2652
p27 Kip1 (D69C12) XP	Rabbit	Cell Signaling/ 3686
p21 Waf1/Cip1 (12D1)	Rabbit	Cell Signaling/ 2947
E2F1	Rabbit	Cell Signaling /3742
MYCN [NCM II 100]	Mouse	Abcam/ ab16898
p-CDK2 T160	Rabbit	Abcam/ ab194868
mAb IgG Isotype Control Alexa 647 Conjugate	Rabbit	Cell Signaling/ 2985
mAb IgG XP(R) Isotype Control	Rabbit	Cell Signaling/3900

mAB IgG1, k Isotype Control	Mouse	Abcam/ab18443

Table 2 Taqman® Real-Time PCR Assays

Gene	Assay ID
MYCN	Hs00232074_m1
C-MYC	Hs00153408_m1
CDKN1A	Hs00355782_m1
CDKN1B	Hs01597588_m1
E2F1	Hs00153451_m1
SKP2	Hs01051864_m1
CCNA2	Hs00996788_m1
CCNE1	Hs01026536_m1
CCND1	Hs00765553_m1
GAPDH	Hs02758991_m1
UBC	Hs00824723_m1
HMBS	Hs00609296_m1
SDHA	Hs00188166_m1

All TaqMan assays were obtained from ThermoFisher Scientific

Drugs

LEE011 (CDK4 inhibitor)	Selleckchem
HLM006474 (E2F inhibitor)	Merck Millipore
U0126 (MEK inhibitor)	Cell Signaling
PD0325901 (MEK inhibitor)	Sigma Aldrich
10058-F4 (MYC inhibitor)	Sigma Aldrich

Antibiotics for cell culture

Blasticidin	Sigma

Penicillin/Streptomycin	PanReac AppliChem
G418	Sigma
Hygromycin B	Sigma
Puromycin	BD Clontech
Zeocin	Invitrogen
Doxycycline	BD Clontech

Media and supplement for cell culture

RPMI 1640 (1mM L-Glutamine, 25mM Hepes)	Gibco, Life Technolofies
RPMI 1640 (with L-Glutamine, without Phenol Red)	PAA, The Cell Culture Company
Fetal Bovine Serum (FCS)	Gibco, Life Technolofies
Fetal Bovine Serum, dialyzed	ThermoFisher

Plasmids

The E2F1pr-d2EGFP-pQCXIP construct was kindly provided by Prof. Guang Yao.It posses a 800bp fragment of the E2F1 promoter followed by a destabilized form of EGFP The plasmids has puromycin resistance.

pFucci orange G1 was kindly provide by University of Viena. The plasmid has the fluorescent protein mKO2 fused to a human part for Cdt1 protein (hCdt1 30-120). It degrades at the start of S phase. Resistance is Neo/Kan and the antibiotic used of selection is G418.

The pMOWS_puroR_mCherry_hCdt1 construct was kindly provided by Prof. Ursula Klingmüller. It is similar to pFucci orange but instead of mKO2 is tagged to mCherry. And the resistance is puromycin.

Table 3 Tissue culture cell lines used in the study

Cell Line	Description	Reference	Selective antibiotics
TET21N	Derived from SH-EP, transgenic inducible *MYCN*, non amplified neuroblastoma cell line	(Lutz, Stohr et al. 1996)	90 µg/ml Hygromycin 200 µg/ml G418
IMR5/75_shRNA MYCN	*MYCN* - amplified neuroblastoma cell line, expresses MYCN shRNA under control of tetracycline repressor	(Muth, Ghazaryan et al. 2010)	5 µg/ml Blasticidin, 45 µg/ml Zeocin
TET21N_hCdt1	Derived from SH-EP, transgenic inducible *MYCN*, with recombinant hCdt1 (30-120)	Generated in collaboration with Tatjana Ryl	90 µg/ml Hygromycin 200 µg/ml G418 7.5 µg/ml Puromycin
IMR5/75_E2F1 Cdt1	*MYCN* - amplified neuroblastoma cell line, expresses MYCN shRNA under control of tetracycline repressor, has Cdt1 and E2F1 constructs	Generated in the present study	5 µg/ml Blasticidin 45 µg/ml Zeocin 1 µg/ml Puromycin 200 µg/ml G418
IMR5/75_E2F1	*MYCN* - amplified neuroblastoma cell line, expresses MYCN shRNA under control of tetracycline repressor, has E2F1 constructs	Generated previously in the Master thesis	5 µg/ml Blasticidin 45 µg/ml Zeocin 1 µg/ml Puromycin

Software

Inkscape

FIJI

FlowJo X

Prism 6

Matlab

R

Bioconductor packages

STAR

HTseq

RSeQC (2.5)

9.2. Methods

9.2.1. Cell culture methods

9.2.1.1. Culturing and cryoconservation of human neuroblastoma cells

All cells were cultivated in RPMI1640 supplemented with 100 U/ml Penicillin/ Streptomycin, and 10% FCS at 37°C, in 5% CO2 atmosphere in a humidified cell culture incubator. The cell culture medium was substituted every 3-4 days, and cells were split at ration 1:5 when they reached subconfluent density. Adherent cells were removed with a solution of PBS and EDTA. Visual observation of cell morphology was conducted under the Zeiss Axiovert microscope, equipped with phase-contrast and bright-field optics. The conservation cells were harvested and resuspended in 4 ml of an ice-cold cryoconservation medium (RPMI with 40% FCS, 10% DMSO). The cellular suspension was dispensed into cryocontainers and incubated at least 24h at -80C prior to deposition into a liquid nitrogen tank for long time storage. For recultivation, frozen cells were quickly thawed and the cryoconservation medium was substituted with a warm fresh growth medium.

9.2.1.2. Transfection of plasmids and selection of transfected cells

Transfections were carried out using the Effectene Transfection Reagent. It is a non-liposomal lipid formulation allowing high transfection efficiency with minimal cytotoxicity. Plasmids were transfected into cells, which were seeded 18-24h before transfection. Transfection was performed according to manufactural instructions using 1 µg DNA. The

transfection medium was replaced by the fresh complete medium 24h post transfection. Selection of stably transfected cells was initiated 24h post transfection by addition of appropriate antibiotics into the growth medium. After selection, transfected cells were sorted into single cells using fluorescence activated cell sorting to generate clonal populations. Individual clones were expanded and analyzed using FACS analysis or time-lapse microscopy.

9.2.1.3. Inhibitors treatment

Inhibitors HLM006474, U0126, PD0325901, were used 2, 4 and 8 μM concentrations on IMR5/75 cells for 24hr. LEE011 was used at 200nM and 10058-F4 at 15 μM.

9.2.1.4. Calculation of growth curves.

At the appropriate time points cells were dethatched with versene. 1mL of cell-versene suspension was collected and 100 μL were counted with the MACSQuant Analyser (Milteny) using propidium iodide staining to exclude dead cells. $2x10^4$ cells were seeded on RTCA slides for impedance measurements and growth rate calculations.

9.2.2. FACS analysis

9.2.2.1. Antibody staining

10^6 cells were pre-fixed with 4% paraformaldehyde (PFA) for 15 minutes at room temperature (RT), then re-suspended in 3ml ice-cold methanol and incubated overnight at -20°C. Cells were then washed in PBS, incubated for 30min in washing buffer (1%BSA, 0,1% TritonX in PBS) and stained with fluorescein-conjugated primary antibodies for 1 h at RT (Table.2). After washing the cells were stained with FxCycle Violet dye for cell cycle analysis. Data was analyzed with FlowJo software, either Dean-Jett-Fox or Watson algorithm was used to determine percentage of cell cycle phases. Cells with a DNA-content below that of the G1-fraction were considered dead.

9.2.2.2. EdU incorporation

Cells were incubated with 10 µM EdU for 30min prior to collection. 10^6 cells were fixed, permeabilized and stained with the Click-iT Plus EdU Flow cytometry Assays Kit.

9.2.2.3. FACS-Single cell sorting (Cell cycle outgrowth)

IMR5/75_E2F1 Cdt1 cells were harvested and re-suspended in ice-cold medium. Cell sorts were performed using FACS sorter Aria II (BD). For each conditions ~600 or more single cells were sorted into 96-well plates according to their cell cycle status. 3 weeks after re-seeding, cells were stained with Cell Titer Blue assay, imaged and the number of colonized wells counted. Three biological replicates were performed.

9.2.2.4. Live-cell microscopy

Around 3000 cells were seeded on 8-well Ibidi µ-slides or Lab-Tek chamber slides in phenol red-free RPMI 1640 medium and imaged every 10 min for up to 48 hr under controlled growth conditions at 37°C, 5% CO2 and 80% humidity. Images were acquired with an inverted widefield microscope (Olympus Cell^R) using an CCD Hamamatsu Orca-ER camera and a 20x lens (UPlanSApo / 0.75). Bright field images were acquired in addition to fluorescence using a light engine lamp. Filters used were EGFP and HcRed.

Cells were tracked manually using FIJI (version 1.48d) (Livak and Schmittgen 2001)

9.2.2.5. Real-time quantitative PCR

Around 6×10^4 live cells were sorted in PBS with RNAse inhibitor based on E2F1 intensitiy and DNA content measured with Vybrant Dye Cycle. Total RNA was isolated with the RNeasy Mini Kit (Qiagen), following manufacturer's instructions. Nucleic acids were quantified in solution using NanoDrop ND-1000 spectrophotometer by measuring absorbance at 260 nm.

RNA for the gene expression measurement was reverse transcribed using the RevertAid H Minus First Strand cDNA Synthesis Kit (Thermo scientific) according to manufacture instructions. Samples to be used in real-time quantitative PCR were diluted with nuclease-free water to the final concentration of 2 ng/µL (equivalent of total RNA) and stored at -20°C until use.

DNA was quantified in 384-well format using the LightCycler 480 Real-Time PCR System, Table5. For the quantitative gene expression studies, cDNA in the amount of 10 ng of equivalent of total RNA was used per well. 5 µL of cDNA (2 ng/µL) was mixed with 6 µL of enzymatic master mix, yielding 11 µL total sample volume. The mRNA level of each target gene was normalized to the relative average amount of the internal reference genes *GAPDH, UBC, SDHA or HMBS*. The internal reference genes and the target genes were analyzed in parallel for each sample. The relative gene expression was calculated using the comparative cycle crossing point ($\Delta\Delta$Cp) method (Livak and Schmittgen 2001).

9.2.3. RNA-sequencing

Around 1 × 10^5 live cells were sorted in PBS with RNAse inhibitor based on Cdt1 and E2F1 intensities and snap frozen in liquid nitrogen. RNA was extracted using Arcturus® PicoPure® Frozen RNA Isolation Kit. ERCC Spike-in control mix-1 (Life technologies) was added to each sample prior to processing (1 µl of a 1:10 dilution of mix-1). RNA from each sample was processed using the RiboGold kit (Epicentre) to remove rRNA. The remaining rRNA-depleted sample was then used to prepare libraries for sequencing. The RNA library prep kit, ScriptSeq Complete Gold Kit (Epicenter) was used for IMR5/75 cells. The Agencourt AMPure XP beads (BeckmanCoulter) were used to purify the cDNA. Barcodes for individual samples were added in order to multiplex 6 samples in each sequencing lane. The qualities of libraries were assessed using a DNA1000 chip on a Bioanalyser (Agilent) to ensure the correct size of libraries and the concentration was measured using the Qbit DNA assay. Sequencing was performed on Illumina platform with HiSeq 2000 Pair-end 100bp sequence type.

RNA-Seq reads alignments and counts of raw reads of sequenced IMR5/75 shRNA cells were mapped to the human genome hg19 using STAR (2.4.0h1) with default parameters. Reads and alignment quality were examined by FastQC (0.10.0) and RSeQC (2.5), respectively. Spike-in sequences were concatenated with the hg19 genome sequence. Read counts were calculated by HTseq via "-s yes".

RNA-Seq data were normalized for each sample, the data sequenced in different lanes was summated, and read counts of genes were normalized by DESeq2 package in R. Normalization size factors were obtained using filtered spike-in raw read counts (≥5 reads in any sample; "absolute" expression) or filtered whole-genome gene read counts (≥10 reads in any sample; "relative" expression). All raw read counts were divided by the size factor to obtain a normalized genes expression value used in all further analyses.

Identification of differentially expressed genes by Likelihood ratio test was implemented by the DESeq2 (Love, Huber et al. 2014) package in R used to find differentially expressed genes with options "independentFiltering = FALSE, cooksCutoff = FALSE". For differential expression, the maximal absolute fold change between MYCN conditions or cell cycle phases had to be ≥ 0.5 and a false discovery rate (FDR) ≤ 0.1. Additional analysis were performed using Ingenuity Pathway Analysis suit under the upstream regulators option (Kramer, Green et al. 2014).

9.2.4. Quantification of Amino Acids

Cell pellets of two million cells were extracted with 0.1 ml ice-cold 0.1 M HCl. Non-thiol-containing amino acids were quantified after specific labeling with the fluorescence dye AccQ-TagTM (Waters) as described in (Yang, A et al. 2015). Cysteine was determined after labeling with monobromobimane (Calbiochem) as described before ((Wirtz and Hell 2007).

9.2.5. Metabolite Analysis by Gas Chromatography/Mass Spectrometry (GC/MS)

9.2.5.1. Extraction

We harvested approximately six million cells of MYCN-high and MYCN-low expressing IMR5/75, as well as MYCN-high IMR5/75 cells treated with MYC inhibitor (10058-F4), or DMSO as control. Intracellular GSH and metabolites of the TCA cycle were analyzed.

Harvested cells were washed twice with 0.9% ice-cold NaCl solution and immediately snap frozen with liquid nitrogen. Frozen pellets were extracted in 180 µl of MeOH for 15 min at 70°C with vigorous shaking. As internal standard, 5 µl ribitol (0.2 mg/ml) were added to each sample. After the addition of 100 µl chloroform, samples were shaken at 37°C for 5 min. To separate polar and organic phases, 200 µl water was added and samples were centrifuged at 11,000× g for 10 min. For the derivatization, 300 µl of the polar (upper) phase were transferred to a fresh tube and dried in a speed-vac (vacuum concentrator) without heating.

9.2.5.2. Derivatization (Methoximation and Silylation)

Pellets were re-dissolved in 20 µl methoximation reagent containing 20 mg/ml methoxyamine hydrochloride (Sigma 226904) in pyridine (Sigma 270970) and incubated for 2 h at 37°C with shaking. For silylation, 32.2 µl N-methyl-N-(trimethylsilyl)trifluoroacetamide (MSTFA; Sigma M7891) and 2.8 µl Alkane Standard Mixture (50 mg/ml C10 – C40; Fluka 68281) were added to each sample. After incubation for 30 min at 37°C, samples were transferred to glass vials for GC/MS analysis.

9.2.5.3. Gas Chromatography/Mass Spectrometry (GC/MS) Analysis

A GC/MS-QP2010 Plus (Shimadzu®) fitted with a Zebron ZB 5MS column (Phenomenex®; 30 m × 0.25 mm × 0.25 µm) was used for GC/MS analyses. The GC was operated with an injection temperature of 230°C and 2 µl sample were injected with

split 10 mode. The GC temperature program started with a 1 min. hold at 70°C followed by a 6°C/min ramp to 310°C, a 20°C/min ramp to 330°C and a bake-out for 5 min. at 330°C using helium as carrier gas with constant linear velocity.

MS was operated with ion source and interface temperatures of 250°C and a scan range (m/z) of 40–1000 with an event time of 0.3 sec.

The “GCMS solution” software (Shimadzu®) was used for data processing.

9.2.6. Analysis of Intracellular ROS

Intracellular reactive oxygen species (ROS) levels were measured in approximately 105 cells using CellROX® (Life technologies). Approximately 105 cells were seeded in 12-well plates and 24 h later cells were treated with 10058-F4 for an additional day. Cells were then fed either with full or cystine-free medium for 24 h. Before ROS being analyzed, CellROX was added to the wells at a final concentration of 5 μM and cells were incubated in a cell culture incubator for 30 min. After 30 min of staining, cells were harvested gently and immediately analyzed by FACSCalibur to measure the signal intensity directly proportional to the level of intracellular ROS.

9.2.7. Analysis of Cell Proliferation by (Sulforhodamine B) SRB Assay

The impact of various medium conditions on cellular proliferation/viability was analyzed using SRB assay as described in great detail by (Vichai and Kirtikara 2006). To determine changes of cellular proliferation upon incubation with various medium conditions, approximately 2 × 104 cells were seeded in full medium in 48-plate format, 24 h prior to the treatment. Cells were then washed once with PBS and fed with the chosen medium. Cell proliferation/viability was analyzed at different incubation time points using SRB assay as described in great detail by Vichai and Kirtikara (Vanicha Vichai 2006, Nature Protocol). In brief, cells were fixed with ice-cold 10% (trichloroacetic acid) TCA for 1 h; fixed cells were then stained with 0.054% w/v SRB for 30 min and

absorbance was measured at 535 nm using a Tecan Ultra plate reader (Tecan, Maennedorf, Switzerland).

10. Results

10.1. MYCN promotes cell cycle entry

10.1.1. Reduction of MYCN leads to prolonged doubling time

Previous studies have found that MYCN boost proliferation(Meyer and Penn 2008). Here we used a tet inducible shMYCN cell line, IMR5/75, that has 75 copies of the MYCN oncogene. The reduction of MYCN is not complete (Figure 11A) but significant. Through the text, MYCN-low cells will be denoted as the cells were MYCN is reduced by the shRNA. There were not reports of doubling times with respect to this particular cell line. To get accurate estimates of doubling times, IMR5/75 cells were counted by FACS over a period of a week to calculate the growth curve (Figure 9B). This result is necessary for further calculations of cell cycle phase lengths that were performed in the further sections. To confirm this result, cell growth was additionally measured by impedance. IMR5/75 cells either with or without the E2F-d2GFP construct were seeded in the RTCA plates. These device measures electron flow on the surface of the plate. Attached cells will interfere with the electron flow generating impedance The higher the cell density the higher the impedance, therefore serving as a readout of cell proliferation. Impedance in some situations could also indicate changes in cell attachment. Overall the results are shown in Figure 9A. The data shows strong accordance between both types of measurements as shown in Figure 9C. MYCN-high cells exhibit a doubling time of around 16-21 hrs and MYCN-low cells between 35-50 hrs. This clearly indicates that reduction of MYCN almost increase by half the length of the cell cycle duration.

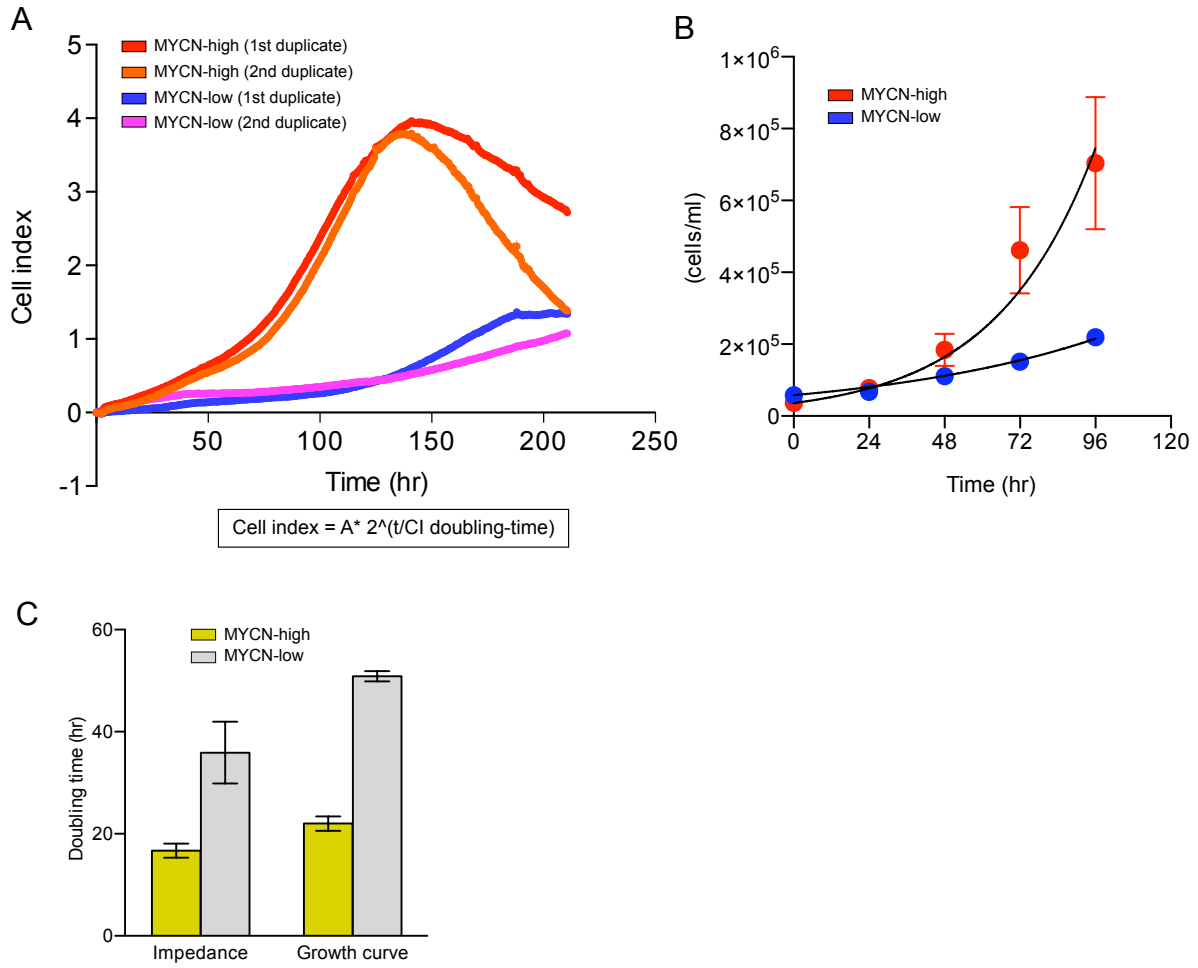

Figure 9 Growth kinetics of MYCN amplified IMR5/75 cells. A) Impedance measurement of cell growth. 2 biological duplicates are shown for MYCN-high/low condition. B) Growth curve calculated by counting viable cells. SEM is calculated from 3 biological replicates. C) Comparison of doubling times calculated

Also interesting to note, MYCN-high cells do not remain viable for longer than 6 days as shown in the impedance data (Figure 9A). Perhaps in confluent conditions ROS levels are overly toxic for active proliferating cells as shown later in the metabolic section.

Calculation of the doubling time is mathematical measure that generalizes a value based on a population measure. To test if this correlates with the actual growth of the cells, MYCN-high cells as an example were sorted in 6-well plates based on G1 DNA content and low E2F-d2GFP reporter (Figure 14A). This reporter cell line previously generated in the Master thesis will be used here in combination with Cdt1-degron marker for characterizing the restriction point in these cells. The results show that after

15hr cells populate all the phases, seemingly correlated with the doubling time calculated based on growth curves and impedance (Figure 10). Interestingly, cells from low E2F-d2GFP levels are still able to grow in the MYCN-high condition. This is confirmed with further experiments later in this thesis, showing that MYCN-high cells do not seem to have a permanent quiescence phenotype.

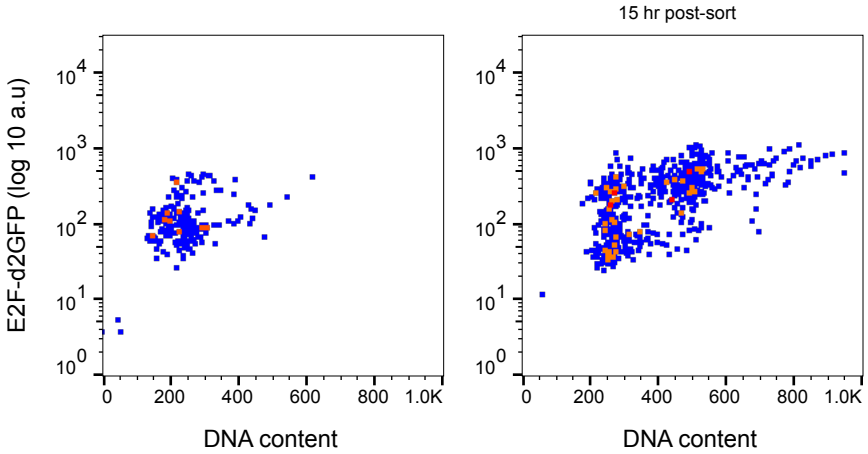

Figure 10 Cell sorting outgrowth. Left panel: MYCN-high cells sorted by low E2F1 promoter activity in G1. Right panel: Measurement of sorted population after 15 hr incubation.

In this particular context, it is important that MYCN is the main driver of the observed phenotype. However the effects can be masked by its homologous c-MYC. However FACS protein staining of c-MYC do not show significant differences upon MYCN reduction (Figure 11A: right panel). Therefore it is safe to say that MYCN is the main driver of the cell cycle effects observed in this particular cell line. The growth measurements showed that MYCN reduction lengthens cell cycle duration by almost a factor of 2. To explore if this is can be explained by the proportion of G0 cells, EdU incorporation was measured after a 30 min pulse. The results indicate that reduction of MYCN increase the proportion of dormant or non-proliferating cells by 10% (Figure 11C). This is still a modest increase but shows that MYCN might be promoting proliferation by inhibiting G1 arrest.

10.1.2. MYCN favors crossing of the restriction point

The Rb-E2F network mostly regulates G1/S transition. The way the mechanism works is by deactivating Rb via phosphorylation leading to E2F1 release from the repressing complexes and increase of E2F1 expression via auto-activation. To explore if the effects observed in the proliferative and dormant fractions are due to changes in the most important G1 regulators (Figure 11B), protein staining of pRb807/811 phosphorylation site (a marker for cell proliferation) E2F1 total protein and d2GFP we co-stained with DNA content staining using FxCycle violet dye. Gates for the cell cycle phases were applied using the Dean Jet Fox model in FlowJo. For each of the cell cycle phases, the distributions were plotted with either the autofluorescence control or the isotype staining. As previously found with EdU incorporation assay, MYCN-low cells accumulate in G1 with almost 10% more cells. The distributions show some interesting behavior. pRb exhibits a bimodal behavior in G1, with almost unchanged levels in the other cell cycle phases. MYCN-low cells exhibit a greater accumulation in the negative pRb fraction as compared to MYCN-high. This shows that MYCN-high cells do maintain a greater proportion of cells in the phosphorylated state, probably the proliferating cells. On the other hand, E2F promoter activity (E2F-d2GFP) exhibits a strong shift in G1 with moderate shifts in the other phases, favoring usually higher promoter activity levels in MYCN-high cells. E2F1 protein levels remain slightly changed in G1 mostly.

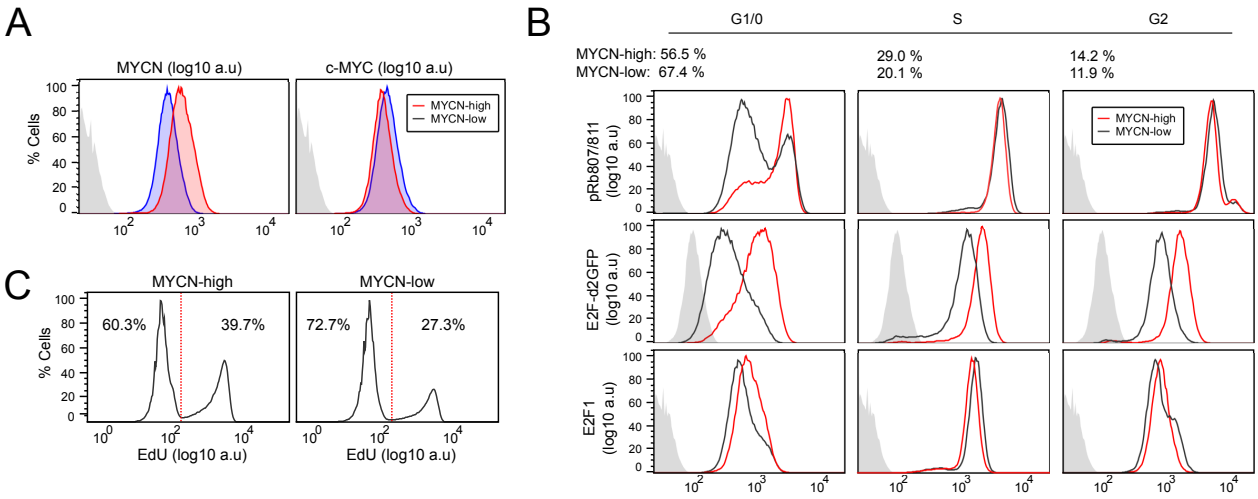

Figure 11 Characterization of the cell system. A) Antibody staining shows MYCN reduction upon shRNA induction. c-MYC levels remain unchanged. B) pRb807/811 and E2F1 staining together with E2F-

d2GFP activity for each cell cycle phase. Faded gray distributions indicate either auto-fluorescence control or isotype. C) EdU incorporation assay. The gate was calculated with the bifurcate option in FlowJo.

Together this indicates that G1 key regulators are strongly affected by MYCN. An interesting point is that E2F1 promoter activity did not show a bimodal behavior as previously reported by (Yao, Lee et al. 2008). However pRb shows a clear bimodality. The relevance of this finding is that its commonly assumed that cell cycle checkpoints work as bistable switches exhibiting ultrasensitive behavior, that means if titration of a signal is performed, the response curve will look sigmoidal, since low amount of signals do not trigger response only until certain threshold is crossed. In single cells measures this ultrasensitivity is observed by bimodal distributions that switch from negative to positive stats without intermediates. This suggest that the bistable switch might be still intact in MYCN-high cells but MYCN might increase the probability of crossing the switch evidenced by a higher proportion of pRb positive cells. As for the case of the the E2F promoter, perhaps external sources of noise could mask the bimodal behavior, but further experiments are required to clarify the noise role in MYC-driven tumors. To investigate further the integrity of the bistable switch, we took advantage of normal heterogeneity of protein levels in cells. We performed a dose response curve of IMR5/75 cells stained with MYCN antibody as the signal and then we looked at the E2F-d2GFP levels of those cells. The MYCN protein distribution was sliced by intervals of 5%, covering all possible MYCN levels using a custom in-house script in FlowJo (Figure 12 left panel). The median values from the obtained distributions after slicing were computed for from the E2F promoter construct and plotted against the median MYCN levels as shown in Figure 12 (right panel). The E2F promoter construct values were normalized to 1 to allow the behavior to be comparable between MYCN-high and low cells. Each point in the dose response curve was mapped to the cell cycle phase using the median values for DNA content. Hill equation was fitted to the data using the least squares method. Interestingly, MYCN-high cells exhibited hyperbolic behavior, typically found in Michaelis-Menten type systems and denoted here by hill coefficient of 1. In contrast, MYCN-low cells showed ultransensitive behavior with hill coefficient of 4, strongly suggesting the existence of a bistable switch as also evindeced by the bimodal

behavior of pRb. Our results suggest that oncogenes might favor crossing of the bistable switches by allowing low input signals to engage directly into the high activation state, in this case the transition from G1 to S phase.

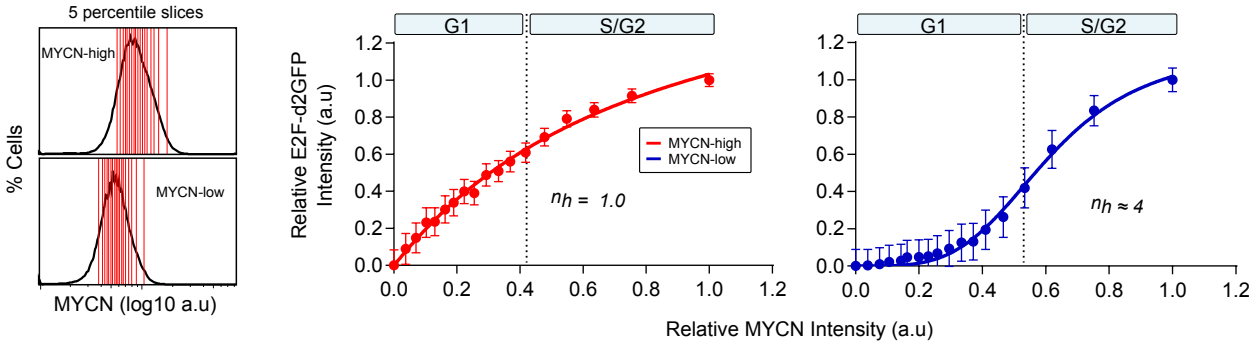

Figure 12 MYCN dose response curve. Left panel: MYCN distributions were sliced by 5% percentiles and the intnsity values were plot against E2F-d2GFP values. Middle panel: MYCN-high dose response exhibits hyperbolic behavior. Right panel: MYCN-low dose response exhibiting sigmodail behavior.

10.2. MYCN drives scape from G0-like state

10.2.1. Cdt1-degron and E2F1-d2GFP reporters define G1 sub-phases

This indicates that MYCN-high cells are perhaps more sensitive to growth signals that MYCN-low cells. A higher probability to cross the restriction point might be due to relatively faster transition or skipping transiently arrested states such as G0. Up to now, only few markers are available that could describe the arrested states in a population of single cells. For that purpose, the previously generated cell line with the E2F-d2GFP promoter construct was transfected with the Cdt1-degron construct which is a marker for G1 length. The schematic of the constructs is depicted in Figure 14A. The Cdt1-degron construct has a Cdt1 fragment that contains a SKP2 degradation site. An example of a microscopic trajectory for Cdt1-degron and E2F-d2GFP dynamics is show in Figure 14B. At the beginning of the cell cycle or birth, the cells are colorless but once cells enter in G1, Cdt1-degron begins to accumulate. Interestingly, this particular MYCN-low cell exhibit higher Cdt1-degron intensity. Previous reports have shown that this might be a proxy for G0 arrest. As for the case of E2F-d2GFP, the patterns look similar between

MYCN-high and low cells with the difference that MYCN-high cells exhibit a higher promoter activity as previously found with the FACS data.

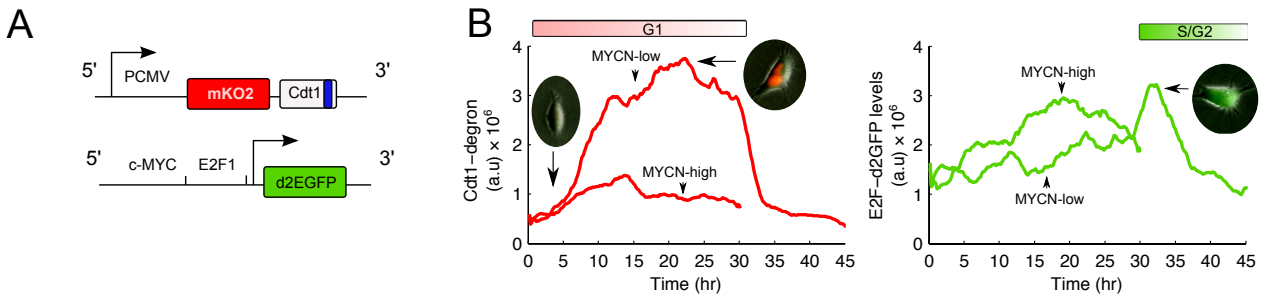

Figure 13 Reporters Cdt1-degron and E2F-d2GFP used to characterized G1 in neuroblastoma cells. A). Schematic representation of the plasmids used. In blue it is indicated the SKP2 recognition site for the Cdt1-degron reporter. E2F-d2GFP reporter scheme with c-MYC and E2F1 biding sites. B) Example trajectories which each of the reporters.

10.2.2. Validation of cell cycle reporters

Since the description of the initial constructs, no proper validation was carried out at the molecular level, for example, correlating promoter activity with mRNA levels or SKP2 levels vs Cdt1-degron levels. To resolve this issue constructs, we performed live cell sorting in E2F-d2GFP cells stained with Vibrant violet dye for live DNA content. Populations were sorted by both GFP level and cell cycle phase. Quantitative PCR measurements for several genes including E2F1 (Figure 15) revealed that the promoter construct reflects the actual gene expression of E2F1 native mRNA (Figure 14A right panel). In a similar fashion, the Cdt1-degron anti-correlates with the protein levels of SKP2 measured by FACS, as expected by its SKP2 degradation site. Thus, we could assume that the reporter constructs are good proxies for E2F1 mRNA and SKP2 activity.

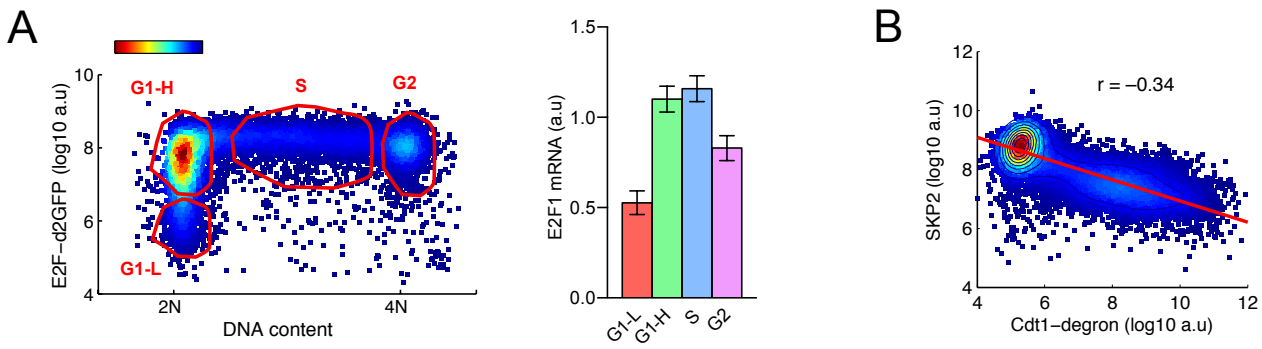

Figure 14 Validation of the reporters. A). E2F-d2GFP vs DNA content plot used to sort populations for qPCR measurements. Middle panel: Shows relative mRNA levels from the sorted populations for E2F1 gene in MYCN-high cells as an example. B) Co-staining of SKP2 and Cdt1-degron showing anti-correlation.

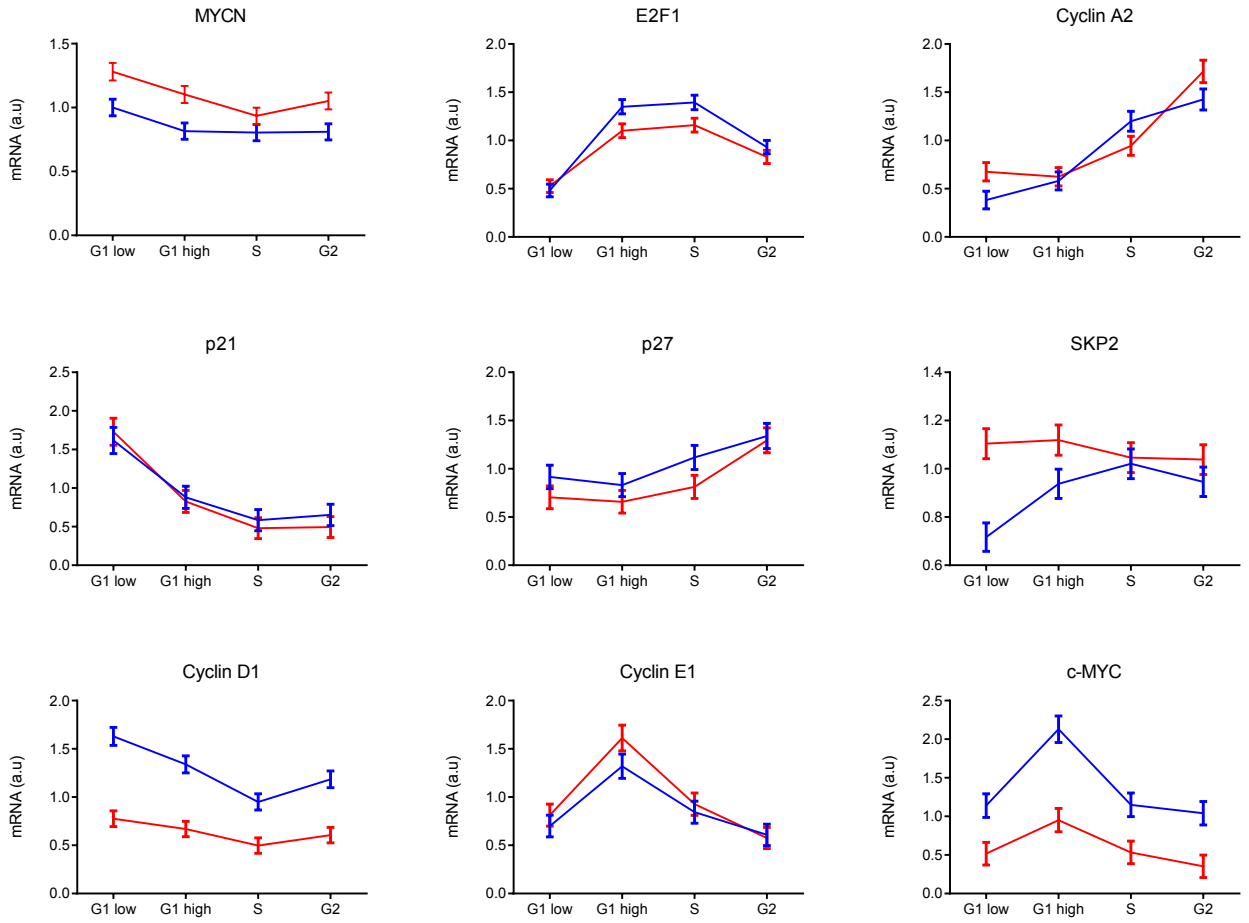

Figure 15 qPCR measurements of additional mRNAs involved in cell cycle regulation. Here is shown in blue the MYCN-low cells and in red MYCN-high cells. The data comes from the previously E2F vs DNA sorted cells. **(**Data generated in collaboration with Tatjana Ryl)

The sorting approach based on cell cycle markers turned to be a valuable tool for evaluating the expression genes in a cell cycle dependent manner. This prototype experiment helped to develop the sorting-RNAseq protocol employed in this thesis. This initial mRNA measurements from sorted cells exhibited interesting patterns. As expected Cyclin A2 rise up in S phase opposite to p21 levels, as expected for normal proliferating cells. Interestingly for SKP2, MYCN-high cells exhibit a constant increase in the levels contrary to MYCN-low cells where it only increased in S phase. Cyclin E is another textbook example where only expression was observed in G1. Cyclin D1 seems more counterintuitive since the levels are reduced in MYCN-high cells but higher in MYCN-low cells. These results might suggest that Cyclin D1 might not be crucial for proliferation in this particular cell type.

10.2.3. MYCN reduction leads to increased Cdt1-degron levels

The single cell trace showed in Figure 13 for MYCN-low showed an increased in Cdt1-degron levels. Additional cells (7 for each condition) were manually tracked and the levels for Cdt1-degron are visualized in Figure 16. A heatmap was created based on intensity levels as shown in the example of Figure 16 (right panel). The first 7 cells are MYCN-high and the remaining ones MYCN-low.

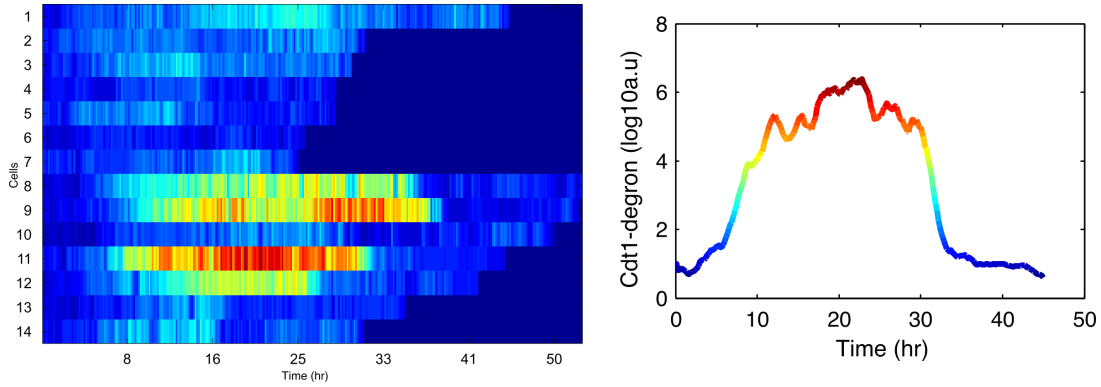

Figure 16 Heatmap representation of Cdt1-degron microscopy trajectories. Left panel: First 7 cells are MYCN-high and the others are MYCN-low cells. Right panel: Representation of the color scheme used on the trajectory to draw the heatmap.

The overall trend is that MYCN-low cells seem to have higher amounts of Cdt1 and therefore longer G1 lengths. The accumulation of Cdt1-degron is interesting as it might indicate that SKP2 function is affected as also shown with the mRNA measurements from sorted cells. However, manual tracking of cells is tedious in IMR5/75 cells since they tend to form clusters, therefore selecting cell boundaries becomes extremely difficult. Future experiments involving CYTOO chips with micro patterns will be an interesting alternative to generate microscopy trajectories and follow progenies in IMR5/75 cells. Even though the sample is small, some cells seem to have additional interesting behaviors. Cell 10 for example has a long cell cycle but fails to increase Cdt1 levels. Cell 1 has as well a long cell cycle as well and classified as MYCN-high but did not increase Cdt1 as well. Even though the heatmap visualization is informative, certain patterns might be not clearly visualized due to the different lengths of the trajectories. One option is to align the trajectories to the universal time. The universal time is

computed as the geodesic distance between two points in the trajectory and calculates the velocity on them. This adjust the “normal” time correcting for shifts and aligning trajectories to identify patterns. As shown in Figure 17, the computed trajectories are then aligned in the Universal time axis. As expected Cdt1-degron signals increased mostly at the beginning as expected for being a G1 marker. E2F-d2GFP starts in later time points and rise up (around 0.5 Universal time) when most of Cdt1-degron signals are stating to drop. An interesting observation is that MYCN-low signals as observed in the previous heatmap do increase in intensity as compared to MYCN-high signals.

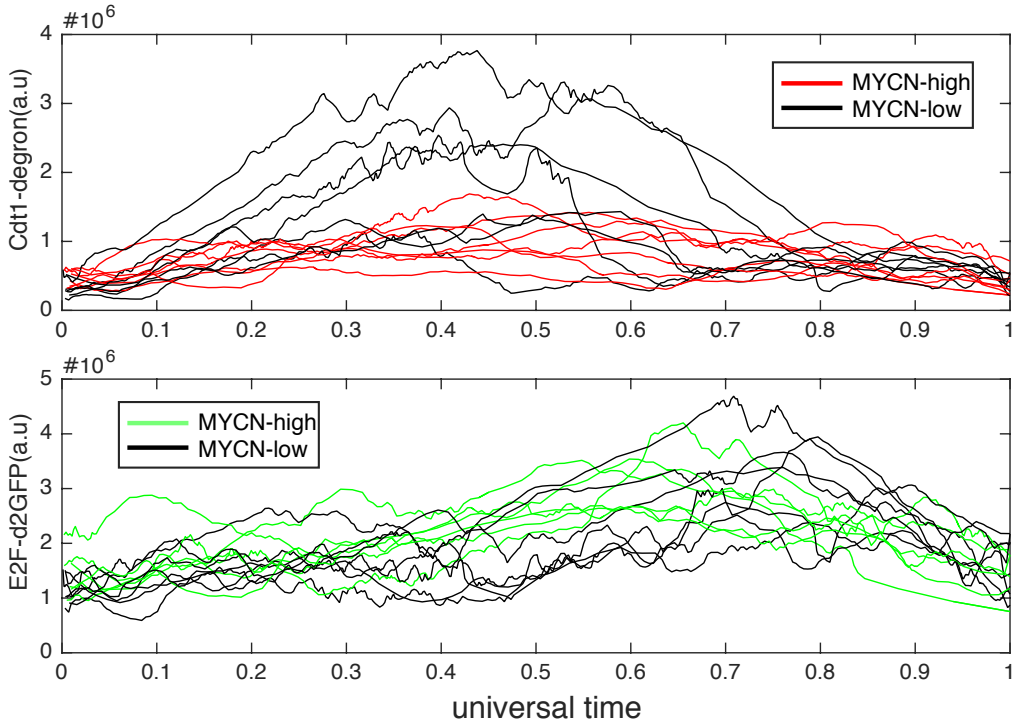

Figure 17 Universal time calculation on microscopy trajectories. (Analysis performed in collaboration with Laleh Haghverdi).

However as for the case of E2F-GFP in MYCN-low cells the behavior reveals some interesting features. It does seem as if E2F1 promoter activity has a relatively small increase, which later stabilizes for the case of MYCN-low cells but for the MYCN-high cells continues in increase. This suggest that perhaps MYCN-low cells enter cell cycle with the machinery necessary to enter commitment and perhaps make an attempt to enter into cell cycle but additional factors promotes delay leading to reduction again of

E2F promoter activity concomitantly with a continue increase of Cdt1-degron. This is later fixed by a newly increase in E2F promoter activity. Another interesting point is that the decision appears to be very fast at the beginning of the cell cycle since MYCN-high cells do not continue increasing Cdt1-degron. This might suggest than an early activity of SKP2 is necessary for degrading inhibitors that might halt cells in the cell cycle.

10.2.4. G0-like state is identified by combination of Cdt1-degron and E2F-d2GFP reporters

Since the number of microscopy trajectories is limited, the further experiments were focused on single cell data in the context of the whole population such as data obtained by FACS. Initial measurements of E2F-d2GFP vs Cdt1-degron in 3 biological replicates revealed a strong difference in MYCN-low cells (Figure 18). In this experiment, cells were gated in G1 using DNA content and the gating approach applied previously. The data shows that cell cycle starts with low Cdt1 and E2F as shown previously in the microscopy trajectories. There seem to be an increase in both signals as cells progress in G1 with a decrese in E2F promoter activity followed by a continuous increase in Cdt1-degron level. This last population seems to appear in both MYCN-high and MYCN-low cells. Interestingly, cells in MYCN-low condition tend to accumulate strongly in this region. This finding strongly correlates with the high Cdt1-degron levels observed in microscopy trajectories in MYCN-low cells.

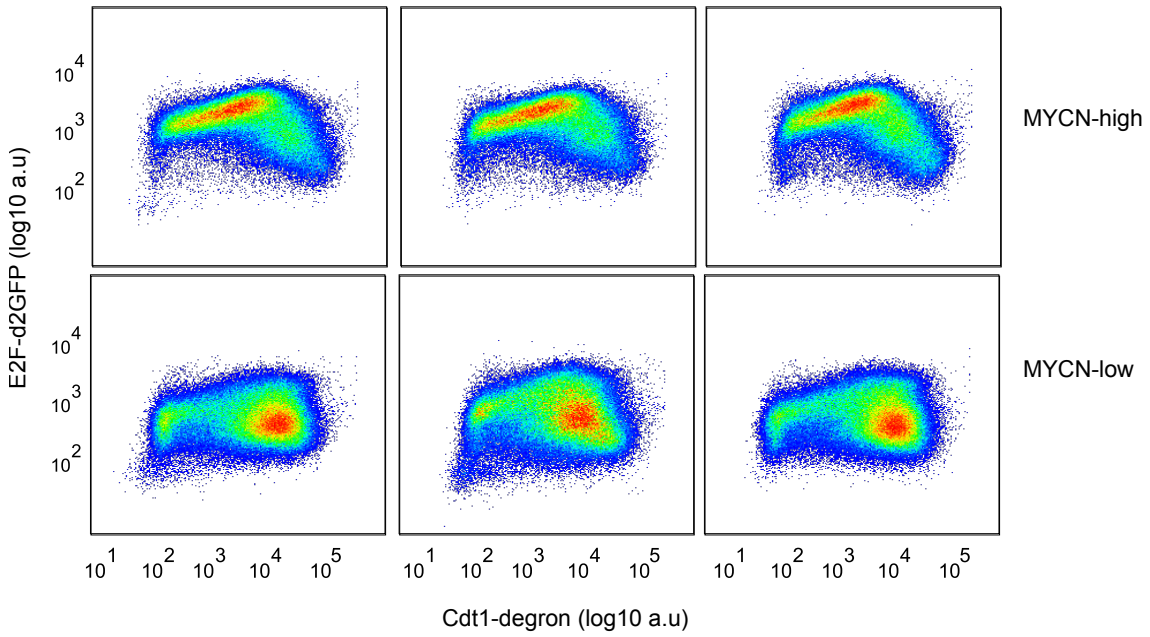

Figure 18 E2F-d2GFP vs Cdt1-degron measurements by FACS. The results indicate 3 different biological replicates in MYCN-high/low condition.

To evaluate if there was a significant difference in the G1 populations, we applied a Expectation-Maximization (EM) algorithm to the gate samples. In this analysis all cells were included and not exclusively G1. This method was implemented in the package Wanderlust (Bendall, Davis et al. 2014) and runs in the Matlab platform. The gating (clustering) method is an iterative algorithm that attempts to find the maximum likelihood of a gaussian mixture model. The clustering algorithm was applied with different number of expected populations (up to 10). Interestingly the algorithm converged to 4 specific populations as shown in Figure 19B. This correlates with the density probability estimation shown by the contours in Figure 19A. To facilitate the reference to this populations, some arbitrary names were given such as G1 early for the initial Cdt1-degron and E2F promoter activity boost, the more steady increase named G1 late, the strong E2F promoter levels and Cdt1-degron negative population as S/G2 and the population with extreme high Cdt1-degron levels and negative E2F promoter activity as G0-like. The names are giving based on the temporal pattern observed in microscopy, however it is important to mention that the names in this data do not attribute any temporal properties since it is a snapshot measurement on a steady state population.

The G0-like term was coined from the previous work from (Spencer, Cappell et al. 2013). In the study, G0-like referred to the state where cells transiently arrest before resuming entry into cell cycle, which seems to be the case after MYCN reduction.

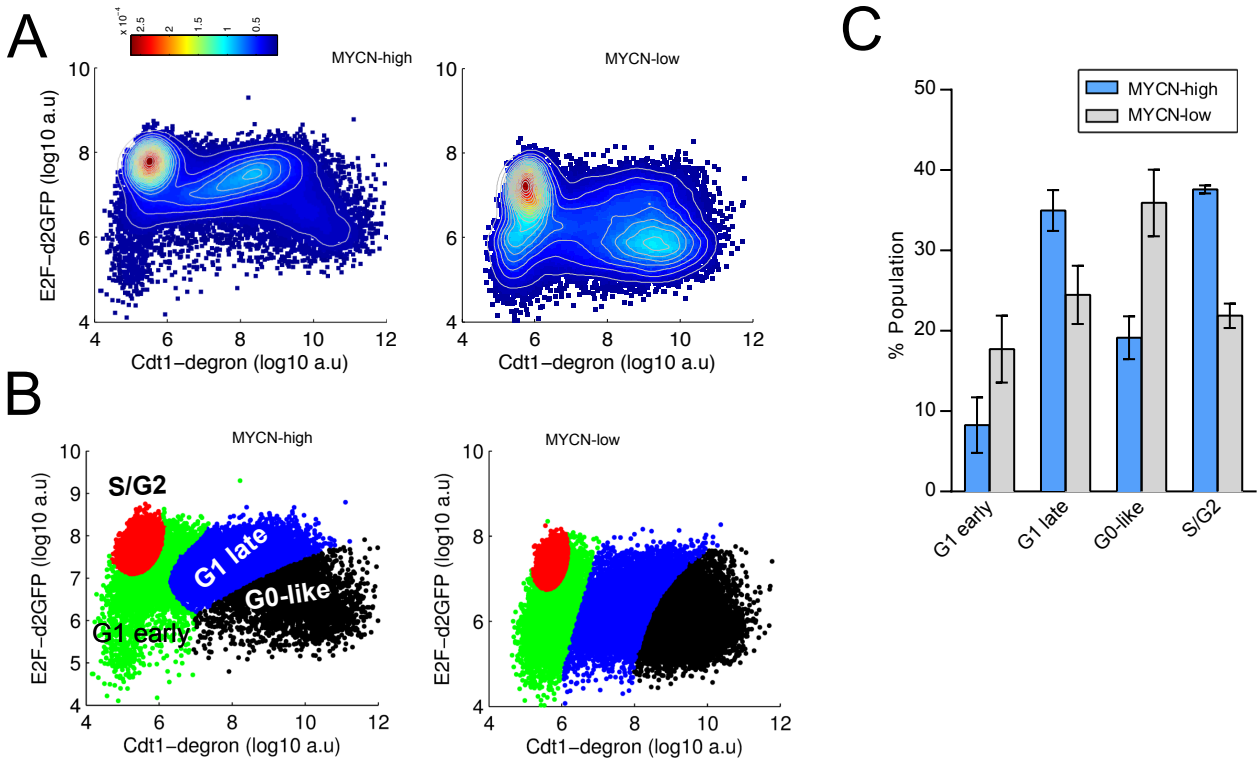

Figure 19 Definition of the populations in G1. A) Probability density plot of MYCN-high/low cells. B) Calculation of gates using the EM algorithm (see text for details). C) Proportion of cells calculated from the gating strategy.

10.2.5. G0-like state is transient and reversible

Proportions of the gated populations detected by the algorithm demonstrate that the G0-like population is significantly higher in MYCN-low as observed previously by visual inspection. Interestingly it seems that cells in G1 early also strongly accumulate in MYCN-low cells, being only G1 late and S/G2 the populations were MYCN-high cells accumulate. This indicates that after MYCN reduction cells might enter a transient state probably due to lack of mitogenic signals which is perhaps solved after a certain specific

amount of time. To test if the G0-like state was really a transient state, again analysies of the microscopy trajectories were performed. The rate of change of Cdt1-degron and E2F promoter activity was measured and plot it using the quiver function in matlab as shown in Figure 20. The arrows indicate the velocity of the particular point and the direction that the trajectory takes in the space. Contour plots were drawn to illustrate the areas where high density of points were observed, this with the purpose of detecting arrested transient states. Interestingly, the traces indicate that MYCN-low cells and perhaps some MYCN-high cells do reduce velocity of progression in the area defined as G0-like state. After certain amount of time cells seem to resume cell cycle by increase in E2F promoter activity and degradation of the Cdt1-degron.

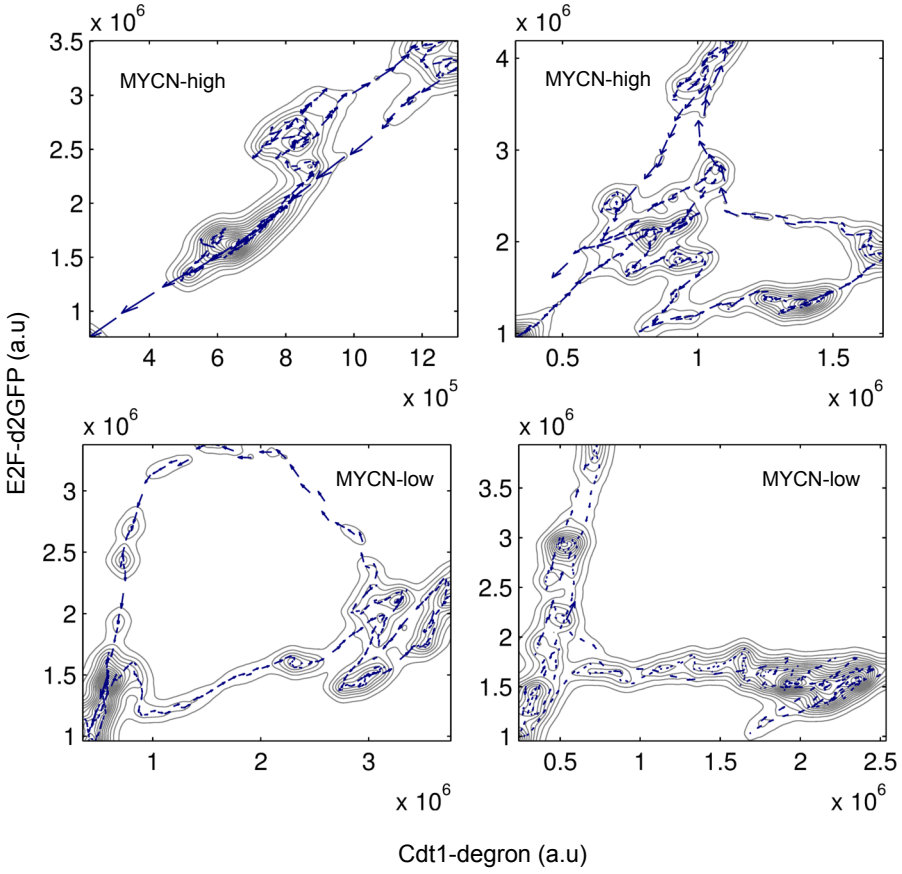

Figure 20. Microscopy trajectories represented as velocity vectors. The derivatives of each time point were calculated with the size of the arrow representing the velocity and the contour plot the density of time points.

Therefore it is a safe assumption to catalogue the G0-like cells as transient state where cells slow down in cell cycle progression but that eventually is resumed leading to cell cycle division. It is possible that since the microscopy trajectories are limited some cells might be arrested for longer or permanently arrested not being able to generate proliferating progeny. To test for this, cells were sorted from the S/G2 and G0-like populations into 96 well plates and let grow for around 3 weeks. Colonies were counted by microscopic inspection and the average number is show in Figure 21. The S/G2 population was used as control of proliferating cells and G0-like cells to test for the ability to produce colonies. Other populations could be sorted, such as the G1 early and G1 late however the growth profiles of these populations could give somewhat mixed results since probably there is where the entry in G0-like is decided. Future experiments should be done to test these 2 additional populations.

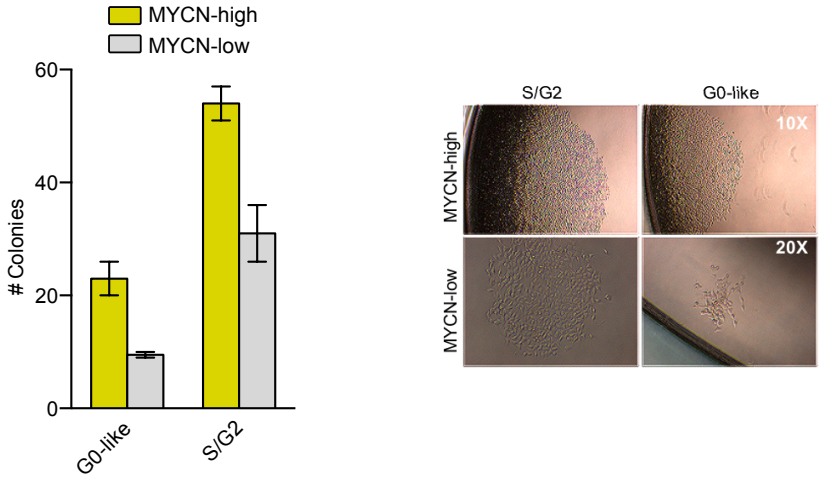

Figure 21 Cell sorting outgrowth from S/G2 and G0-like populations. Left panel: Average number of colonies counted for all conditions. Right panel: Microscopy pictures of some example colonies.

Colony counting shows (Figure 21 left panel) that G0-like cells are capable of generating colonies either in MYCN-high or low condition. Interestingly enough the colonies generated by the G0-like cells coming from MYCN-high cells are larger in number. This could indicate that MYCN-high cells in G0-like state have some “advantage” that allows faster proliferation, perhaps the levels of MYCN itself. S/G2 colonies are still lower in MYCN-low cells but this might due to some cells from that population entering the G0-like state. An aspect that might also play a role is the inheritance from the previous cell

cycle could also explain why the G0-like state cells either with MYCN or not do not repopulate at the same proportion as the S/G2 cells. However to strongly verify ths point which is in theory interesting, is to collect more microscopy trajectories and perform lineage analysis.

One of the advantages of the snapshot data is that gives an overview of the cells in the whole population and allows to identify small subpopulations that might be missed by averaging the population or not enough single cell throughput for microscopy trajectories. However the disadvantage is that the dynamics or temporal information will be missing. Early mathematical analysis (Watanabe and Okada 1967) has shown that under certain conditions such as ensuring exponential transitions among the states one could infer temporal properties of the data. For example based on steady state data such as DNA content proportions and using the doubling time one could simply estimate the time spent in each of the phases, but it is not a simple proportion since the model takes into account the effects of doubling the population after each division and cell loss. The original model was used for G1, S and G/M populations but here instead we used the proportions discovered by the clustering analysis on the E2F-d2GFP vs Cdt1-degron FACS data. We assumed that populations are in constant transit among states and that cell loss is relatively constant. The results are shown in Figure 22A:

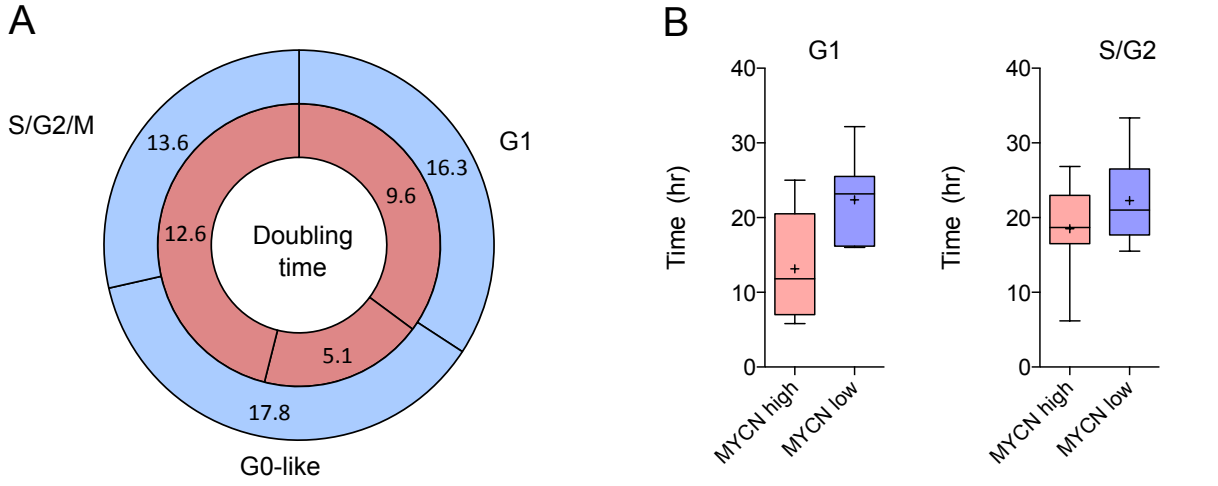

Figure 22 Calculation of G1 and G0-like length. A) Steel formulas were used to calculate the G1, G0-like and S/G2 length based on the proportions determined in Figure 19 and doubling time calculated in Figure 9. B) G1 and S/G2 length calculated from microscopy trajectories.

10.2.6. G0-like state can be induced by mitogen starvation

The calculations revealed that G0-like state in MYCN-low cells could last approximately 20 hrs, which is almost one cell cycle. However G1 (composed here by G1 early and Late) also accounts for an important part of the cell cycle lengthening of around 16 hrs. This could be explained by the accumulation of cells in G1 early as observed in the proportions in Figure 19B. Interestingly G0-like length in MYCN-high cells is very short, of around 5 hrs. This might explain why MYCN-high cells could generate potentially more colonies in the MYCN-high condition.

Together this indicates that cells with high MYCN enter cell cycle faster via skipping the G0-like state. This is tightly connected to the restriction point of the cell cycle. Cells in the mitogen sensitive window respond by increasing E2F levels until the point that the transition becomes irreversible without the need of mitogens. If cells lack enough mitogen signals they enter the quiescence state. The definition of quiescence is somewhat arbitrary as in some cases might indicate a more permanent state. However to test if the G0-like state defined previously is related to the quiescence or G0 state, we performed serum deprivation of the G1-gated IMR5/75 cells and analyzed the behavior of the E2F promoter and Cdt1-degron reporters as shown in Figure 23.

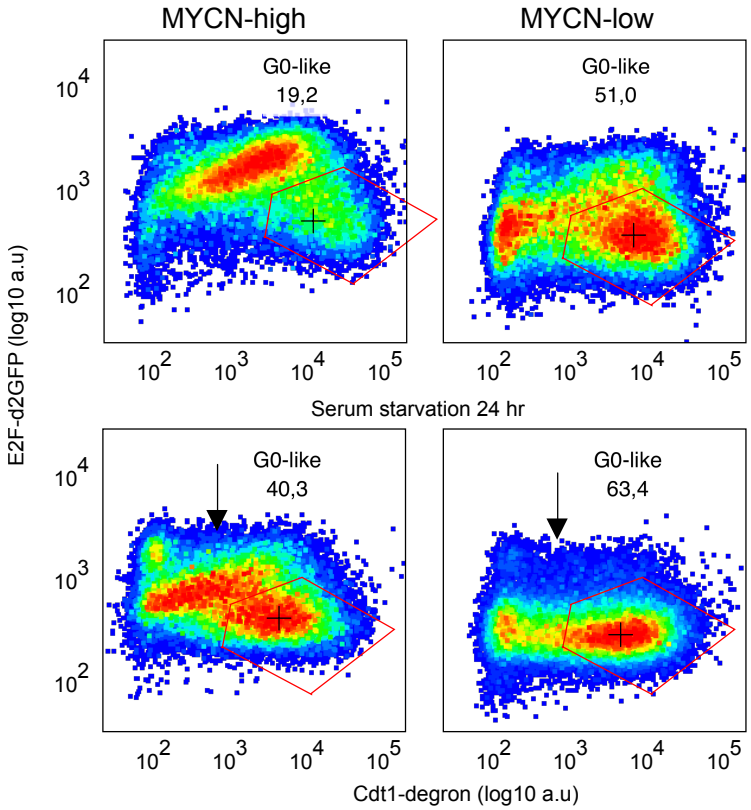

Figure 23 Serum starvation of MYCN-high/low cells. The data represents the increase in G0-like state proportions after complete serum starvation for 24 hr.

Interestingly, the cells indeed accumulated in the G0-like state after 24 hrs of serum deprivation independently of the status of MYCN. Around 20% more were arrested in G0-like for the MYCN-high condition and almost 10% more for the MYCN-low case. However the treatment also strongly affected G1 early and late E2F promoter activity. This shows that a stronger effect in the mitogen signal abrogates even the intial E2F boost in G1 early and late. This effect is more pronounced in the MYCN-low situation. Perhaps one mechanism that could explain the data is defining the G0-like state as an endpoint phenotype where cells arrive after not fulfilling the requirements for cell division, but in some cases like in the reduction of MYCN, cells can still enter the G0-like state after making fail attempt with an initial E2F boost.

10.2.7. G0-like state is unresponsive to p21 and p27 knockdown

Among the regulators of G0 are the cell cycle inhibitors p21 and p27. Especially p27 acts by inhibiting CDK2 and promoting cell cycle arrest (Sherr 1996). On the other hand p21 seems to be involved in cell cycle arrest after DNA damage (Gartel, Ye et al. 2001). However the quiescence CDK2 reporter study (Spencer, Cappell et al. 2013) showed that cells could still be arrested in G0-like via specifically p21 induction. To evaluate if either p21 or p27 are involved in the regulation or maintenance of the G0-like state, siRNA inhibition was performed by liposomal transfection with different siRNA doses. The results for 10μM treatment are shown in Figure 24.

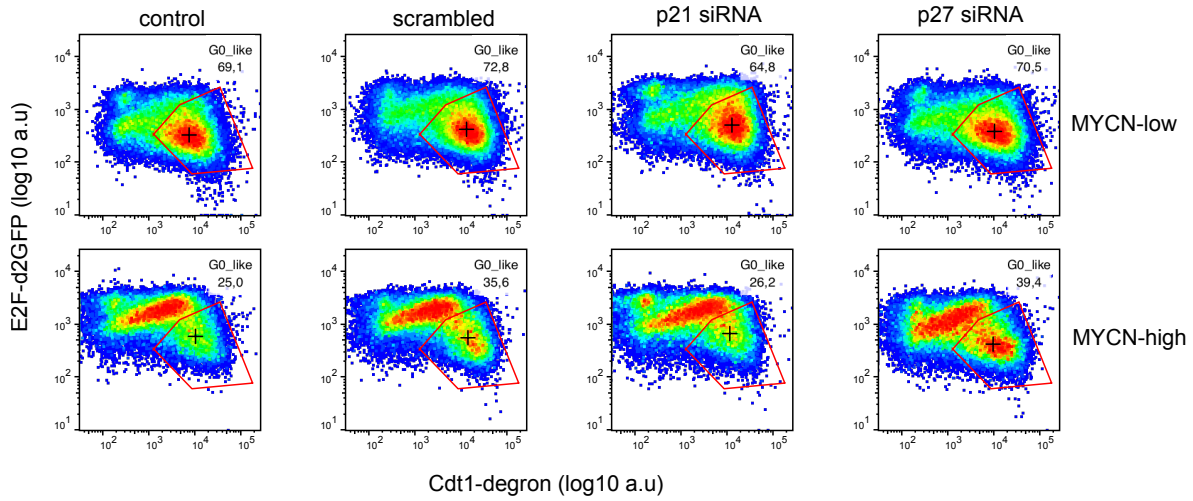

Figure 24 siRNA knockdown of p21 and p27 in MYCN-high/lowc cells. Control cells represent cells treated with lipofectamine. Scrambled are cells treated with unspecific siRNAs. The p21 and p27 siRNAs were used at a concentration of 10 μM for 48 hrs.

Surprisingly p21 and p27 inhibition did not influence the proportion of cells in the G0-like state. This come as surprise since those are the classical inhibitors associated with the G0 phenotype. However one possibility is that some cells might not require the same set of inhibitors to control cell cycle regulation as pointed out in (Spencer, Cappell et al. 2013). To test if p57, which is a stronger inhibitor of cell cycle (Matsuoka, Edwards et al. 1995), was involved, we performed protein staining in IMR5/75 cells and p57 distributions were gated by cell cycle phase (Figure 25).

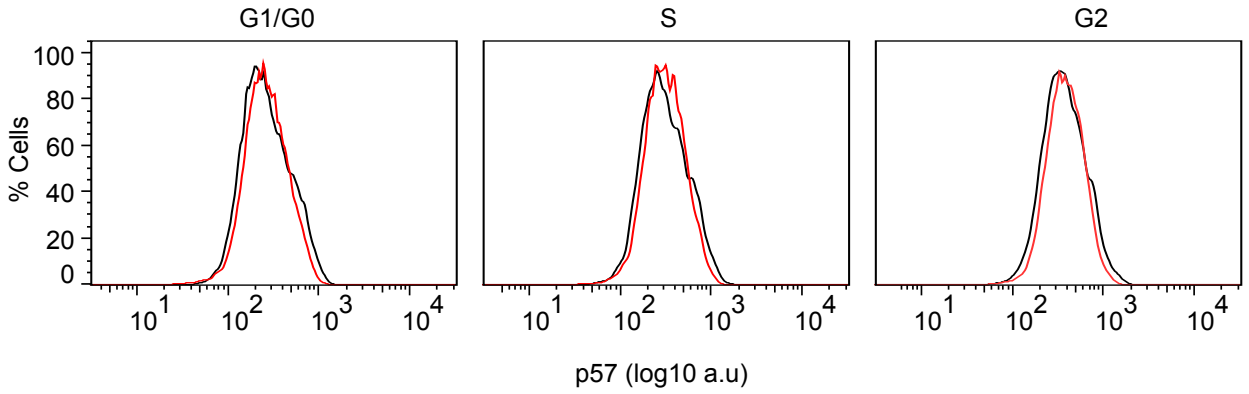

Figure 25 p57 stainings of MYCN-high/low cells.

p57 levels remained unchanged in all cell cycle phases and independently of MYCN status. The results indicate that there might other potential regulators of the G0-like state, which do not necessarily involve the classical cell cycle inhibitors.

10.2.8. G0-like state can be identified in other cell systems

Together, the data shows that the system Cdt1-degron and E2F-d2GFP in combination allows a very complete description of all cell cycle phases and G1 sub phases present in in amplified neuroblastoma cells. The novelty relies on the ability to detect the G0-like state, which is strongly affected by MYCN reduction. Serum starvation experiments indicate that the G0-like state is driven by mitogen signaling which strongly suggests that the system developed here allows accurate monitoring of the transition through the restriction point. However it is useful to validate the system in other cell types to confirm if the G0-like state can still be detected independently of the cell system. To accomplish that task, the reporters were also transfected into HeLA cell line. This particular cell system is interesting since Rb and p53 are inactivated by the papilloma virus infection (Giacinti and Giordano 2006). This explains the fast growth rate of this cell line. The data from all cell cycle phases is shown in Figure 26. As expected, the cells do exhibit increase in E2F promoter activity and Cdt1-degron levels, but there is complete absence of the G0-like state as confirmed by the measurements in two different clones. This could be an indication of the absence of active Rb, which impedes cell cycle arrest.

Additionally p53 might also play a role, since p21 might not be expressed or remain in low levels.

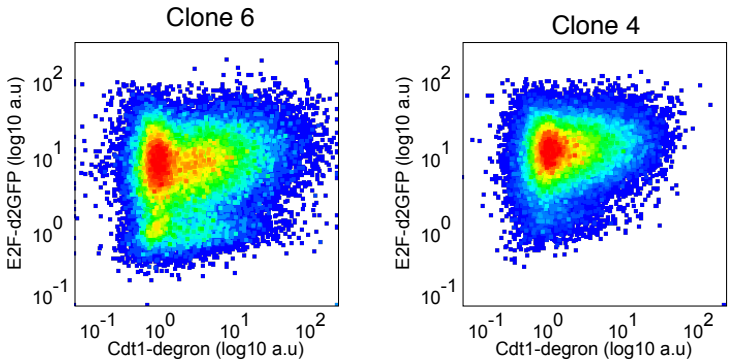

Figure 26 E2F-d2GFP and Cdt1-degron data in HeLa cells. Two different single cell clones were used for comparison

As shown in Figure 11B, Rb phosphorylation correlates with E2F promoter activity in G1. This becomes useful as different cell lines with construct might have antibiotic resistance that could To evaluate if the G0-like state can be detected in another neuroblastoma cell line with no MYCN amplification, the Tet21N cell line was used that carries an inducible MYCN system. As comparison, IMR5/75 Cdt1-degron only were also co-stained with the pRb807/811 antibody. Indeed, the G0-like appeared evident in this combination of markers. Tet21N cells exhibited a higher number of G0-like cells compared to IMR5/75 which could be caused by the sensitivity of this cell line to cell-contact arrest.

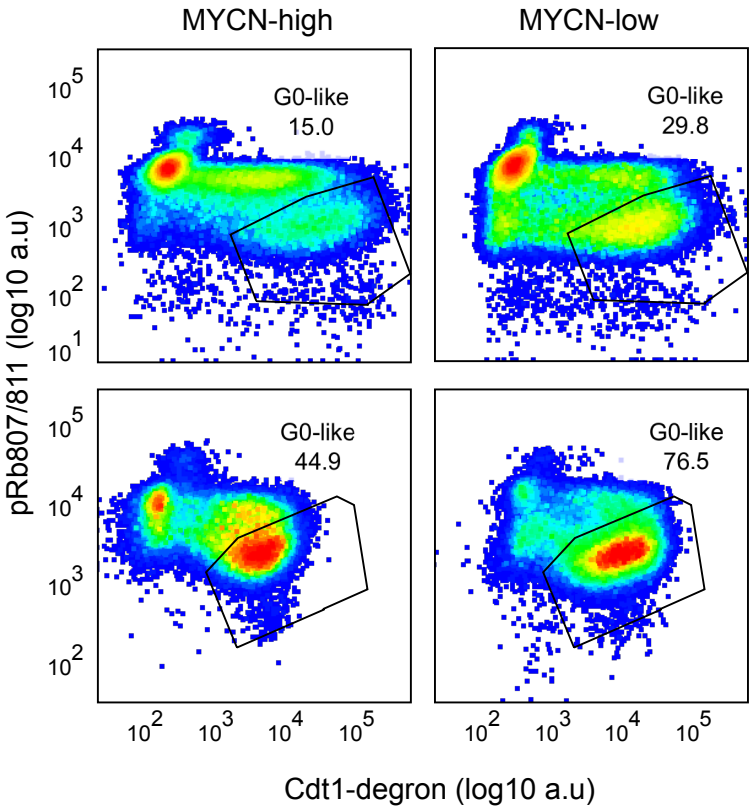

Figure 27 Detection of G0-like state in Tet21N cells. Upper panel: IMR5/75 cells with Cdt1-degron only construct co-stained with pRb807/811. Lower panel: Tet21N cells with same co-staining as IMR5/75 cells.

10.3. Cell cycle regulators promote commitment at G1 early under high levels of MYCN

10.3.1. SKP2 and pRb levels are reset after cell division more strongly in MYC-low cells

These results clearly show that the Cdt1-degron in combination with E2F1 promoter or pRb staining could distinguish the G0-like in other cell systems. Further experiments could include the optimization of the reporters with brighter fluorescent proteins more suitable for microscopy. Of note, the G0-like state when using the pRb staining shows a separation on pRb levels already from the start of the cell cycle. This is an interesting question since it is not known where exactly in G1 that MYCN exerts its proliferative effects. It is probable that MYCN might modulate other cell cycle regulators favoring cell cycle entry and scape from the G0-like state, which could happen either in G1 early or

potentially in G2/M. To address this question other regulators of cell cycle were co-stained with the Cdt1-degron and E2F promoter system. The co-staining was performed in different samples, meaning that each sample with Cdt1-degron, E2F-d2GFP and DNA content was co-stained with an additional protein. This is a limitation and relies in the difficulty of co-staining several proteins on the same cell when lacking antibodies labeled with spectral compatible characteristics. Additionally when using secondary antibodies, species of origin impose a problem since many antibodies are produced usually from mouse or rabbit. However, by using the cell cycle markers as common frame one could in principle compare patterns among different samples preserving some validity since the patters are highly reproducible. One important aspect is to make sure that cells are always in the exponential phase. The results of the stainings are shown in Figure 28:

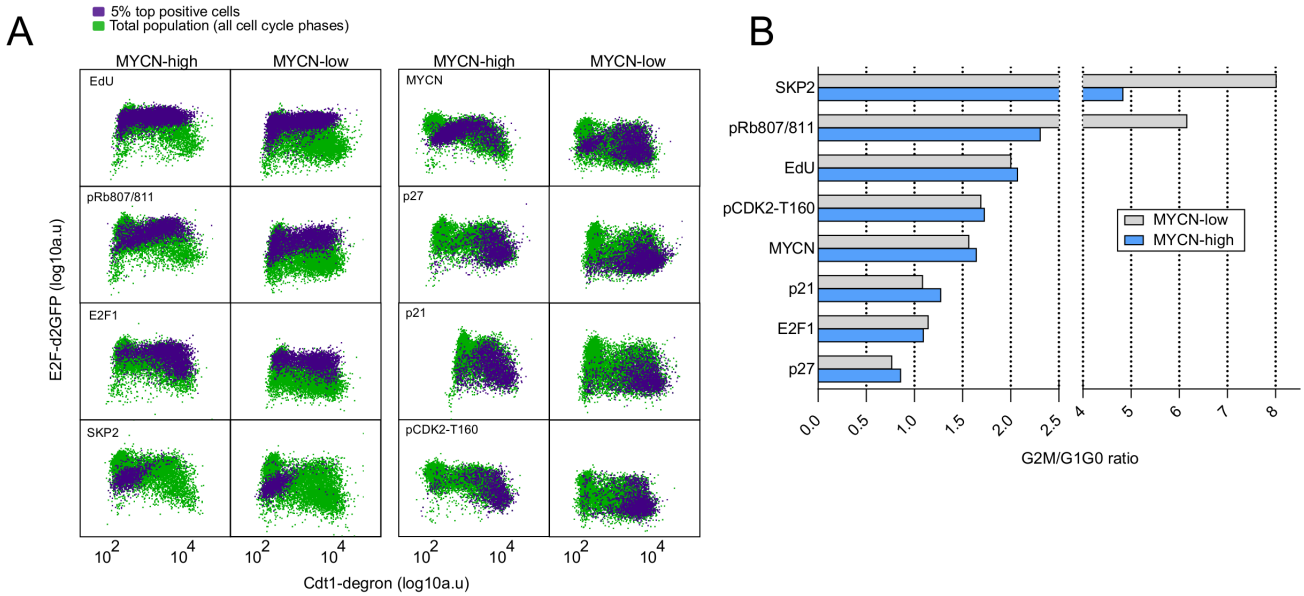

Figure 28 Localization of regulators of cell cycle in the E2F-d2GFP vs Cdt1-degron plot. A) protein stainings were gated by 5% highest intensity population (positive cells) and highlighted on E2F-d2GFP vs Cdt1-degron plot. B) G2M/G1G0 ratio of the different regulators.

The E2F-d2GFP and Cdt1-degron axis is displayed for each of the proteins. To locate where each of the proteins is located in the cell cycle axis, the histograms were segmented by the 5% of the positive populations. This ensures that only positive cells for a particular marker are chosen. The positive cells then are highlighted to find in which cell cycle phase they are clustered. The patterns show some interesting

characteristics. EdU labeling used here as control, shows that active proliferating cells are clustered on the top where the S/G2 region is located and part of the G1 late region. As for pRb, it shows correspondence with EdU staining however active pRb seems to reach the region for G1 early as well. E2F1 protein clusters in the area similarly populated by pRb but in addition seems to be present in the G0-like state. SKP2 on the other hand it is only present in G1 early. For the case of the inhibitors (p21 and p27) they cluster in the G0-like region. However, as shown previously in Figure 24, siRNA knockdown of these inhibitors did not affect significantly the G0-like proportion of cells. pCDK2 which is a marker for active CDK2 and therefore proliferative cells, shows surprisingly clustering in the G0-like area. Lastly, MYCN seems to be populating G1 early region in similar way as SKP2, one of its direct targets. This might suggest that MYCN might prepare cells already in G1 early rather than in G2. Interestingly, G0-like cells do also exhibit accumulation of MYCN, this also comes as surprise since one logical assumption was that G0-like cells could enter this state due to lack of MYCN. Overall, the patterns of the regulators do match with the expected behavior with some interesting exceptions. However there is no an evident difference in patterns regarding to MYCN levels, by simple inspection MYCN-high and low cells do behave similarly. However it is interesting to note that MYCN, pRb and SKP2 levels are higher in G1 early and nearly absent in S/G2. This suggest that the point of commitment might start already very early after birth. To evaluate if G2/M levels could dictate the fate in the following cell cycle, we calculated the median levels of the proteins in G2/M and dividing these values by the ones calculated in G1. In theory, most of proteins if there is no active degradation or dephosphorylation, they should half after division. For example, DNA content is 4N in Mitosis and once cells divide the daughter cells should inherit 2N DNA content. A perfect G2M/G10 ratio would agree with this phenomenon. The results are shown in Figure 28B. As expected, EdU ratio is a perfect 2 and it is identical for MYCN-high or low cells. Interestingly p21 and p27 do not seem to change from the moment of division and the next cell cycle. Strikingly SKP2 and pRb change dramatically in MYCN-low cells indicated here by the ratios of 8 and 6 respectively.

10.3.2. pRb is phosphorylated in MYCN-high cells at the moment of birth

To investigate what is the reason for the high G2M/G10 ratios, the same procedure used to calculate the MYCN dose response curve was applied here to slice the Cdt1 distribution by 5% percentile and look at the distributions of the regulators: pRb, SKP2 and as controls E2F1 protein and p21. As shown in Figure 29, some interesting changes are observed at the moment of birth. In the top left corner, the pRb distributions show distinct behaviors during G1 with respect to MYCN levels. MYCN-low cells (on the right) exhibit a bimodal behavior with pronounced amount of pRb negative cells. The behavior does not change through G1 progression and in the G0-like region (last 7 slices) cells do completely arrest with low pRb levels. As for the case of MYCN-high cells, the cells are mostly shifted to the positive pRb mode, indicating that MYCN-high cells are already committed to cell cycle at the moment of birth. SKP2 also exhibits a similar trend, although less pronounced than pRb, SKP2 seems to be shifted to high levels in MYCN-high context and slightly more SKP2 negative cells in the MYCN-low case.

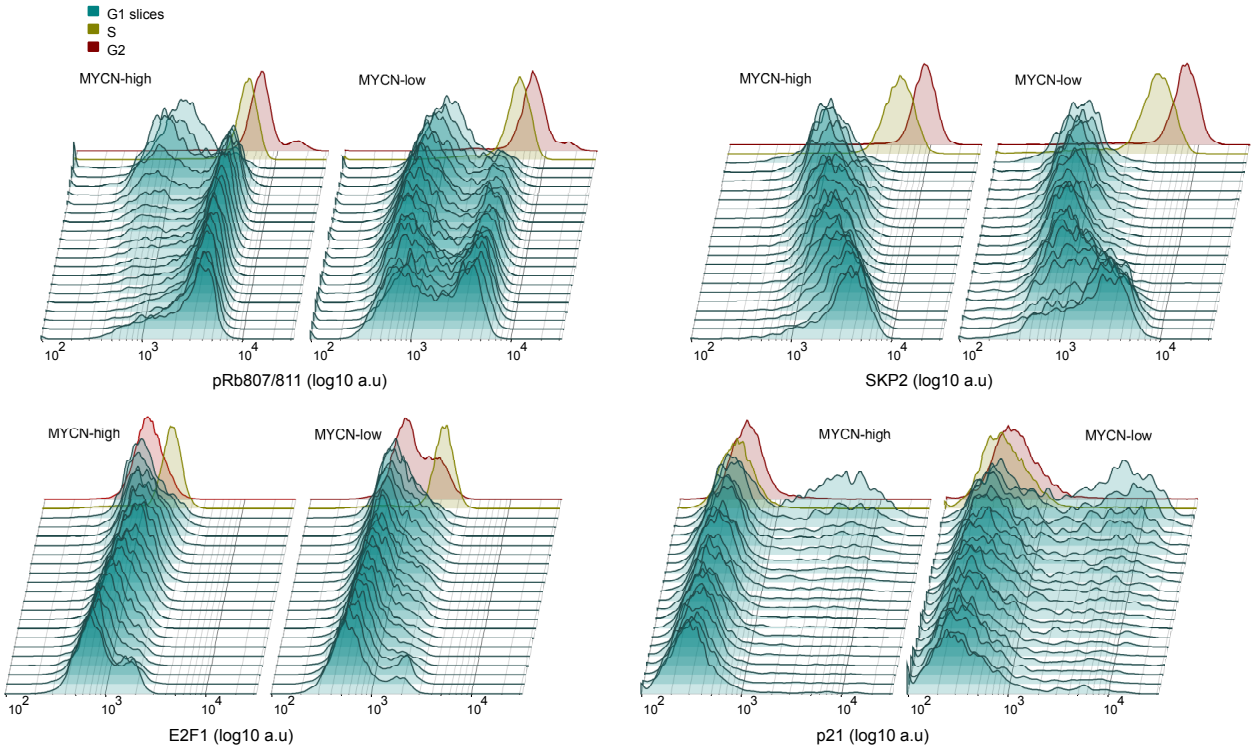

Figure 29 Cdt1 slices and distributions of important cell cycle regulators. Cdt1-degron plot was sliced by 5% percentiles and the distributions for pRb, SKP2, E2F1 and p21 are shown

The S and G2 levels of both pRb and SKP2 remain very similar in MYCN-high and low conditions, so the reason of the change in G2M/G10 ratio might be related to the strong differences in G1 early at the moment of birth. E2F1 and p21 do not show evident changes at the moment of birth, although there is a slight increase in E2F1 positive cells in MYCN-high condition and slightly higher variance in p21 levels. This gives additional evidence excluding the role p21 in driving the G0-like phenotype after MYCN reduction opposed to what it was previously found by (Spencer, Cappell et al. 2013). It is also important to clarify that the levels at S/G2 phases are coming from cells that enter cell cycle, perhaps recovering from the passage through the G0-like state. This suggests that during G1 there might be 2 populations of cells that share an initial trajectory but then it bifurcates into a branch that goes further in S and G2 phases and the remaining branch entering the G0-like state.

Thus, the slicing approach suggest two main findings: 1) pRb and SKP2 are strongly affected in G1 early and this could be the responsible for the cell fate, 2) p21 does not seem to play an important role in the initial commitment.

10.4. Diffusion maps analysis to extract dynamics from snapshot data

10.4.1. Diffusion maps detect a bifurcation in G1 early

The disadvantage of the slicing approach is that it only allows for a visual inspection of the potential changes in the distributions. Therefore a more rigorous mathematical analysis is needed to accurately determine potential bifurcation points, and perhaps infer dynamics from the snapshot data to detect significant changes in the progression of the reporters. As stated earlier in the introduction, dynamics from snapshot data can be extracted under certain assumptions such constant flow among populations with negligible loss rate. To accomplish that task, the Diffusion pseudotime algorithm was used (Haghverdi, Buttner et al. 2016). The previously generated data for each of the cell cycle regulators was used (except EdU data). Around 1000 cells were used for the analysis, and data was log-transformed for the fluorescence channels while leaving the scatters (side and forward) and DNA content as linear. For this type of analysis the main goal is to include as many markers as possible, however as explained above, the stainings were performed 1 per sample separately. To solve that issue, metacells were constructed. The process consists in aligning cells via common markers such as Cdt1-degron and E2F-d2GFP and then proceeds to add all the other markers to create a dataset as if one sample was measured. This procedure allows a more accurate comparison of the markers regarding one particular common axis. Technically, for creating the metacells, we first chose a reference data file, in this case the isotype control which only has the cell cycle markers and no protein stainings. For 1000 randomly chosen cell in the reference file, 3 nearest neighbors were found in the remaining 7 data files using the shared markers (FSC, SSC, Cdt1-degron, E2F-d2GFP, DNA content). The value of the additional protein from each file was taken from those neighboring cells, resulting in n*3 total metacells, each with 5+7 feature measurements.

Once the metacells are created, the starting cell is set from the Cdt1-degron and E2F1-d2GFP plot and then diffusion map calculation follows. The algorithm detects the most likely trajectory the potential bifurcation points. The data can be interpreted as a principal component analysis (PCA) plot where the different markers contribute to the direction of the trajectory. In the Figure 30, both diffusion maps are plot it for the MYCN-high and low conditions. The map is color coded by the DNA content to indicate the direction of the cell cycle progression.

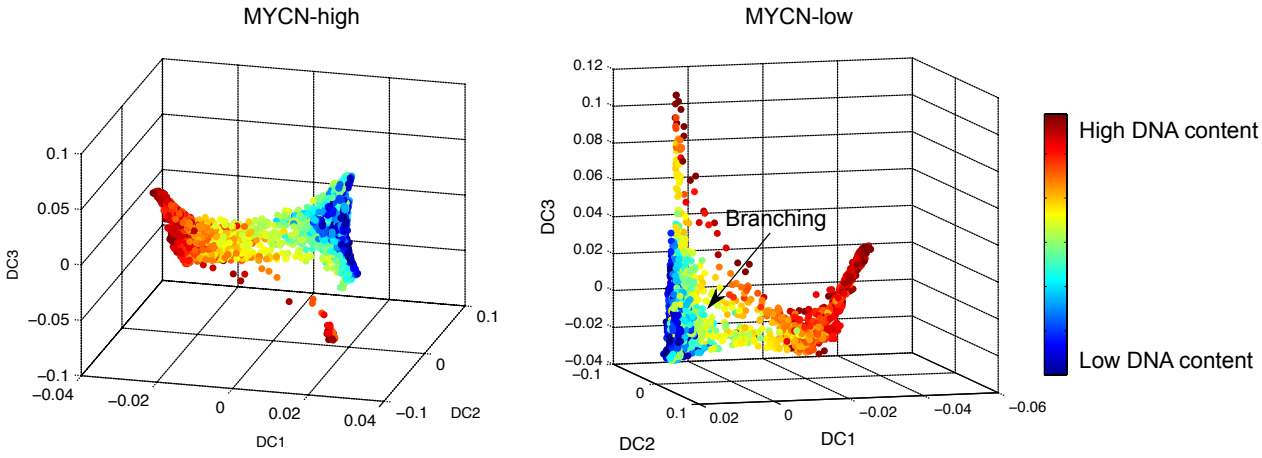

Figure 30 Diffusion maps of metacells constructed from all the different cell cycle regulators. Right panel: Branching point is illustrated in MYCN-low as an example. Color scale is based on DNA content. (Analysis performed in collaboration with Laleh Haghverdi).

The direction of progression starts with the blue area indicating G1 and goes further into the highest DNA content (depicted in red) to the G2/M phase. Interestingly, the diffusion maps exhibit bifurcation at early stage in the progression. The bifurcation is more pronounced in MYCN-low as expected due to the higher density of G0-like population. MYCN-high cells still exhibit a represents the G0-like state. The unbiased detection of the bifurcation point predicts that in fact the entrance into G0-like state might be already defined in G1 early. This confirms the previous assumption based on robust mathematical analysis. Once the diffusion map is calculated, the trajectories for the other proteins can be plot it with respect to the diffusion pseudotime (DPT), which is a random-walk-based distance that is computed based on simple Euclidian distances in the 'diffusion map space'. This measure gives the sense of dynamics of the snapshot

data. As stated earlier, this computational method could provide useful information that is otherwise impossible to obtain experimentally without incurring in artifacts, specially the ones caused by cell cycle synchronization. To confirm the validity of the DPT calculation we first check if the dynamics predicted by DPT reflects the biological set up, we performed plots of the E2F1-d2GFP and Cdt1-degron markers by color coding DPT. Smoothing of the data was performed to obtain the average trajectory. The results in Figure 31 show strong resemblance to the trajectories obtained from microscopy (See Figure 20).

10.4.2. Dynamics extracted from snapshot data correlates with microscopy data

From the dynamical point of view, the analysis also shows that MYCN-low cells spend more time in the G0-like state, which can easily be visualized by looking at DPT values of the trajectory that moves towards the S/G2 area. In MYCN-low cells, this area corresponds to 2000 value of DPT and in MYCN-high to the 1500 DPT value. Another interesting observation is the difference in the slope of the trajectory at the start of the cell cycle. MYCN-high cells do exhibit a steep increase in E2F1-d2GFP values compared to MYCN-low cells. This pattern was previously discussed with the analysis of microscopy trajectories and some trajectories show that cells could generate a fail attempt to increase E2F1 promoter activity and the withdraw from cell cycle entering the G0-like state. However the average trajectory calculated here only indicates that there is not significant increase in E2F promoter activity but only slow accumulation of Cdt1-degron until reaching the G0-like levels. More microscopy trajectories are needed to clarify this point at the single cell dynamics. However it is safe to assume that the trajectories draw from snapshot data is a good representation of the dynamical properties of the system as confirmed with the few microscopy trajectories.

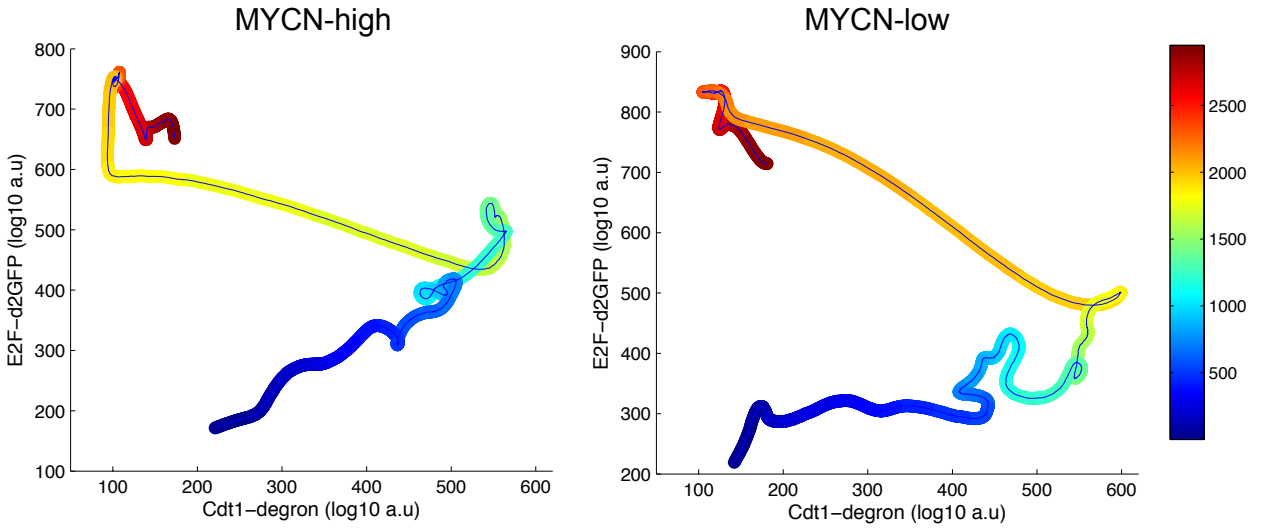

Figure 31 E2F-d2GFP and Cdt1-degron trajectories from snapshot data calculated with DPT. Color scale represents the diffusion pseudotime. (Analysis performed in collaboration with Laleh Haghverdi).

10.4.3. Dynamical analysis revealed E2F1 as an early regulator of cell commitment

Since the algorithm could successfully reproduce the dynamical behavior observed by the cell cycle markrs, it becomes more interesting to evaluate the dynamics of the other protein markers. For that purpose, the protein dynamics extracted from the DPT analysis were plotted as heatmap with prior normalization of the values from 0-1 to render the intensities comparable. The results are shown in Figure 32.

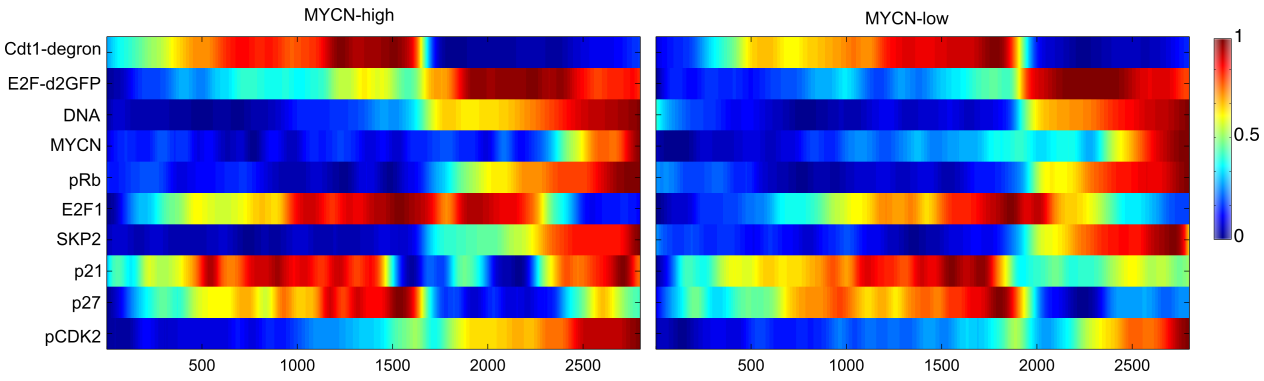

Figure 32 Trajectories of other cell cycle regulators with respect to DPT. Color scale represents normalized intensity of the regulators. (Analysis performed in collaboration with Laleh Haghverdi).

As previously shown with the microscopy data, the Cdt1-degron reporter marks the G1 length. The intensity falls at around 1600 for MYCN-high cells and 2000 for MYCN-low cells. This confirms again the longer G1 length of MYCN-low condition. E2F promoter activity increases after the drop in Cdt1-degron levels and it is mimicked by the DNA content in both conditions. MYCN itself does not seem to increase comparatively in both conditions but only at the end of the cell cycle. E2F1 protein, on the other hand, increases earlier in MYCN-high cells reaching the maximum at around 1000 DPT as compared to 1500 in MYCN-low cells. The other regulators do not seem to differ strongly in the dynamics; only pCDK2 seems to be the highest in G2/M mimicking MYCN levels. pRb and SKP2 did not appeared in this analysis as predominantly up-regulated in G1 early as compared to the slicing analysis. One reason for the discrepancy is intensity normalization was performed to compare all the markers and that could mask the initial boost of some markers. So it is suggested that combination of different analysis is a better alternative for making conclusions of the mechanism.

10.5. Mitogenic signaling cooperates with MYCN to favor cell cycle commitment in G1 early

10.5.1. Common growth factors do not induce proliferation in Neuroblastoma cells

In summary the data suggests that pRb, SKP2 and E2F1 levels are strongly affected in G1 early as revealed by slicing analysis and DPT. Perhaps some initial E2F boost could be present in MYCN-low cells but the data does seem to indicate that the decision is already done at the beginning of the cell cycle. It is still not possible to exclude that some events happening in G2/M might be involved in dictating the differences observed in G1 early. The mechanism of how MYCN can cause alteration of SKP2 and E2F1 could be transcriptional as found previously by others (Bell, Lunec et al. 2007, Bretones, Acosta et al. 2011) and the hyper-phosphorylation of Rb might be due as well to the overexpression of CDK4 (Gogolin, Ehemann et al. 2013). However it is interesting to point out that at least for the neuroblastoma system, the classical cell cycle inhibitors

(p21 and p27) might not be strongly involved in favoring the G0-like state but rather its maintenance. The chain of events could hypothesized as follows: an early Rb phosphorylation via CDK4 could lead to a fast E2F1 activation and promotion of a higher SKP2 boost already present in higher levels and therefore the destruction of some X inhibitor which might be playing the role in favoring the G0-like state, and all of this should be happening at the beginning of the cell cycle. However CDK4 do require Cyclin D1 as partner for activation, so one possibility is that MYCN could cooperate with mitogenic signals to start its early actions and favoring cell cycle commitment. To test this hypothesis, we first did an attempt to identify a single growth factor that could induce neuroblastoma cell growth. The reason is to more specifically track the effects to a particular pathway since serum stimulation is a myriad of different signals with multiple unspecific events. For the experiment, cells were starved for 24 hrs and then stimulated for additional 24 hrs with specific growth factors as shown in Figure 33. Viable attached (left panel) and floating (right panel) cells were counted using FACS.

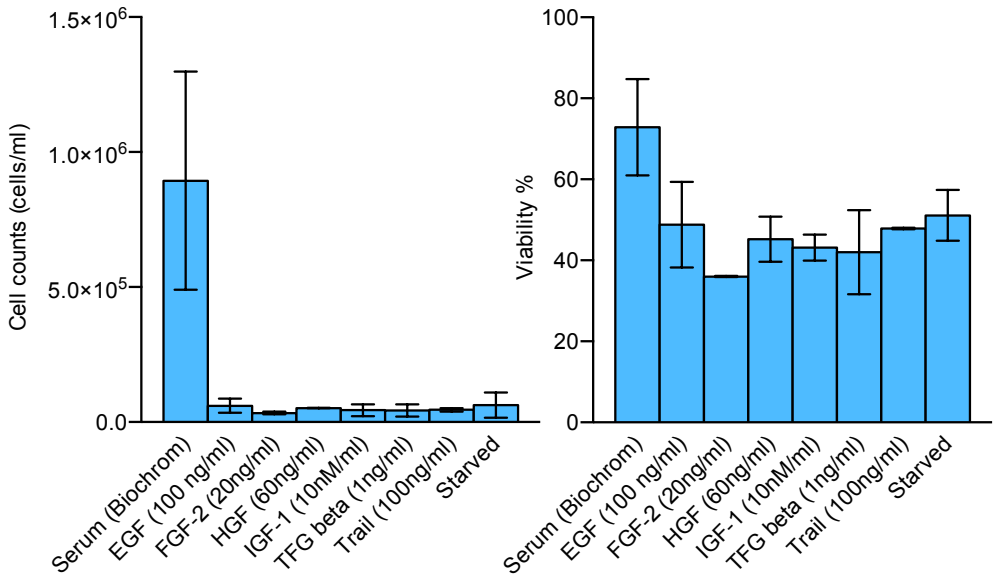

Figure 33 Growth factor stimulation of IMR5/75 cells. Left panel: Attached viable cells counted by FACS after 24hr serum starvation followed by specific growth factor stimulation. Right panel: viable cells from the same experiment in the supernatant.

Surprisingly from the list of growth factors used (in addition to TRAIL and TGF-beta as negative controls) the cells fail to proliferate and the effects were similar to the starvation condition. Of note, for this particular experiment, higher doses of growth factors were given as compared to values published in literature. The negative results might be due to very specific combination of growth factors required by the neuroblastoma cells. Given these results another approach was taken instead, in this case signaling inhibitors were used to test if specific signaling components cooperate with MYCN to favor cell cycle commitment in G1 early

Cells were treated for 30 or 60 min with specific inhibitors in the presence of serum, and the phosphorylation of the target protein was measured by western blot. Titration of different doses on IMR5/75 cells revealed the amount of inhibitor needed to shut down a specific pathway. The inhibitors used were MEK, PI3K, AKT and PDK and as control serum starvation was performed to evaluate the reduction of ERK phosphorylation. (Figure 34)

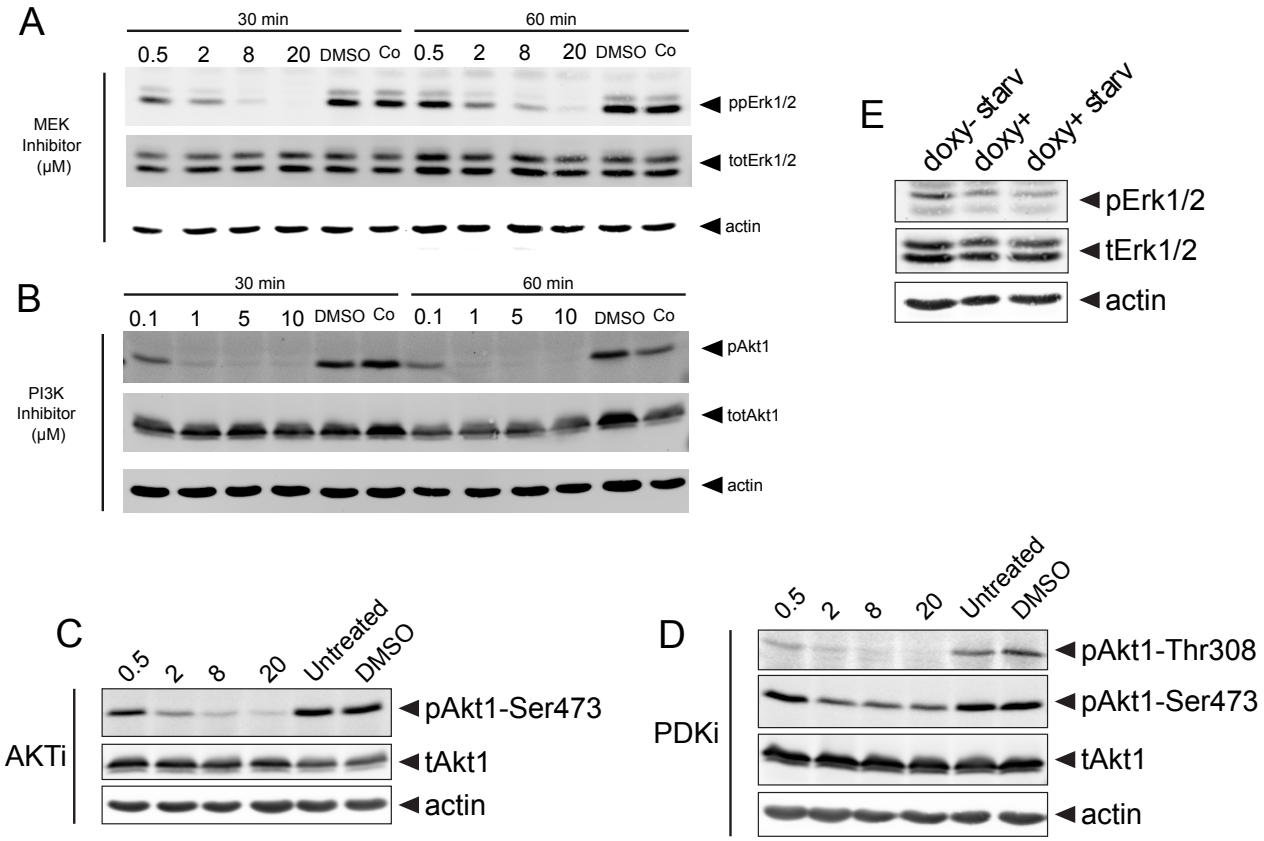

Figure 34 Western blots of phospho proteins involved in MAPK and AKT signaling after inhibitors treatment. A) and B) cells treated with different doses of MEKi and PI3Ki in presence of serum for 30 and 60 min. C) and D) cells treated for 30 min with AKTi and PDKi. E) Serum starvation for 30 min and pERK measurements. (Experiment performed in collaboration with Dmytro Dvornikov).

The results show that in general for most of the inhibitors, the dose needed to shut down the signaling pathway to 50-80% is around 1-4 μM, with the exception of the PDK inhibitor that with 0.5 μM dose was enough to block almost 90% of Akt phosphorylation.

Once identified the dose, a quick experiment was performed to determine toxicity and effects on the cell cycle of MYCN-high cells. Cells were treated with relatively high doses of the inhibitors and E2F-d2GFP and DNA content was measured after 24 hrs and 56 hrs, and results are shown in Figure 35:

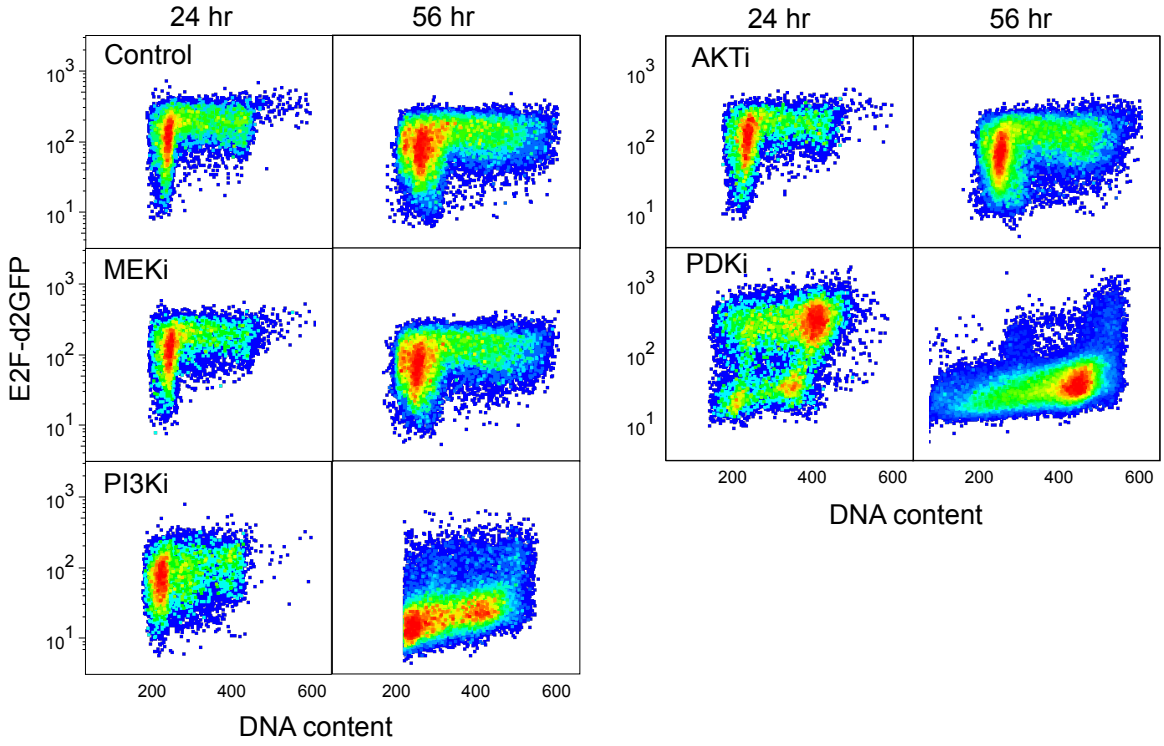

Figure 35 Screen of inhibitors in the E2F-d2GFP cells. Cells were treated for the times shown fixed and stained for DNA content.

10.5.2. MEK inhibition overrides the initial E2F promoter activity in G1 early

The treatments show that MEK and AKT inhibitors do not perturb the qualitative cell cycle pattern in the time points tested in comparison to the control. However, for the PI3Ki and PDKi, strong cell dead was observed together with cell cycle arrest for the surviving cells. PDKi seemed to induce G2 arrest, which became evident at 56 hrs, and for the PI3Ki, the cell cycle arrest occurred at G1 and G2. In both situations, E2F-d2GFP levels were reduced. Even though MEKi and AKTi did not show strong differences in cell cycle, it is still possible that it can G0-like depending on the dose. For that reason, the experiments were repeated with the Cdt1-degron and E2F1-d2GFP cell line by using the MEKi together with E2Fi and CDK4i used here as controls. The purpose was to investigate the effects of this inhibitors in G1 early and the relationship with G0-like state.

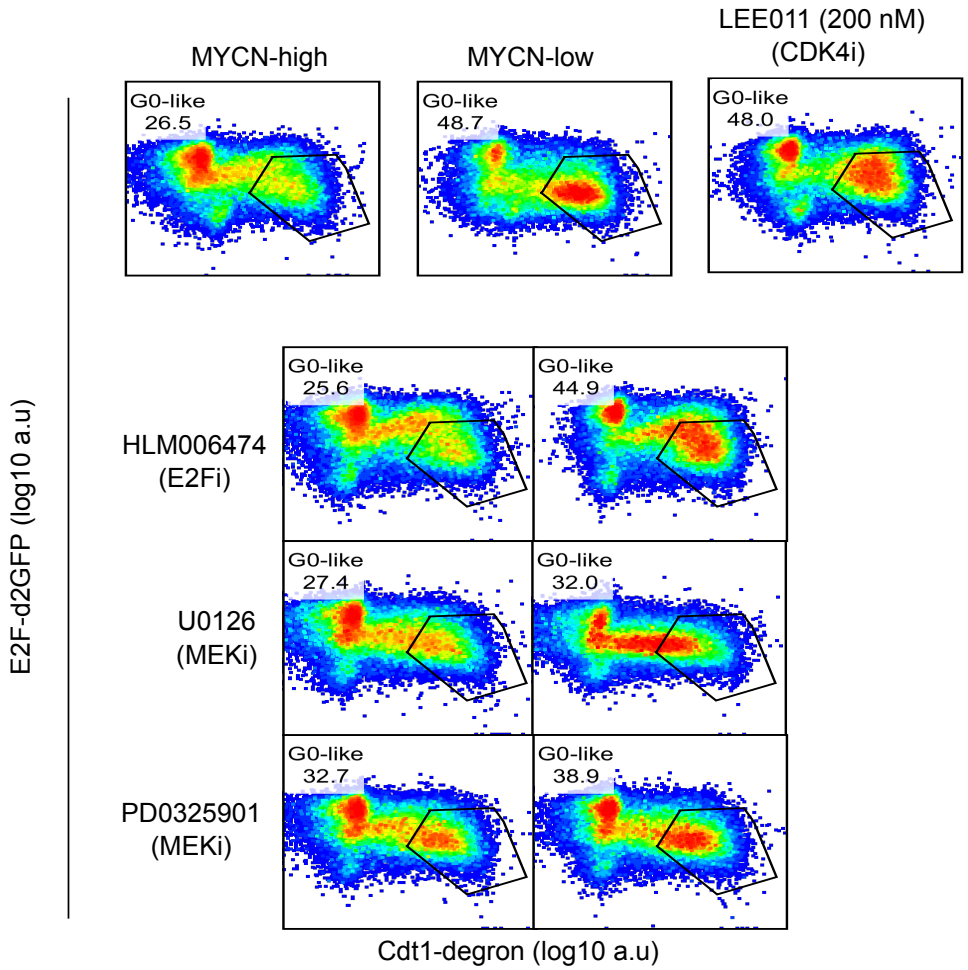

Figure 36 Selected set of inhibitors used to evaluate the G0-like population. Cells were incubated separately for 24 hr with each of the inhibitors shown.

As shown in Figure 36, all the inhibitors tested affected the G0-like population although in different ways. The CDK4i induced a strong G0-like arrest, reproducing the effects caused by MYCN reduction as expected. The E2Fi induced G0-like arrest as expected but interestingly the initial E2F1 boost was preserved in the doses tested. This finding was surprising as it was expected that the E2F1 inhibitor would abolish E2F1 in G1 early as well. Both MEK inhibitors (U0126 and the more recent one PD0325901) did show an interesting pattern. As previously observed with the serum starvation experiment (Figure 23), the inhibitors managed to override the initial E2F boost, so it does seem as if cells do not increase E2F promoter activity and only Cdt1-degron is accumulated reaching the G0-like state. Together this might indicate that mitogen signaling might cooperate

with MYCN scape the G0-like state. As explained in the previous experiments, it is still unclear why MYCN-low cells might have this initial E2F1 boost and still enter G0-like state at least from the trajectories observed and from the snapshot data. However there might be the possibility that the picture for most of the cells is a start in G1 early with no E2F boost and only Cdt1-degron accumulation. In some other cells this initial boost is necessary to scape the G0-like state. It is interesting to speculate that MYCN might provide this initial E2F1 boost that prevents cells to reach the G0-like state. Apparently this initial boost is also not overridden by CDK4 or E2F1 inhibition so there might another control mechanisms driven by mitogenic signaling that might be responsible for the G1 early response.

10.6. Analysis of Gene expression profiles from sorted cells identify key regulators of G0-like state in MYCN-high cells

10.6.1. Sorted cells using cell cycle markers is a better alternative than cell synchronization

To answer this question, RNA sequencing from the different populations was performed. Cells were cultivated under exponential growth, collected, re-suspend it in buffer with RNAse inhibitor to prevent RNA degradation and sorted according to the intensities of the 4 classical populations: G1 early, G1, late, G0-like and S/G2. The dead cells were excluded via TOPRO-3 staining. The same procedure was performed for cells in the MYCN-low condition and the collected cells were snap-frozen in liquid nitrogen for further RNA extraction and sequencing. The gating scheme for the sorting procedure is illustrated in Figure 37. An important aspect to note is that the gates in this case are relatively arbitrary since the clustering algorithm is not available on the sorting machine. For setting the G1 early gate for example, it was important to only gate the populations that are colorless, since cells start to accumulate Cdt1-degron or E2F1-d2GFP relatively fast after cell division as observed in microscopy trajectories. To our knowledge it is the first time that unperturbed cell cycle dependent data is generated in neuroblastoma cells. Especially since previous cell cycle studies only used time courses of chemically

synchronized cells, which was discussed before to be an important source of artifacts. An additional advantage of this type of data is that it allows to compare to previous gene expression profiles obtained for G0 or quiescent cells. The reporters allows direct visualization of the G0-like population in contrast to the CDK2 reporter study where it was only possible to detect the G0-like cells after normalizing nucleus and cytoplasmic intensity therefore not suitable for cell sorting.

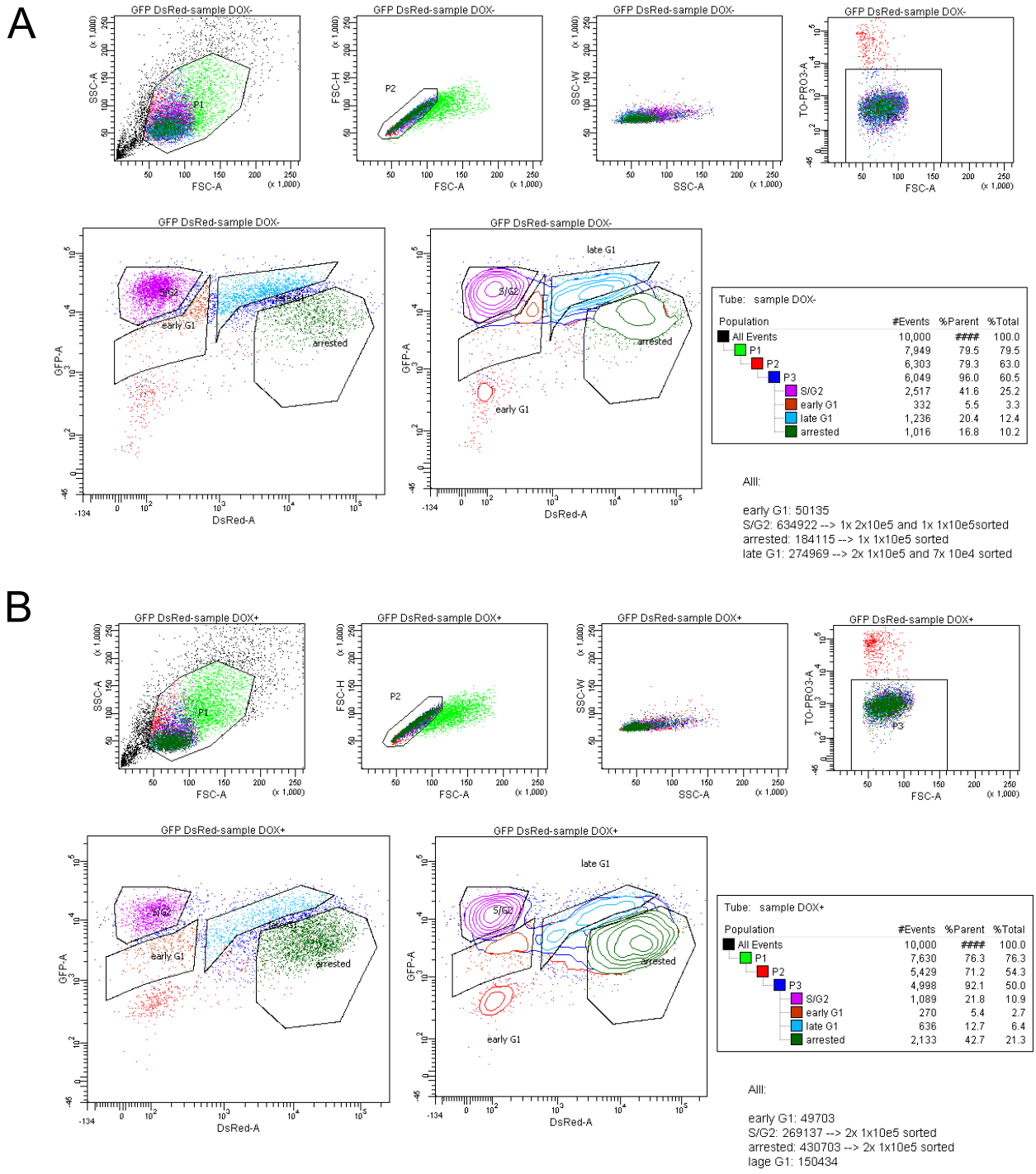

Figure 37 Sorting scheme of Samples used for RNA sequencing. (See text for details).

After data processing (Reads aligning, calculation of expression values) the samples per each population were compared as MYCN-high vs MYCN-low to calculate the

differentially expressed genes. Genes were filtered by 0.1 FDR (false discovery rate) and 0.5 log2 fold change. Around 1119 genes were found to be differentially expressed in G1 early upon reduction of MYCN. This population represents the one with largest number of differentially expressed genes in G1 (Figure 38 A).

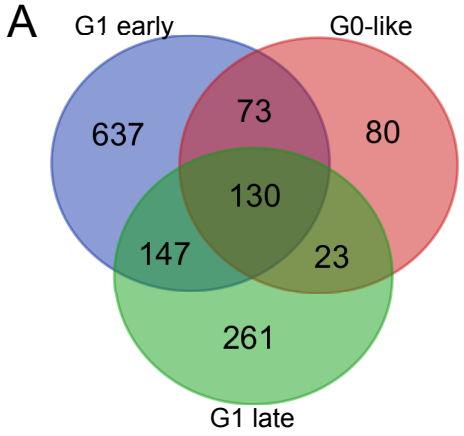

KEGG enrichment unique genes

Population (unique)	KEGG pathway	p-value (Benjamini)
G0-like	Ribosome	≤ 0.05
G1 early	DNA replication, **Mismatch repair**, Ribosome biogenesis, Cell cycle	≤ 0.05

KEGG enrichment all populations

Population	KEGG pathway	p-value (Benjamini)
G1 early	DNA replication, Cell cycle	≤ 0.05
G1 late	PI3K-Akt/MAPK signaling pathway	0.4
G0-like	Pathways in Cancer (TGF-b, CDK4, Bcl)	0.08
S/G2	p53 signaling pathway	0.6
Unsorted	DNA replication, Cell cycle	≤ 0.05

Figure 38 Enrichment analysis of the differentially expressed genes in G1 sub-phases. A) Ven diagram plot illustrating genes commonly regulated among the different sub-phases. Right panel: Table showing the pathways enriched in the different populations. Only 4 populations showed significant enrichment. (RNAseq procedure performed by Tatjana Ryl and RNAseq data processing in collaboration with Chunxuan Shao).

10.6.2. G0-like transcriptional program under MYCN control is distinct from mitogen-starvation program in fibroblasts and stem cells

A Venn diagram was performed to compare the number of genes that are exclusively regulated in each of the G1 sub-phases as shown in Figure 38A. 130 genes are involved in all of the sub-phases with only 80 genes being exclusively regulated in the G0-like state. 637 genes are exclusively regulated in G1 early. Gene enrichment analysis is a common method to obtain a global picture of the gene function from a set of genes. The analysis was performed with the DAVID platform selecting the KEGG pathway option (Jiao, Sherman et al. 2012). The results are shown in Figure 38 (right panel). The first table shows the pathway enrichment in the 80 only G0-like and 637 G1 early genes. For the G0-like genes, the ribosome pathway was enriched, which relates to genes involved

in translation and protein synthesis. As for the case of G1 early, genes involved in multiple processes, such as DNA replication and DNA repair were enriched. Of note, the DNA repair genes might be an interesting finding since it has been proposed that cells could enter the G0-like state due to random DNA damage (Spencer, Cappell et al. 2013), so one hypothesis could be that MYCN skips G0-like state with the influence of a more effective repair machinery (A topic that was addressed in Tatjana Ryl's dissertation). When evaluating the pathway enrichment of the separate populations, no significant pathways were found with the exception of G1 early and unsorted cells. The information provided by pathway enrichment was not particularly useful to tease out the difference between G1 early and G0-like. Another option is to compare the G0-like differentially expressed genes with respect to G0 or quiescent cells expression profiles from published data to tease out common regulatory mechanisms. Two studies (Venezia, Merchant et al. 2004, Coller, Sang et al. 2006) generated comprehensive expression profiles of fibroblasts and hematopoietic stem cells under quiescence. The procedure to generate quiescence was mitogen starvation and contact inhibition for the fibroblast study and induction of proliferation and then collection of quiescent cells for the stem cell study. To test the hypothesis if the G0-like state caused by MYCN withdrawal has commonalities with the genes differentially regulated in other quiescent states, we compared the genes from G1 early and G0-like vs the list of genes found in the other studies. The results are shown in Figure 39:

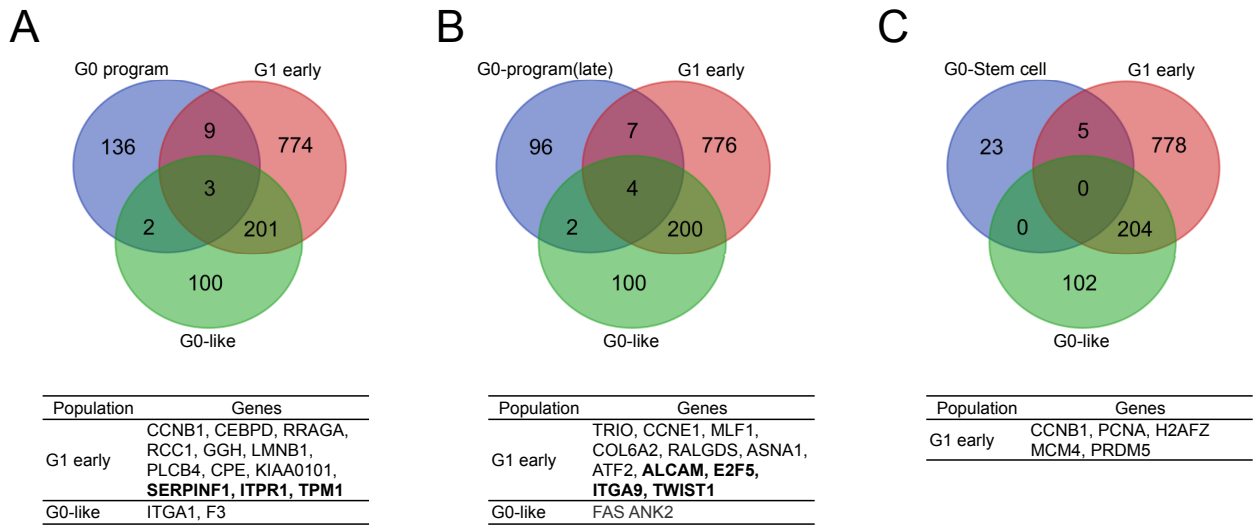

Population	Genes
G1 early	CCNB1, CEBPD, RRAGA, RCC1, GGH, LMNB1, PLCB4, CPE, KIAA0101, **SERPINF1, ITPR1, TPM1**
G0-like	ITGA1, F3

Population	Genes
G1 early	TRIO, CCNE1, MLF1, COL6A2, RALGDS, ASNA1, ATF2, **ALCAM, E2F5, ITGA9, TWIST1**
G0-like	FAS ANK2

Population	Genes
G1 early	CCNB1, PCNA, H2AFZ MCM4, PRDM5

Figure 39 Comparison of differentially expressed G0-like genes in neuroblastoma versus published data. (See text for details).

Surprisingly very few genes were conserved among the different datasets. In Mitogen starvation for a short period (Figure 39A), the data shows that as few as 2 genes were shared with G0-like gene set. For the G1 early case, the overlap is also not evident. The same case it is observed for the mitogen starvation condition for longer times (around 2 weeks) (Figure 39B). Lastly, the stem cell data does not show any gene in common with the G0-like state. This results suggest that the genes affected by MYCN in the context of the G0-like state could be essentially different by the program employed by other cells when arresting in quiescence. This supports the theory that quiescence or G0-like state is an indistinguishable state with potentially different transcriptional programs.

The last analysis indicates, that a set of genes might be specifically acting in concert with MYCN preventing the cells to enter the G0-like state, which might differ from the genes involved in the maintenance of the G0 state in other cells. Another approach to look at the expression data is by differential expression of genes by cell cycle phase rather than MYCN status. In this approach, a pairwise comparison is made between phases that are close in the transition. For example, one could determine the differentially expressed genes of G1 early vs G1 late phase. And the genes could be compared by visual inspection among conditions such as MYCN levels. This approach

was applied here to identify the genes responsible for the transitions, with specific focus on G1 early to G1 late transition and G1 late to G0-like.

10.6.3. Outlook: RABL6, potential new MYCN-driven regulator of cell cycle commitment

The analysis of differential expression was carried out as before with DSeq2 platform. The obtained list of genes was 3 per each MYCN condition. With the list of differentially expressed genes another analysis was performed. To perform this analysis, Ingenuity Pathway Analysis tool was used. (Kramer, Green et al. 2014). This platform performs an analysis called causal network analysis. This analysis is based on a proprietary database that stores experimental observations of nearly 5 million findings manually curated from literature and different databases. The network contains ~40.000 nodes representing mostly genes, proteins, chemical compounds, microRNA molecules and biological functions. The nodes are connected by ~1'480.000 edges representing cause–effect relationships related to expression, transcription, activation, molecular modification and transport as well as binding events. In some cases the edges have a causal direction, activating or inhibiting. Based on this data set, statistical analysis is performed (Z-score calculation) to predict based on the list of differentially regulated genes which potential regulator has the highest number of interactions (Kramer, Green et al. 2014). The results for the different transitions are shown in Figure 40. The data shows some interesting features.

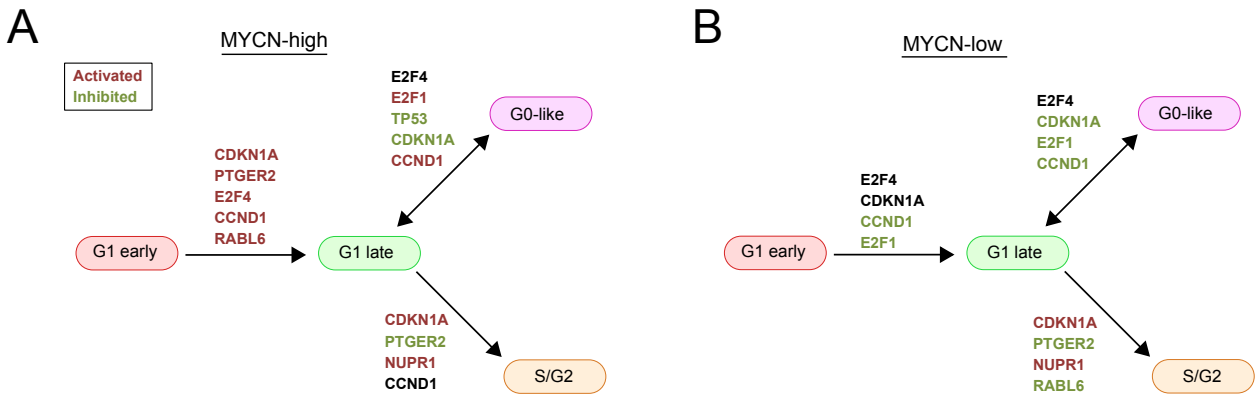

Figure 40. Upstream regulator analysis performed Ingenuity Pathway analysis suite

The transition from G1 early to G1 late exhibits some differences between MYCN-high vs. low conditions. For the case of MYCN-high cells, Cyclin D1 (CCND1) is activated which correlates with growth signaling activation. Interestingly, CDKN1A (p21) is also activated together with E2F4. Surprisingly these two genes are involved in the quiescence phenotype. Two more genes are additionally activated, PTGER2 and RABL6. The RABL6 gene is an interesting candidate since it has been shown to prevent G1/S arrest (Hagen, Muniz et al. 2014). As for the case of MYCN-low cells, E2F1 and Cyclin D1 are inhibited, with E2F4 and p21 enriched but no sign for activation. The transition to G0-like also exhibits some interesting properties. MYCN-high cells unlike MYCN-low preserve the activation of E2F1 and CCND1, potentially providing an advantage to scape the G0-like state as compared to MYCN-low cells. The G1 late to S/G2 transition shows that RABL6 is inhibited in the MYCN-low condition.

The results shown in this thesis seems to point to an special mechanisms of how MYCN-high cells avoid the G0-like state and therefore the increase in the growth rate. Cells after division could potentially have acquired an advantage from the previous cell cycle. MYCN-high cells start proliferation similarly than MYCN-low cells, but RABL6 activation is more predominant leading to inactivation of p16, which is a well-known inhibitor of CDK4. This inactivation might lead to even stronger Rb phosphorylation observed at the moment of birth. As a consequence, this leads to an E2F1 increase, which could protect cells in case they arrive to the G0-like state. SKP2, on the other hand, might be also playing a role by further degrading p16. Finally, mitogen signaling in cooperation with MYCN might favor the activation of RABL6, which occurs at the beginning of the cell cycle. The initial E2F boost might be just a consequence of high levels of CDK4, which are probably not sufficient for cells to cross the restriction point and therefore leading cells entering the G0-like state (and perhaps leaving this state at different rates). As an outlook, testing the role of p16 and RABL6 will be crucial for the understanding of MYCN's role in the commitment to cell cycle at G1 early.

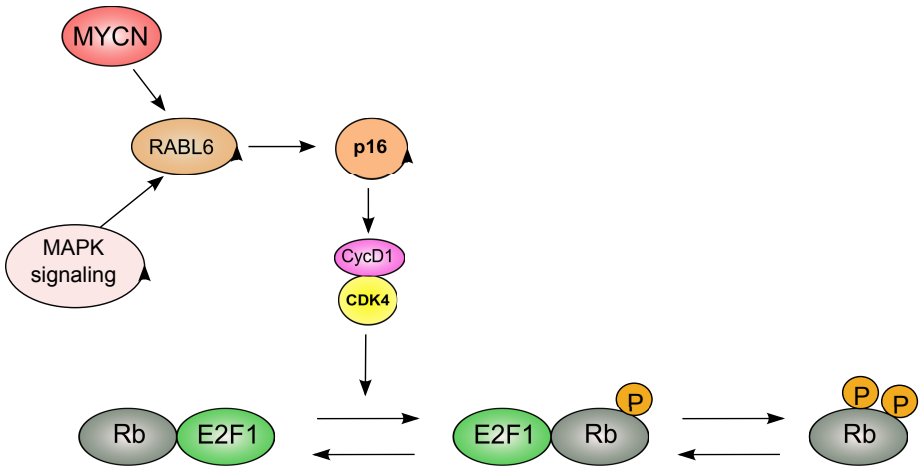

Figure 41 Proposed mechanism for G0-like scape in MYCN-high cells

10.7. MYCN-high cells are highly sensitive to ROS imbalances

10.7.1. MYCN-high cells are strongly addicted to the amino acid cystine

Another aspect of the oncogenic properties of MYCN is cell metabolism. To investigate metabolic vulnerabilities of MYCN-high cells we first measure amino acid concentrations via GC/MS protocol. The intention of this measurement was to eavluate if potentially other aminoacids are essential specifically for MYCN-high cells. This is based on previous finding showing a strong depedence of c-MYC and MYCN high cells on glutamine metabolism (Ren, Yue et al. 2015).

In the course of analyzing the global amino acid metabolism in the presence of MYCN, we measured the intracellular amino acid levels in IMR5/75 MYCN-amplified cells (Figure 42A). We sought to determine whether MYCN levels could affect amino acid concentrations. The results show that MYCN-low cells exhibited lowered intracellular levels of almost all amino acids by at least 2-fold. Treatment of cells with the c-MYC/Max inhibitor 10058-F4 that targets MYCN/max interaction yielded similar results (Figure 42A). In particular, cysteine levels were drastically lowered by almost ten-fold when comparing MYCN-high and MYCN-low cells and by 4-fold in DMSO vs 10058-F4-treated cells. Single amino acid depletion revealed that MYCN-high cells are drastically

sensitive to cystine deprivation, (oxidized form of aminoacid cysteine present in the medium) causing massive cell death whereas MYCN-low cells remained unaffected (Figure 42B). Inhibition of MYCN prevented cystine deprivation-mediated cell death. Glutamine deprivation impaired MYCN-high cell viability but much less pronounced as compared to cystine deprivation. Microscopy images shows the massive cell dead after cystine deprivation (Figure 42C). Together this indicates that neuroblastoma cell lines with increased MYCN levels evaluated here, are highly dependent on cystine, the precursor of cysteine, for cell survival.

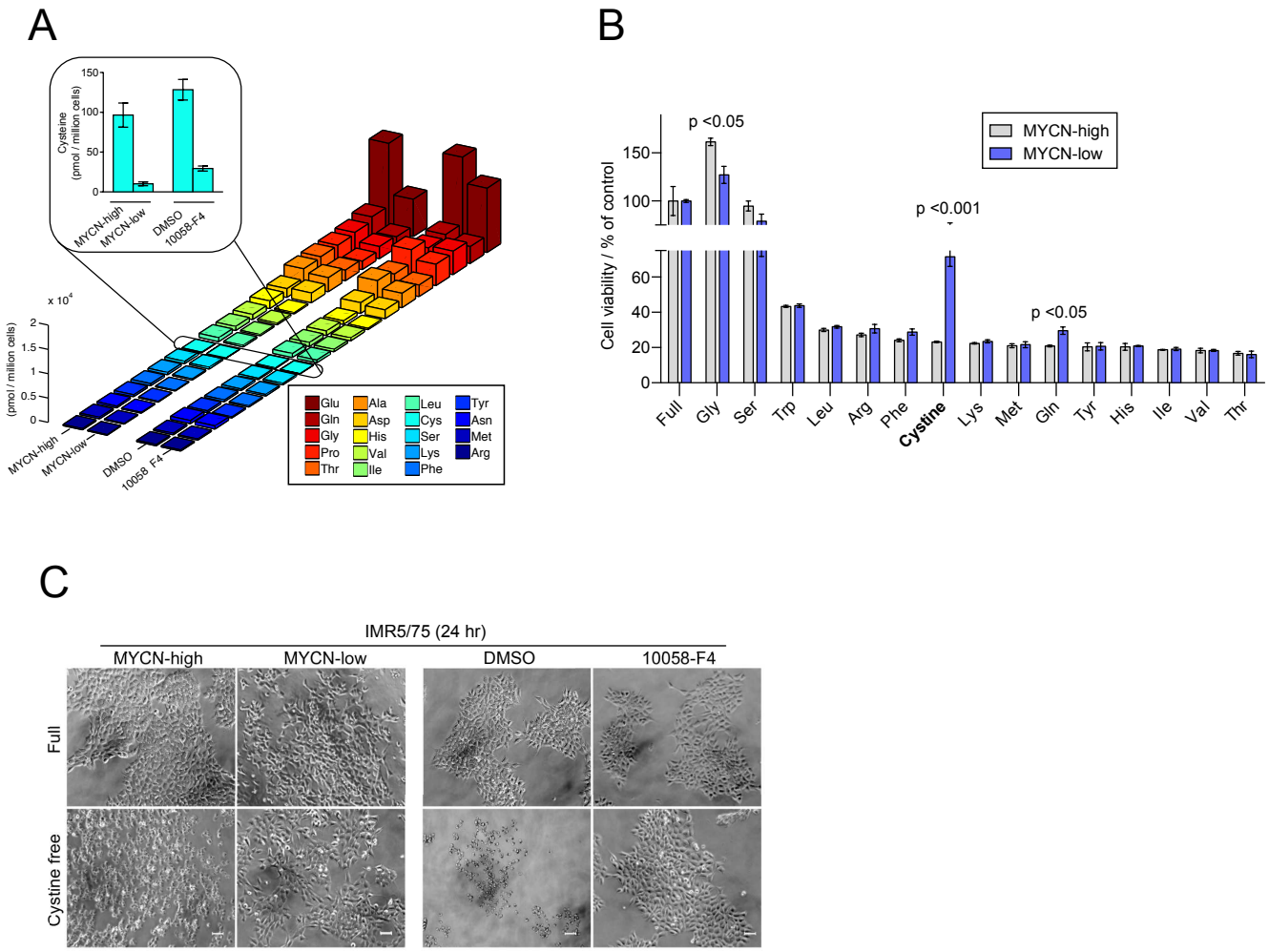

Figure 42 Analyses of Amino Acid Uptake, and Strong Addiction of MYCN-Amplified Neuroblastoma Cells to Cysteine (Reduced Form of Cystine Presence in Cell Culture Medium) (A) Quantification of intracellular amino acid levels. MYCN was either inhibited using 30 µM MYCN inhibitor (10058-F4), interfere with MYC/MAX interaction, or reduced by MYCN-shRNA-Tet-inducible system in IMR5/75 neuroblastoma cells for 4 days. * $p < 0.05$, *** $p < 0.001$ (t-test), indicating statistical significance.

Data are presented as an average of six independent samples. (B) Standardized cell viability of knockdown and inhibitor treated IMR5/75 sh-MYCN neuroblastoma cells. Data are presented as an average of triplicates and normalized to MYCN-high NT or DMSO control (full medium). (C) Light microscopic pictures representing IMR5/75 neuroblastoma cells in the presence or absence of cystine (oxidized form of amino acid cysteine) in cell culture medium for 24 hr. MYCN level was reduced using MYCN-shRNA-Tet-inducible system (left) or cells treated with MYCN inhibitor prior to the cystine starvation (right). In both conditions the picture was taken 24 hr post cystine starvation. Massive cell death can be observed upon cystine starvation in cells expressing high-level of MYCN (left). Scale bar: 50 µm. (Data was acquired in collaboration with Hamed Alborzinia)

We observed that MYCN-high cells accumulate large amounts of cysteine compared with MYC-low cells (Fig. 1A-B). The dual role of cysteine consists of protein synthesis and as a crucial precursor of GSH production. To examine potential synthetic lethal interactions of MYCN with metabolic pathways, data mining from a previously executed siRNA screen was performed. The screen was initially done by Sina Gogolin from Frank Westermman lab and the data is presented with her permission. The screen was carried out in 384-well format by transfecting IMR5/75 cells in triplicate wells, each with three different siRNAs targeting a single gene. Several candidate hits in metabolic processes were found to be significantly lethal in MYCN-high condition, in particular genes involved in the GSH biosynthesis pathway, lipid peroxidation, and glycolysis. We found GSR and GSTM1 to cause synthetic lethality upon downregulation in IMR5/75 cells (Figure 43A). Interestingly, we observed GPX6 to be synthetic lethal in the same context, and the effects are compared to GAPDH as control.

10.7.2. Cystine deprivation leads to ROS production and cell death

Intracellular measurements of glutathione levels revealed a 2-fold increase in IMR5/75 cells (Figure 43B). Knockdown and pharmacological inhibition of MYCN resulted in substantial reduction of intracellular GSH levels correlated with low cysteine levels (Figure 43B). Supplementing cystine-free medium with glutathione or cysteine preserved cell integrity in cystine-deprived cells overexpressing MYCN (Figure 43D). Glutathione maintains redox balance by eliminating ROS and counteracting its deleterious effects.

ROS are produced mainly by the mitochondrial respiratory chain and in some cases by cytosolic NADPH oxidases (NOXs) (Gorrini, Harris et al. 2013)To investigate the mitochondrial ROS production, we used CellROX staining. We observed that ROS levels are significantly lower in MYCN-high cells (Figure 43C). 16 h after cystine deprivation, mitochondrial ROS levels increased about 2-fold relative to basal levels in MYCN-high cells (Figure 43C). Together the results show that ROS can trigger cell death specifically in MYCN-high cells under cystine or GSH reduction.

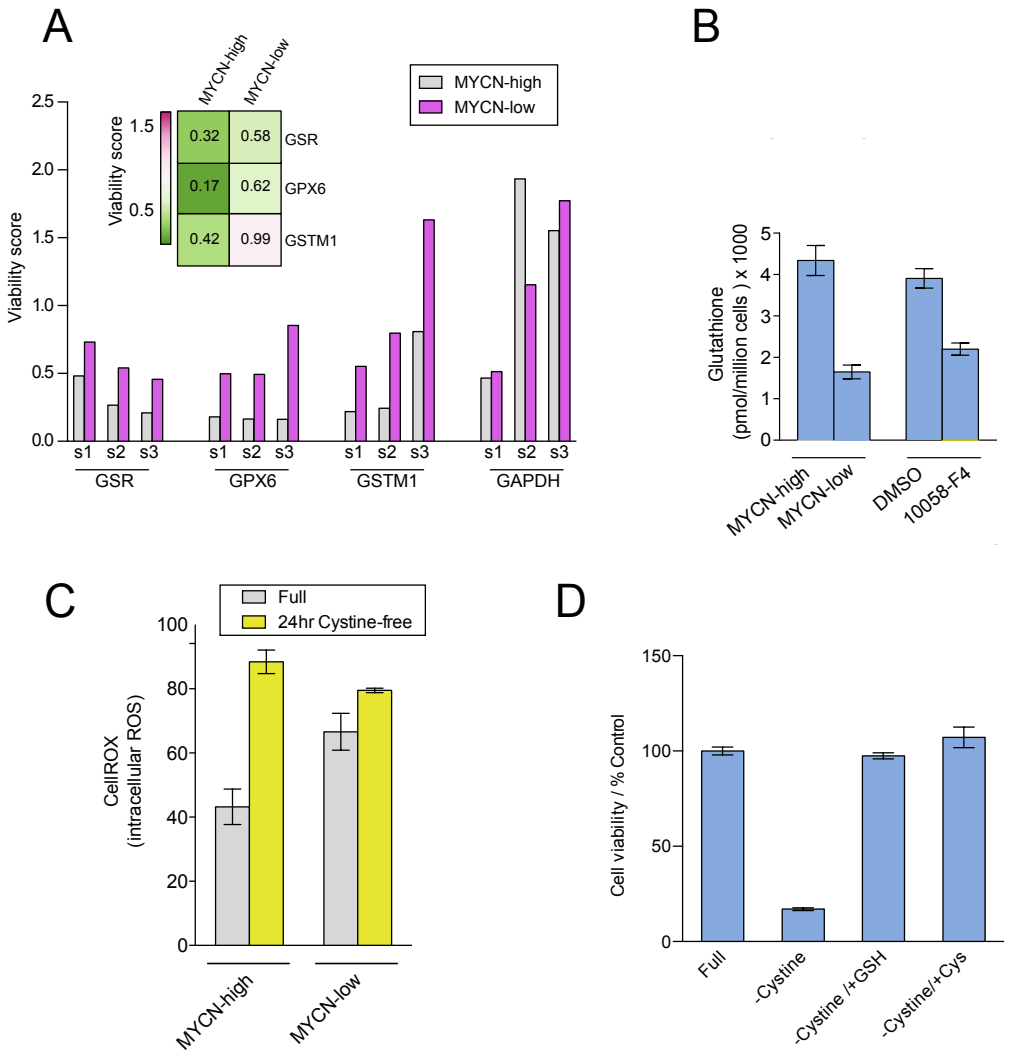

Figure 43 GSH pathway is overly active in MYCN-high cells to detoxify ROS. A) High throughput siRNA synthetic lethality screen, clearly indicating that enzymes from GSH pathway are synthetic lethal with MYCN. The bar plot shows the viability in IMR5/75 cells expressing high and low levels of MYCN. 3

different siRNAs sequences were used per gene for this experiment. GAPDH was used as a negative control. B) Intracellular analysis of glutathione level in IMR5/75 neuroblastoma cells using GC/MS. MYCN level was either reduced MYCN-shRNA Tet-inducible systems or inhibited by 10058-F4 MYCN inhibitor. C) Quantification of intracellular of level ROS in IMR5/75 neuroblastoma cells, in the presence or absence of cystine for 24 hr. MYCN level was reduced using shRNA-Tet-inducible system in IMR5/75 neuroblastoma cells. D) Standardized cell viability of MYCN-amplified IMR5/75 neuroblastoma cells in the presence (indicated as Full), absence of cystine (indicated as –Cystine), in the absence of cystine but in the presence of GSH in the medium (indicated as –Cystine/+GSH), and in the absence of cystine but in the presence of cysteine in the medium (indicated as –Cystine/+Cys) for 24 hr. Data are presented as an average of triplicates. (Data was acquired in collaboration with Hamed Alborzinia)

10.7.3. MYCN sensitizes cells to ferroptosis under cystine deprivation

Cystine deprivation induced massive cell death in MYCN-high cells. To evaluate the mechanism of cell death, we inhibited apoptosis and ferroptosis under cystine deprivation conditions (Figure 44A). We applied apoptosis and autophagy inihibitors z-VAD-fmk, and Ferrostatin-1. Only for the case of Ferrostatin-1, we could substantially rescued MYCN-high cells under cystine deprivation (Figure 44A). This result suggests a novel association of MYCN and ferroptosis. The ferroptosis inducer erastin that causes GSH depletion was used here to test sensitivity of MYC-high cells to ferroptosis. Indeed, we confirmed that erastin triggers ferroptosis exclusively in MYCN-high cells (Figure 44B and 44C).

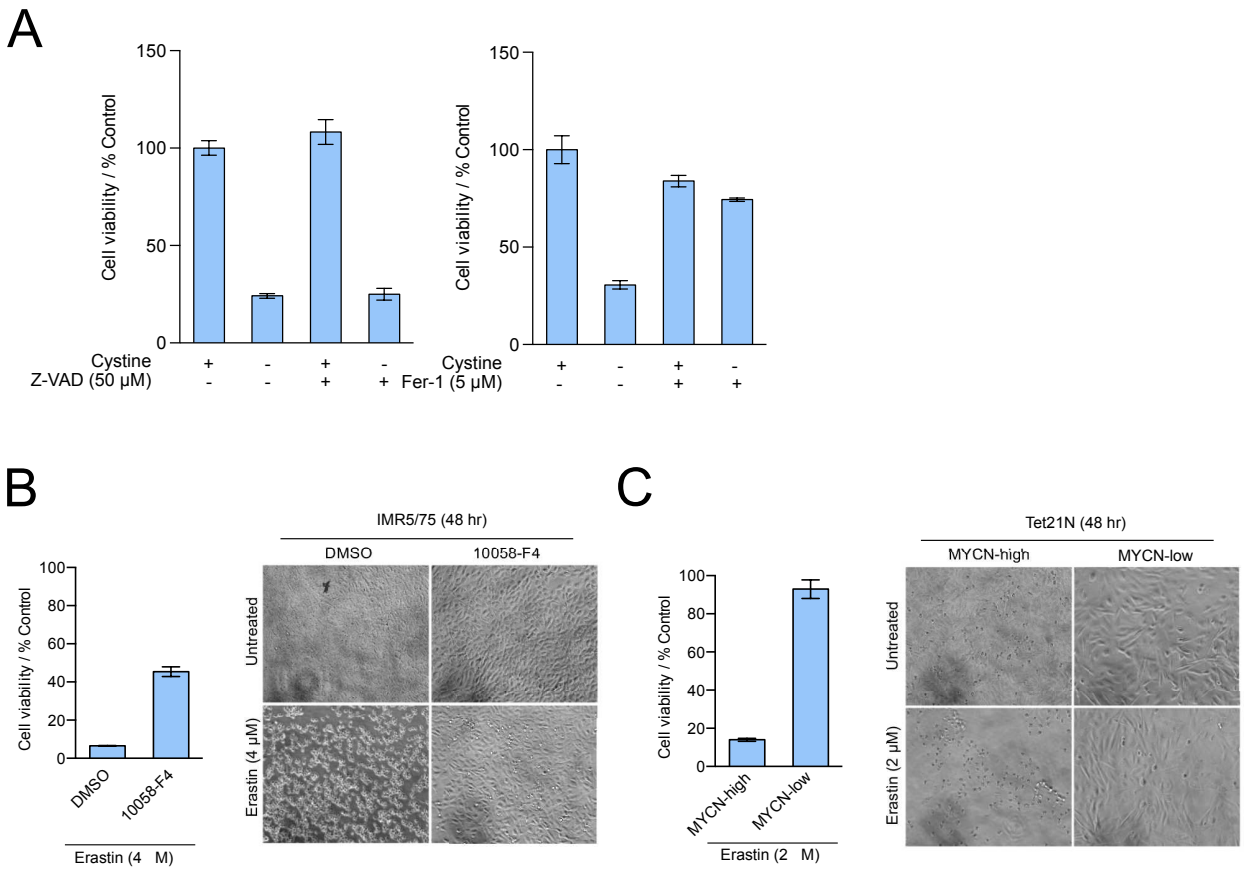

Figure 44 . Cystine Depletion Triggers Ferroptosis-Dependant Cell Death. A) Standardized cell viability of MYCN-amplified neuroblastoma cells in the presence or absence of cystine, and co-treated with 50 µM of z-VAD-fmk (z-VAD), a broad pan-caspase inhibitor and DMSO control for 24 hr. Data presented as an average of triplicates and standardized to NT (full medium). Right panel: Standardized cell viability of MYCN-amplified neuroblastoma cells in the presence or absence of cystine, and 5 µM ferrostatine-1 for 24 hr. Single dose treatment of Erastin in IMR5/75 B) and C) Tet21N cells either with MYC inhibitor treatment or MYCN induction. Light microscopic pictures representing MYCN-amplified neuroblastoma cells, Scale bar: 50 µm. (Data was acquired in collaboration with Hamed Alborzinia)

11. Discussion

In neuroblastoma, MYCN promotes uncontrolled proliferation leading to high-risk and poor prognosis tumors (Cheung, Murray et al. 2013). The role of MYCN in cancer has been widely studied specially in regulation of proliferation, however the exact mechanism of how MYCN oncogene regulates cell cycle remains poorly understood (Huang and Weiss 2013). Here we used neuroblastoma as a model to understand cell

cycle regulation driven by MYCN, in particular the G1 transition that has been previously shown to be strongly influenced by MYCN (Gogolin, Ehemann et al. 2013). IMR5/75 cells (carrying 75 copies of MYCN) with a tet inducible system for MYCN shRNA were used to downregulate MYCN levels at the point of affecting proliferation denoted here by MYCN-low condition and MYCN-high for the normal level situation. One of the caveats of the study is that MYCN reduction is mild as shown in Figure 11A. A personal communication from Frank Westermann relates that further reduction of MYCN to lower levels leads to strong cell death. Despite these limitations, the system still shows a delay in proliferation, which was observed in the growth kinetics. Previous experiments in mouse fibroblasts showed that enforced expression of c-MYC could lead to cell cycle entry in quiescence cells (Armelin, Armelin et al. 1984). The effects were enough to block exit from cell cycle, and in the case of embryos this was completely independent of growth factors (Piedra, Delgado et al. 2002). However these studies relied on a more phenotypic definition of quiescence. Our data showed that MYCN cells can increase the number of proliferating cells so as probably showed for the c-MYC case, there was the suspicion that MYCN could also foster the exit from quiescence. The problem as discussed in the introduction, is that the quiescence phenotype is only defined as a cell cycle arrest in the absence of mitogens. The study from (Spencer, Cappell et al. 2013) shed light on the dynamical properties of quiescence (or more accurately defined the G0-like state). One of the highlights of the study is that for the first time it was possible to observe the entry into G0-like in real time, and the realization that cells could stochastically enter this state by influence of p21 levels from the previous cell cycle. Therefore it was safe to assume that if c-MYC could alter the quiescence state, then having markers to detect quiescence and evaluating the effects of its homologous MYCN, one could learn something about the mechanism. Here we found that E2F-d2GFP which was observed to be a marker for the restriction point, when in combination with the Cdt1-degron reporter allowed the visualization of the G0-like state. This came as a surprise since it was not expected that the combination of the reporters could clearly unmask a population present at high Cdt1-degron levels and low E2F1-d2GFP. Further experimental validations of this population done in this thesis showed a similar result observed by (Spencer, Cappell et al. 2013). This population was transient and

reversible in nature. One of the important findings with respect to this population is the fact that it happens in the area defined here as G1 late. This is of relevance since just based on E2F-d2GFP levels, the G0-like and G1 early states are not distinguishable.

This goes in agreement, with c-MYC knockout studies that found elongated G1 and G2 with lower CDK4 and CDK2 activity. The experiments showed that either c-MYC or MYCN could speed up the cell cycle of slow proliferating cells (Berns, Hijmans et al. 2000). Therefore, the evidence in our experiments shows that the reason why MYCN as well might promote acceleration of the cell cycle is by preventing cells to enter the G0-like state, and this was only possible by the finding of the reporter combination that allowed the visualization of the G0-like state.

The colony sorting procedure showed as well an interesting result. When sorting G0-like cells, the colony results showed that MYCN-low cells generate less number of colonies as compared to the MYCN-high cells. The same goes for cells sorted from the S/G2 population. When comparing G0-like and S/G2 in both conditions, G0-like cells generated less number of colonies. One possible explanation is survival, perhaps G0-like cells could be more sensitive to stressors such as sorting, which is a mechanical force applied onto the cells membrane. However as shown in the example pictures of colonies, it seems that G0-like cell colonies are smaller. This could lead to an alternative explanation. It might be possible that G0-like cells carry an inheritance factor (MYCN?) that is passed onto daughter cells rendering to a homogeneous population. This hypothesis could be supported by a recent study (Sandler, Mizrahi et al. 2015) showing that cell division times of cousin cells are correlated. In the study, live cell imaging and tracking was performed over 60 generations, and several hundreds of cell pairs were analyzed. Interestingly, mother daughter correlation was low, but cousins were highly correlated. One explanation was that the circadian clock could exert an influence in the cell cycle duration. This could suggest that even though, cell cycle regulators are probably reset in each cell cycle some inheritance is still present and manifest in later generations. The only way to tease out this question will be by performing lineage analysis of IMR5/75 cells with the reporters used in this thesis.

When performing the FACS analysis it was interesting to observe that in both cases, MYCN-low and MYCN-high cells do have an initial boost of E2F1 levels. This was clearly observed in the FACS data and slightly clear in the microscopy trajectories due to the limitations of tracking IMR5/75 cells. The presence of initial E2F promoter activity which still leads to the G0-like state seems to go in disagreement to the results shown by (Spencer, Cappell et al. 2013). In Figure S3A of that study, the combination Cdt1-degron and CDK2 reporter showed that cells with very high Cdt1 levels exhibit no CDK2 activity. However the study published by (Dong, Maddali et al. 2014) showed that quiescent cells might still have some weak E2F1 responses. In their paper, the quiescence phenotype was not defined by absence of E2F1 activity but rather due to the amplitude. So there is still possibility that G0-like cells even though CDK2 activity is not reached completely, some E2F1 promoter activity might be still present via stochastic activation from remaining free E2F1 free.

Serum starvation treatment showed that cells could arrest in the G0-like state. This confirms that the state defined by MYCN withdrawal is related to the state defined as quiescence via mitogen withdrawal. However, it has been proposed that quiescence is controlled either by p21 (Spencer, Cappell et al. 2013) and p27 (Oki, Nishimura et al. 2014). Knockdown of these inhibitors did not show any significant rescue of cells in the G0-like state. This result was unexpected since at least for epithelial cells and other cell systems, the G0-like state defined by mitogen withdrawal depended exclusively on p27, and in a newly generated reporter for quiescent cells is based on the degradation properties of p27 (Oki, Nishimura et al. 2014). Protein stainings also showed an accumulation of these inhibitors in the G0-like state (Figure 28A). One possibility as mentioned in the results section is that p21 and p27 might play a role in the maintenance of the G0-like state, but perhaps the initial decision to enter or not the G0-like state might be influenced by other regulators. At least for the case of c-MYC, knockout of p21 or p27 in mouse embryos can still lead to cell cycle arrest when repressing c-MYC targets via a double negative mutant (Berns, Martins et al. 2000). This indicates that either p21 or p27 are dispensable for cell cycle arrest in the presence of MYCN.

Stainings of the different cell cycle regulators and the observation of their localization in the Cdt1-degron and E2F-d2GFP plot indicated that there is no influence of MYCN in where these regulators are expressed at least from the global behavior. Some regulators such as activated CDK2 phosphorylated in the residue Thr160 was surprisingly located in the G0-like region. A recent study showed that pCDK2 is controlling the passage through the restriction point and its phosphorylation is influenced by mitogens (Mueller, Huard et al. 2015). One reason could be experimental error, however 3 different antibodies were tested and they all generated the same results. Another possibility is that CDK2 activation might occur only in G1 late (Mueller, Huard et al. 2015), but when no sufficient CDK2 is activated, the arrest could be triggered and the levels be carried out to the G0-like state. The same situation was observed for MYCN. But in the case of MYCN, other factors such as localization and perhaps activation via phosphorylation might play additional role in having the full activity of MYCN (Huang and Weiss 2013).

The slicing approach of the Cdt1-degron distributions and the histograms derived from it gave an important source of information. To our knowledge it was not shown before that cells in G1 early exhibited already high levels of pRb in the MYCN-high case. This leads to several consequences. Cells might be born with a relative advantage from the previous cell cycle and being committed even if growth factor signals are not present yet. However comparison of the distributions for the different cell cycle regulators did not show difference in the G2 levels. Perhaps another regulator might be involved. One candidate could be CDK4. Constant high levels of CDK4 as described for the case of MYCN, can lead to already phosphorylation events at the moment of birth. However as previously shown (Narasimha, Kaulich et al. 2014), CDK4 alone might prime cells for cell cycle entry via monophosphorylation but quantum hyperphosphorylation via CDK2 is still needed in G1 late.

Another novelty of the work presented here is the use of diffusion maps to extract dynamics from snapshot data. As previously discussed in the introduction, one of the main caveats of cell cycle studies are the artifacts caused by cell synchronization. After validation of the reporters Cdt1-degron and E2F-d2GFP it was possible to set up a common cell cycle axis to use it as a frame of reference to calculate the dynamics of

different regulators. The results showed remarkably reproducibility with the microscopy traces validating the approach (Figure 31). The trajectories showed interesting dynamics. E2F1 protein was the one that peaked earlier in MYCN-high cells. This goes in accordance with the pRb bimodality at birth found via the slicing approach. The reason why perhaps pRb early boost was not detected in this analysis might be due to averaging effects when calculating the trajectories. One solution is to calculate DPT and analyze the trajectories in a distribution-wise manner. That is an interesting analysis for future improvements of the algorithm. Together, this shows that MYCN effects in G1 early could be reduced to Rb phosphorylation and E2F1 expression. As for the case of E2F1, many mechanisms are involved in controlling not only protein stability and gene expression (Donjerkovic and Scott 2000) which makes the regulation complex, but perhaps just simply direct activation of the E2F1 promoter might be necessary for the intial boost. To our knowledge this has not been proven yet, so further experiments are needed to evaluate the different sites of the E2F1 promoter and their association with MYCN binding and activation.

Inhibitors of cell cycle and mitogen signaling were used to validate the mechanism of arrest (Fig 36). CDK4 inhibition (LEE011) leads to accumulation of G0-like cells in MYCN-high cells resembling the effect of MYCN reduction, providing evidence for the CDK4 hypothesis. E2F inhibition with the HLM006474 inhibitor resulted in the same effect. MEK inhibitors U0126 and PD0325901 caused a different pattern of arrest. Cells accumulated uniformly on different levels of Cdt1 with no increase in E2F promoter activity. This might suggest that the initial boost of E2F activity might be related to correct functioning of MAPK cascade. More recently it has been proposed that targeting signaling pathways could be an effective therapy for neuroblastoma tumors.(Tanaka, Higashi et al. 2016). Data regarding ERK and MYCN is scarce, but early studies in c-MYC showed that intact MAPK signaling is necessary for c-MYC phosphorylation which prevents its degradation (ref). One could speculate, that a similar situation could happen for MYCN, although more studies are needed in this area. Very recently, by using a combination of MEK and CDK4 inhibitors the authors induced strong reduction of tumor growth in neuroblastoma samples (Hart, Rader et al. 2016), this strongly supports the findings presented here, since inhibitors that only induce G0-like arrest such as CDK4

inhibitors might still allow the initial E2F boost. This could be a dangerous option since those cells could potentially leave G0-like and enter in S phase.

To investigate the regulatory program of the different cell cycle states in G1, RNA-seq measurements of live-sorted populations was performed. Differential expression of genes was calculated based on MYCN-high versus low condition. Interestingly, G1 early showed the highest number of regulated genes among the different G1 populations. For the G0-like and G1 early populations only 80 and 637 were regulated exclusively on those populations. To gain further insight into genes involved in G0-like, comparison of gene lists were performed against previously published set of genes implicated in G0-regulation in fibroblasts and stem cells. Interestingly very little overlap was found among MYCN regulated genes and genes involved in G0 arrest (e.g mitogen withdrawal) in all different gene lists. This result might suggest that a different regulatory program might be involved in allowing the entrance to G0-like under MYCN-low conditions, as compared to the classical G0 program. A different approach to tease out the regulatory machinery responsible for G0-like and MYCN was taken. This time differential expression analysis was performed by cell cycle phase, comparing groups such as G1 early/G1 late, G1 late/G0-like and G1 late/S/G2. From the list of differentially regulated genes, Of note, RABL6 appeared to be activated in MYCN-high cells in the transition from G1 early to G1 late. This is an interesting prediction since the information about RABL6 (REBL1) is scarce. Very recent paper discussed the role of RABL6 in osteosarcoma, where it serves as a promoter of cell cycle entry. Inhibitor of RABL6 in this tumor induced G1 arrest (Tang, Ji et al. 2016). Another study found overexpression of RABL6 in around 67% of breast cancer samples (Montalbano, Jin et al. 2007). The mechanism of how RABL6 promotes cell growth is not known. This constitutes an interesting molecule that could be studied in more detail in the relationship with MYCN. The only data available about possible regulators interacting with RABL6 come from yeast-two hybrid studies (Tompkins, Hagen et al. 2006). One interesting regulator coming from this data set was p16, which has been shown to induce cell cycle arrest by inhibition of CDK4 in G1 early (Donjerkovic and Scott 2000).

The model proposed here suggests that MYCN expression in G1 early leads to increased E2F1 and CDK4 levels, which lead to Rb phosphorylation. Apparently this

could be enogh for cells to prevent entry into quiescence state. MAPK pathway might prevent MYCN degradation, fostering the proliferative effects. RABL6 can serve as a potential target that together with MYCN could cooperate to inhibit p16, contributing as well to prevent G0-like entry.

The MYC proto-oncogene is strongly involved in cancer proliferation and metabolism (Hanahan and Weinberg 2011). Several MYC-regulated genes participate in mitochondrial biogenesis, glutamine and glucose metabolism. An altered redox balance has been implicated in MYC-driven tumorigenesis as a strategy to cope with metabolic stress deriving from excessive proliferation (Cairns, Harris et al. 2011). Our studies have shown that MYC appears to enforce vulnerability to cystine deprivation and selectively induces cell death via ferroptosis. This mechanism of cell death is distinct from that of apoptosis and autophagy.

MYC boosts intracellular amino acid levels and alters the expression of enzymes of amino acid metabolism (Zirath, Frenzel et al. 2013), though the detailed regulation process remains unclear. One possibility seems to be by driving protein synthesis through activation of ribosomal proteins and translation initiation factors (van Riggelen, Yetil et al. 2010). MYC cooperates with mammalian target of rapamycin (mTOR) and eukaryotic translation initiation factor 4E binding protein-1 (4EBP1) in regulating protein synthesis. Targeting mTOR has been suggested as a therapeutic approach in Myc-driven hematological cancers (Pourdehnad, Truitt et al. 2013). Among the upregulated amino acids, we observed that the intracellular level of cysteine increased to almost ten-fold in MYCN-high condition. Cysteine is the reducing agent of GSSH and mitigates ROS levels, which has mostly detrimental effects (Paulsen and Carroll 2013). Upon single amino acid deprivation we found that MYC/MYCN-high cells specifically undergo cell death when either cystine or glutamine is restricted. Glutamine deprivation has been shown to induce apoptosis in *MYC*-amplified cells (Wise, DeBerardinis et al. 2008, Qing, Li et al. 2012). We observed that cell death upon cystine deprivation is independent of media composition and strongly selective in MYCN-high cells. Consistent with our findings, inhibition of cystine uptake rather than glutamine deprivation seemed to target triple-negative breast cancer tumors more effectively (Timmerman, Holton et al. 2013).

The role of ROS in cancer development is not yet fully understood. On one hand, ROS could influence cell signaling, but when in excess it can contribute to DNA damage and, as shown more recently, to lipid peroxidation and ferroptosis (Gorrini, Harris et al. 2013, Sabharwal and Schumacker 2014). GSH is the main antioxidant in mammalian cells, and its function is tightly coupled to cystine availability. We found that MYCN-high cells exhibited increased levels of GSH, while mitochondrial ROS remained almost identical in MYCN-high/low conditions. Expression of MYC was shown to induce ROS, whereas it lowered the levels via activation of NRF2 and its target genes if endogenously expressed (DeNicola, Karreth et al. 2011). We found that mitochondrial ROS increased specifically in MYCN-high cells under cystine deprivation. Adding glutathione prevented cell death in MYCN-high cells.

We systematically tested the mechanisms of cell death involved in cystine deprivation. Using chemical inhibitor of apoptosis we could not prevent cell death under cystine deprivation conditions. Only ferrostatin-1 could completely restore cell viability. This evidence was further confirmed by treatment with erastin showing that MYC/MYCN-high cells selectively undergo ferroptosis. These results are supported by previous evidence showing that reduction of cystine uptake induces ferroptosis (Jiang, Kon et al. 2015). We found that MYC might enhance sensitivity to ferroptosis via multiple mechanisms. Of note, glutaminolysis and possibly high iron uptake (Wu, Polack et al. 1999, O'Donnell, Yu et al. 2006, Gao, Monian et al. 2015) together with a strong dependence on the glutathione pathway could lead to higher susceptibility of MYC-driven tumors to ferroptosis. We propose that activation of ferroptosis can be exploited as a new therapeutic approach to target MYC-driven tumors

12. Conclusions

In the present thesis, the mechanisms employed by MYCN to promote cell proliferation and sustain cell metabolism were explored.

The results showed that MYCN reduces G1 length by preventing cells to enter in the G0-like state. The successful combination of Cd1-degron and E2F-d2GFP reporters allowed to visualize the G0-like state which is an important step for understanding the regulation of the restriction point in Neuroblastoma cells.

MYCN seems to act specifically in G1 early at the moment of birth via increased Rb phosphorylation and early E2F1 expression. Cell cycle inhibitors p21 and p27 do not seem to play an important role in driving MYCN-low cells into the quiescence state.

MEK inhibition revealed a strong synergy with MYCN at G1 early by promoting the intial E2F promoter boost. Perhaps a combined therapy of MEK inhibition with other cell cycle inhibitors such as CDK4 or E2F could be more effective in treating neuroblastomas, as recently suggested by (Hart, Rader et al. 2016)

Gene expression profiles from G0-like cells originated by MYCN reduction do not share a significant number of differentially regulated genes with respect to other expression profiles of cells in quiescence. This suggest that the G0-like program is specific for cells addicted to MYCN.

As an outlook, RABL6 seems to be a promissory target in controlling cell cycle commitment at G1 early. Further experiments are needed to confirm this hypothesis driven by the analysis of sorted RNA-seq data.

.

13. References

Alam, J., D. Stewart, C. Touchard, S. Boinapally, A. M. Choi and J. L. Cook (1999). "Nrf2, a Cap'n'Collar transcription factor, regulates induction of the heme oxygenase-1 gene." J Biol Chem **274**(37): 26071-26078.

Alexandrov, L. B., S. Nik-Zainal, D. C. Wedge, S. A. Aparicio, S. Behjati, A. V. Biankin, G. R. Bignell, N. Bolli, A. Borg, A. L. Borresen-Dale, S. Boyault, B. Burkhardt, A. P. Butler, C. Caldas, H. R. Davies, C. Desmedt, R. Eils, J. E. Eyfjord, J. A. Foekens, M. Greaves, F. Hosoda, B. Hutter, T. Ilicic, S. Imbeaud, M. Imielinski, N. Jager, D. T. Jones, D. Jones, S. Knappskog, M. Kool, S. R. Lakhani, C. Lopez-Otin, S. Martin, N. C. Munshi, H. Nakamura, P. A. Northcott, M. Pajic, E. Papaemmanuil, A. Paradiso, J. V. Pearson, X. S. Puente, K. Raine, M. Ramakrishna, A. L. Richardson, J. Richter, P. Rosenstiel, M. Schlesner, T. N. Schumacher, P. N. Span, J. W. Teague, Y. Totoki, A. N. Tutt, R. Valdes-Mas, M. M. van Buuren, L. van 't Veer, A. Vincent-Salomon, N. Waddell, L. R. Yates, I. Australian Pancreatic Cancer Genome, I. B. C. Consortium, I. M.-S. Consortium, I. PedBrain, J. Zucman-Rossi, P. A. Futreal, U. McDermott, P. Lichter, M. Meyerson, S. M. Grimmond, R. Siebert, E. Campo, T. Shibata, S. M. Pfister, P. J. Campbell and M. R. Stratton (2013). "Signatures of mutational processes in human cancer." Nature **500**(7463): 415-421.

Armelin, H. A., M. C. Armelin, K. Kelly, T. Stewart, P. Leder, B. H. Cochran and C. D. Stiles (1984). "Functional role for c-myc in mitogenic response to platelet-derived growth factor." Nature **310**(5979): 655-660.

Bell, E., J. Lunec and D. A. Tweddle (2007). "Cell cycle regulation targets of MYCN identified by gene expression microarrays." Cell Cycle **6**(10): 1249-1256.

Bendall, S. C., K. L. Davis, A. D. Amir el, M. D. Tadmor, E. F. Simonds, T. J. Chen, D. K. Shenfeld, G. P. Nolan and D. Pe'er (2014). "Single-cell trajectory detection uncovers progression and regulatory coordination in human B cell development." Cell **157**(3): 714-725.

Berns, K., E. M. Hijmans, E. Koh, G. Q. Daley and R. Bernards (2000). "A genetic screen to identify genes that rescue the slow growth phenotype of c-myc null fibroblasts." Oncogene **19**(29): 3330-3334.

Berns, K., C. Martins, J. H. Dannenberg, A. Berns, H. te Riele and R. Bernards (2000). "p27kip1-independent cell cycle regulation by MYC." Oncogene **19**(42): 4822-4827.

Berthold, F., J. Boos, S. Burdach, R. Erttmann, G. Henze, J. Hermann, T. Klingebiel, B. Kremens, F. H. Schilling, M. Schrappe, T. Simon and B. Hero (2005). "Myeloablative megatherapy with autologous stem-cell rescue versus oral maintenance chemotherapy

as consolidation treatment in patients with high-risk neuroblastoma: a randomised controlled trial." Lancet Oncol **6**(9): 649-658.

Bretones, G., J. C. Acosta, J. M. Caraballo, N. Ferrandiz, M. T. Gomez-Casares, M. Albajar, R. Blanco, P. Ruiz, W. C. Hung, M. P. Albero, I. Perez-Roger and J. Leon (2011). "SKP2 oncogene is a direct MYC target gene and MYC down-regulates p27(KIP1) through SKP2 in human leukemia cells." J Biol Chem **286**(11): 9815-9825.

Brodeur, G. M. (2003). "Neuroblastoma: biological insights into a clinical enigma." Nat Rev Cancer **3**(3): 203-216.

Brodeur, G. M., R. C. Seeger, M. Schwab, H. E. Varmus and J. M. Bishop (1984). "Amplification of N-myc in untreated human neuroblastomas correlates with advanced disease stage." Science **224**(4653): 1121-1124.

Cairns, R. A., I. S. Harris and T. W. Mak (2011). "Regulation of cancer cell metabolism." Nat Rev Cancer **11**(2): 85-95.

Cappell, S. D., M. Chung, A. Jaimovich, S. L. Spencer and T. Meyer (2016). "Irreversible APC(Cdh1) Inactivation Underlies the Point of No Return for Cell-Cycle Entry." Cell **166**(1): 167-180.

Cheung, L., J. E. Murray, M. Haber and M. D. Norris (2013). The MYCN Oncogene.

Chipumuro, E., E. Marco, C. L. Christensen, N. Kwiatkowski, T. Zhang, C. M. Hatheway, B. J. Abraham, B. Sharma, C. Yeung, A. Altabef, A. Perez-Atayde, K. K. Wong, G. C. Yuan, N. S. Gray, R. A. Young and R. E. George (2014). "CDK7 inhibition suppresses super-enhancer-linked oncogenic transcription in MYCN-driven cancer." Cell **159**(5): 1126-1139.

Chong, J. L., P. L. Wenzel, M. T. Saenz-Robles, V. Nair, A. Ferrey, J. P. Hagan, Y. M. Gomez, N. Sharma, H. Z. Chen, M. Ouseph, S. H. Wang, P. Trikha, B. Culp, L. Mezache, D. J. Winton, O. J. Sansom, D. Chen, R. Bremner, P. G. Cantalupo, M. L. Robinson, J. M. Pipas and G. Leone (2009). "E2f1-3 switch from activators in progenitor cells to repressors in differentiating cells." Nature **462**(7275): 930-934.

Coller, H. A., L. Sang and J. M. Roberts (2006). "A new description of cellular quiescence." PLoS Biol **4**(3): e83.

Dang, C. V. (2011). "Therapeutic targeting of Myc-reprogrammed cancer cell metabolism." Cold Spring Harb Symp Quant Biol **76**: 369-374.

DeNicola, G. M., F. A. Karreth, T. J. Humpton, A. Gopinathan, C. Wei, K. Frese, D. Mangal, K. H. Yu, C. J. Yeo, E. S. Calhoun, F. Scrimieri, J. M. Winter, R. H. Hruban, C. Iacobuzio-Donahue, S. E. Kern, I. A. Blair and D. A. Tuveson (2011). "Oncogene-induced Nrf2 transcription promotes ROS detoxification and tumorigenesis." Nature **475**(7354): 106-109.

Dixon, S. J., K. M. Lemberg, M. R. Lamprecht, R. Skouta, E. M. Zaitsev, C. E. Gleason, D. N. Patel, A. J. Bauer, A. M. Cantley, W. S. Yang, B. Morrison, 3rd and B. R. Stockwell (2012). "Ferroptosis: an iron-dependent form of nonapoptotic cell death." Cell **149**(5): 1060-1072.

Dolma, S., S. L. Lessnick, W. C. Hahn and B. R. Stockwell (2003). "Identification of genotype-selective antitumor agents using synthetic lethal chemical screening in engineered human tumor cells." Cancer Cell **3**(3): 285-296.

Dong, P., M. V. Maddali, J. K. Srimani, F. Thelot, J. R. Nevins, B. Mathey-Prevot and L. You (2014). "Division of labour between Myc and G1 cyclins in cell cycle commitment and pace control." Nat Commun **5**: 4750.

Donjerkovic, D. and D. W. Scott (2000). "Regulation of the G1 phase of the mammalian cell cycle." Cell Res **10**(1): 1-16.

Evans, L., L. Chen, G. Milazzo, S. Gherardi, G. Perini, E. Willmore, D. R. Newell and D. A. Tweddle (2015). "SKP2 is a direct transcriptional target of MYCN and a potential therapeutic target in neuroblastoma." Cancer Lett **363**(1): 37-45.

Everson, T. C. (1964). "Spontaneous regression of cancer." Ann N Y Acad Sci **114**(2): 721-735.

Gao, M., P. Monian, N. Quadri, R. Ramasamy and X. Jiang (2015). "Glutaminolysis and Transferrin Regulate Ferroptosis." Mol Cell **59**(2): 298-308.

Gartel, A. L., X. Ye, E. Goufman, P. Shianov, N. Hay, F. Najmabadi and A. L. Tyner (2001). "Myc represses the p21(WAF1/CIP1) promoter and interacts with Sp1/Sp3." Proc Natl Acad Sci U S A **98**(8): 4510-4515.

Gatta, G., A. Ferrari, C. A. Stiller, G. Pastore, G. Bisogno, A. Trama, R. Capocaccia and R. W. Group (2012). "Embryonal cancers in Europe." Eur J Cancer **48**(10): 1425-1433.

Giacinti, C. and A. Giordano (2006). "RB and cell cycle progression." Oncogene **25**(38): 5220-5227.

Gogolin, S., V. Ehemann, G. Becker, L. M. Brueckner, D. Dreidax, S. Bannert, I. Nolte, L. Savelyeva, E. Bell and F. Westermann (2013). "CDK4 inhibition restores G(1)-S arrest in MYCN-amplified neuroblastoma cells in the context of doxorubicin-induced DNA damage." Cell Cycle **12**(7): 1091-1104.

Gong, J., F. Traganos and Z. Darzynkiewicz (1995). "Growth imbalance and altered expression of cyclins B1, A, E, and D3 in MOLT-4 cells synchronized in the cell cycle by inhibitors of DNA replication." Cell Growth Differ **6**(11): 1485-1493.

Gorrini, C., I. S. Harris and T. W. Mak (2013). "Modulation of oxidative stress as an anticancer strategy." Nat Rev Drug Discov **12**(12): 931-947.

Green, S. A. and M. E. Bronner (2013). "Gene duplications and the early evolution of neural crest development." Semin Cell Dev Biol **24**(2): 95-100.

Hagen, J., V. P. Muniz, K. C. Falls, S. M. Reed, A. F. Taghiyev, F. W. Quelle, F. A. Gourronc, A. J. Klingelhutz, H. J. Major, R. W. Askeland, S. K. Sherman, T. M. O'Dorisio, A. M. Bellizzi, J. R. Howe, B. W. Darbro and D. E. Quelle (2014). "RABL6A promotes G1-S phase progression and pancreatic neuroendocrine tumor cell proliferation in an Rb1-dependent manner." Cancer Res **74**(22): 6661-6670.

Haghverdi, L., M. Buttner, F. A. Wolf, F. Buettner and F. J. Theis (2016). "Diffusion pseudotime robustly reconstructs lineage branching." Nat Methods **13**(10): 845-848.

Hanahan, D. and R. A. Weinberg (2011). "Hallmarks of cancer: the next generation." Cell **144**(5): 646-674.

Hart, L. S., J. Rader, P. Raman, V. Batra, M. R. Russell, M. Tsang, M. Gagliardi, L. Chen, D. Martinez, Y. Li, A. Wood, S. Kim, S. Parasuraman, S. Delach, K. A. Cole, S. Krupa, M. Boehm, M. Peters, G. Caponigro and J. M. Maris (2016). "Preclinical therapeutic synergy of MEK1/2 and CDK4/6 inhibition in neuroblastoma." Clin Cancer Res.

Horiuchi, D., B. Anderton and A. Goga (2014). "Taking on challenging targets: making MYC druggable." Am Soc Clin Oncol Educ Book: e497-502.

Huang, M. and W. A. Weiss (2013). "Neuroblastoma and MYCN." Cold Spring Harb Perspect Med **3**(10): a014415.

Ianari, A., T. Natale, E. Calo, E. Ferretti, E. Alesse, I. Screpanti, K. Haigis, A. Gulino and J. A. Lees (2009). "Proapoptotic function of the retinoblastoma tumor suppressor protein." Cancer Cell **15**(3): 184-194.

Iyer, V. R., M. B. Eisen, D. T. Ross, G. Schuler, T. Moore, J. C. Lee, J. M. Trent, L. M. Staudt, J. Hudson, Jr., M. S. Boguski, D. Lashkari, D. Shalon, D. Botstein and P. O. Brown (1999). "The transcriptional program in the response of human fibroblasts to serum." Science **283**(5398): 83-87.

Jiang, L., N. Kon, T. Li, S. J. Wang, T. Su, H. Hibshoosh, R. Baer and W. Gu (2015). "Ferroptosis as a p53-mediated activity during tumour suppression." Nature **520**(7545): 57-62.

Jiao, X., B. T. Sherman, W. Huang da, R. Stephens, M. W. Baseler, H. C. Lane and R. A. Lempicki (2012). "DAVID-WS: a stateful web service to facilitate gene/protein list analysis." Bioinformatics **28**(13): 1805-1806.

Jirawatnotai, S., Y. Hu, W. Michowski, J. E. Elias, L. Becks, F. Bienvenu, A. Zagozdzon, T. Goswami, Y. E. Wang, A. B. Clark, T. A. Kunkel, T. van Harn, B. Xia, M. Correll, J. Quackenbush, D. M. Livingston, S. P. Gygi and P. Sicinski (2011). "A function for cyclin D1 in DNA repair uncovered by protein interactome analyses in human cancers." Nature **474**(7350): 230-234.

Jones, S. M. and A. Kazlauskas (2001). "Growth-factor-dependent mitogenesis requires two distinct phases of signalling." Nat Cell Biol **3**(2): 165-172.

Kafri, R., J. Levy, M. B. Ginzberg, S. Oh, G. Lahav and M. W. Kirschner (2013). "Dynamics extracted from fixed cells reveal feedback linking cell growth to cell cycle." Nature **494**(7438): 480-483.

Kamb, A., S. Wee and C. Lengauer (2007). "Why is cancer drug discovery so difficult?" Nat Rev Drug Discov **6**(2): 115-120.

Kramer, A., J. Green, J. Pollard, Jr. and S. Tugendreich (2014). "Causal analysis approaches in Ingenuity Pathway Analysis." Bioinformatics **30**(4): 523-530.

Lien, E. C., C. A. Lyssiotis, A. Juvekar, H. Hu, J. M. Asara, L. C. Cantley and A. Toker (2016). "Glutathione biosynthesis is a metabolic vulnerability in PI(3)K/Akt-driven breast cancer." Nat Cell Biol **18**(5): 572-578.

Lindeman, G. J., S. Gaubatz, D. M. Livingston and D. Ginsberg (1997). "The subcellular localization of E2F-4 is cell-cycle dependent." Proc Natl Acad Sci U S A **94**(10): 5095-5100.

Livak, K. J. and T. D. Schmittgen (2001). "Analysis of relative gene expression data using real-time quantitative PCR and the 2(-Delta Delta C(T)) Method." Methods **25**(4): 402-408.

Love, M. I., W. Huber and S. Anders (2014). "Moderated estimation of fold change and dispersion for RNA-seq data with DESeq2." Genome Biol **15**(12): 550.

Lutz, W., M. Stohr, J. Schurmann, A. Wenzel, A. Lohr and M. Schwab (1996). "Conditional expression of N-myc in human neuroblastoma cells increases expression of alpha-prothymosin and ornithine decarboxylase and accelerates progression into S-phase early after mitogenic stimulation of quiescent cells." Oncogene **13**(4): 803-812.

Macdonald, J. I. and F. A. Dick (2012). "Posttranslational modifications of the retinoblastoma tumor suppressor protein as determinants of function." Genes Cancer **3**(11-12): 619-633.

Maris, J. M. (2010). "Recent advances in neuroblastoma." N Engl J Med **362**(23): 2202-2211.

Mateyak, M. K., A. J. Obaya and J. M. Sedivy (1999). "c-Myc regulates cyclin D-Cdk4 and -Cdk6 activity but affects cell cycle progression at multiple independent points." Mol Cell Biol **19**(7): 4672-4683.

Matsuoka, S., M. C. Edwards, C. Bai, S. Parker, P. Zhang, A. Baldini, J. W. Harper and S. J. Elledge (1995). "p57KIP2, a structurally distinct member of the p21CIP1 Cdk inhibitor family, is a candidate tumor suppressor gene." Genes Dev **9**(6): 650-662.

Matthay, K. K., J. G. Villablanca, R. C. Seeger, D. O. Stram, R. E. Harris, N. K. Ramsay, P. Swift, H. Shimada, C. T. Black, G. M. Brodeur, R. B. Gerbing and C. P. Reynolds (1999). "Treatment of high-risk neuroblastoma with intensive chemotherapy, radiotherapy, autologous bone marrow transplantation, and 13-cis-retinoic acid. Children's Cancer Group." N Engl J Med **341**(16): 1165-1173.

Merlo, L. M., J. W. Pepper, B. J. Reid and C. C. Maley (2006). "Cancer as an evolutionary and ecological process." Nat Rev Cancer **6**(12): 924-935.

Meyer, N. and L. Z. Penn (2008). "Reflecting on 25 years with MYC." Nat Rev Cancer **8**(12): 976-990.

Montalbano, J., W. Jin, M. S. Sheikh and Y. Huang (2007). "RBEL1 is a novel gene that encodes a nucleocytoplasmic Ras superfamily GTP-binding protein and is overexpressed in breast cancer." J Biol Chem **282**(52): 37640-37649.

Morrish, F., N. Neretti, J. M. Sedivy and D. M. Hockenbery (2008). "The oncogene c-Myc coordinates regulation of metabolic networks to enable rapid cell cycle entry." Cell Cycle **7**(8): 1054-1066.

Mosse, Y. P., M. Laudenslager, L. Longo, K. A. Cole, A. Wood, E. F. Attiyeh, M. J. Laquaglia, R. Sennett, J. E. Lynch, P. Perri, G. Laureys, F. Speleman, C. Kim, C. Hou, H. Hakonarson, A. Torkamani, N. J. Schork, G. M. Brodeur, G. P. Tonini, E. Rappaport, M. Devoto and J. M. Maris (2008). "Identification of ALK as a major familial neuroblastoma predisposition gene." Nature **455**(7215): 930-935.

Mueller, S., J. Huard, K. Waldow, X. Huang, L. A. D'Alessandro, S. Bohl, K. Borner, D. Grimm, S. Klamt, U. Klingmuller and M. Schilling (2015). "T160-phosphorylated CDK2 defines threshold for HGF dependent proliferation in primary hepatocytes." Mol Syst Biol **11**(3): 795.

Muth, D., S. Ghazaryan, I. Eckerle, E. Beckett, C. Pohler, J. Batzler, C. Beisel, S. Gogolin, M. Fischer, K. O. Henrich, V. Ehemann, P. Gillespie, M. Schwab and F. Westermann (2010). "Transcriptional repression of SKP2 is impaired in MYCN-amplified neuroblastoma." Cancer Res **70**(9): 3791-3802.

Narasimha, A. M., M. Kaulich, G. S. Shapiro, Y. J. Choi, P. Sicinski and S. F. Dowdy (2014). "Cyclin D activates the Rb tumor suppressor by mono-phosphorylation." Elife **3**.

Nie, Z., G. Hu, G. Wei, K. Cui, A. Yamane, W. Resch, R. Wang, D. R. Green, L. Tessarollo, R. Casellas, K. Zhao and D. Levens (2012). "c-Myc is a universal amplifier of expressed genes in lymphocytes and embryonic stem cells." Cell **151**(1): 68-79.

O'Donnell, K. A., D. Yu, K. I. Zeller, J. W. Kim, F. Racke, A. Thomas-Tikhonenko and C. V. Dang (2006). "Activation of transferrin receptor 1 by c-Myc enhances cellular proliferation and tumorigenesis." Mol Cell Biol **26**(6): 2373-2386.

Oki, T., K. Nishimura, J. Kitaura, K. Togami, A. Maehara, K. Izawa, A. Sakaue-Sawano, A. Niida, S. Miyano, H. Aburatani, H. Kiyonari, A. Miyawaki and T. Kitamura (2014). "A novel cell-cycle-indicator, mVenus-p27K-, identifies quiescent cells and visualizes G0-G1 transition." Sci Rep **4**: 4012.

Pardee, A. B. (1974). "A restriction point for control of normal animal cell proliferation." Proc Natl Acad Sci U S A **71**(4): 1286-1290.

Pauklin, S. and L. Vallier (2013). "The cell-cycle state of stem cells determines cell fate propensity." Cell **155**(1): 135-147.

Paulsen, C. E. and K. S. Carroll (2013). "Cysteine-mediated redox signaling: chemistry, biology, and tools for discovery." Chem Rev **113**(7): 4633-4679.

Pavet, V., M. M. Portal, J. C. Moulin, R. Herbrecht and H. Gronemeyer (2011). "Towards novel paradigms for cancer therapy." Oncogene **30**(1): 1-20.

Peifer, M., F. Hertwig, F. Roels, D. Dreidax, M. Gartlgruber, R. Menon, A. Kramer, J. L. Roncaioli, F. Sand, J. M. Heuckmann, F. Ikram, R. Schmidt, S. Ackermann, A. Engesser, Y. Kahlert, W. Vogel, J. Altmuller, P. Nurnberg, J. Thierry-Mieg, D. Thierry-Mieg, A. Mariappan, S. Heynck, E. Mariotti, K. O. Henrich, C. Gloeckner, G. Bosco, I. Leuschner, M. R. Schweiger, L. Savelyeva, S. C. Watkins, C. Shao, E. Bell, T. Hofer, V. Achter, U. Lang, J. Theissen, R. Volland, M. Saadati, A. Eggert, B. de Wilde, F. Berthold, Z. Peng, C. Zhao, L. Shi, M. Ortmann, R. Buttner, S. Perner, B. Hero, A. Schramm, J. H. Schulte, C. Herrmann, R. J. O'Sullivan, F. Westermann, R. K. Thomas and M. Fischer (2015). "Telomerase activation by genomic rearrangements in high-risk neuroblastoma." Nature **526**(7575): 700-704.

Piedra, M. E., M. D. Delgado, M. A. Ros and J. Leon (2002). "c-Myc overexpression increases cell size and impairs cartilage differentiation during chick limb development." Cell Growth Differ **13**(4): 185-193.

Pourdehnad, M., M. L. Truitt, I. N. Siddiqi, G. S. Ducker, K. M. Shokat and D. Ruggero (2013). "Myc and mTOR converge on a common node in protein synthesis control that confers synthetic lethality in Myc-driven cancers." Proc Natl Acad Sci U S A **110**(29): 11988-11993.

Qing, G., B. Li, A. Vu, N. Skuli, Z. E. Walton, X. Liu, P. A. Mayes, D. R. Wise, C. B. Thompson, J. M. Maris, M. D. Hogarty and M. C. Simon (2012). "ATF4 regulates MYC-mediated neuroblastoma cell death upon glutamine deprivation." Cancer Cell **22**(5): 631-644.

Ren, P., M. Yue, D. Xiao, R. Xiu, L. Gan, H. Liu and G. Qing (2015). "ATF4 and N-Myc coordinate glutamine metabolism in MYCN-amplified neuroblastoma cells through ASCT2 activation." J Pathol **235**(1): 90-100.

Robert, C., A. Ribas, J. D. Wolchok, F. S. Hodi, O. Hamid, R. Kefford, J. S. Weber, A. M. Joshua, W. J. Hwu, T. C. Gangadhar, A. Patnaik, R. Dronca, H. Zarour, R. W. Joseph, P. Boasberg, B. Chmielowski, C. Mateus, M. A. Postow, K. Gergich, J. Elassaiss-Schaap, X. N. Li, R. Iannone, S. W. Ebbinghaus, S. P. Kang and A. Daud (2014). "Anti-programmed-death-receptor-1 treatment with pembrolizumab in ipilimumab-refractory advanced melanoma: a randomised dose-comparison cohort of a phase 1 trial." Lancet **384**(9948): 1109-1117.

Rubin, S. M. (2013). "Deciphering the retinoblastoma protein phosphorylation code." Trends Biochem Sci **38**(1): 12-19.

Sabharwal, S. S. and P. T. Schumacker (2014). "Mitochondrial ROS in cancer: initiators, amplifiers or an Achilles' heel?" Nat Rev Cancer **14**(11): 709-721.

Sabo, A., T. R. Kress, M. Pelizzola, S. de Pretis, M. M. Gorski, A. Tesi, M. J. Morelli, P. Bora, M. Doni, A. Verrecchia, C. Tonelli, G. Faga, V. Bianchi, A. Ronchi, D. Low, H. Muller, E. Guccione, S. Campaner and B. Amati (2014). "Selective transcriptional regulation by Myc in cellular growth control and lymphomagenesis." Nature **511**(7510): 488-492.

Sakaue-Sawano, A., H. Kurokawa, T. Morimura, A. Hanyu, H. Hama, H. Osawa, S. Kashiwagi, K. Fukami, T. Miyata, H. Miyoshi, T. Imamura, M. Ogawa, H. Masai and A. Miyawaki (2008). "Visualizing spatiotemporal dynamics of multicellular cell-cycle progression." Cell **132**(3): 487-498.

Sandler, O., S. P. Mizrahi, N. Weiss, O. Agam, I. Simon and N. Q. Balaban (2015). "Lineage correlations of single cell division time as a probe of cell-cycle dynamics." Nature **519**(7544): 468-471.

Schachter, M. M., K. A. Merrick, S. Larochelle, A. Hirschi, C. Zhang, K. M. Shokat, S. M. Rubin and R. P. Fisher (2013). "A Cdk7-Cdk4 T-loop phosphorylation cascade promotes G1 progression." Mol Cell **50**(2): 250-260.

Sclafani, R. A. and T. M. Holzen (2007). "Cell cycle regulation of DNA replication." Annu Rev Genet **41**: 237-280.

Setty, M., M. D. Tadmor, S. Reich-Zeliger, O. Angel, T. M. Salame, P. Kathail, K. Choi, S. Bendall, N. Friedman and D. Pe'er (2016). "Wishbone identifies bifurcating developmental trajectories from single-cell data." Nat Biotechnol **34**(6): 637-645.

Shaw, J., K. Payer, S. Son, W. H. Grover and S. R. Manalis (2012). "A microfluidic "baby machine" for cell synchronization." Lab Chip **12**(15): 2656-2663.

Sherr, C. J. (1996). "Cancer cell cycles." Science **274**(5293): 1672-1677.

Spencer, S. L., S. D. Cappell, F. C. Tsai, K. W. Overton, C. L. Wang and T. Meyer (2013). "The proliferation-quiescence decision is controlled by a bifurcation in CDK2 activity at mitotic exit." Cell **155**(2): 369-383.

Tanaka, T., M. Higashi, K. Kimura, J. Wakao, S. Fumino, T. Iehara, H. Hosoi, T. Sakai and T. Tajiri (2016). "MEK inhibitors as a novel therapy for neuroblastoma: Their in vitro effects and predicting their efficacy." J Pediatr Surg.

Tang, H., F. Ji, J. Sun, Y. Xie, Y. Xu and H. Yue (2016). "RBEL1 is required for osteosarcoma cell proliferation via inhibiting retinoblastoma 1." Mol Med Rep **13**(2): 1275-1280.

Timmerman, L. A., T. Holton, M. Yuneva, R. J. Louie, M. Padro, A. Daemen, M. Hu, D. A. Chan, S. P. Ethier, L. J. van 't Veer, K. Polyak, F. McCormick and J. W. Gray (2013). "Glutamine sensitivity analysis identifies the xCT antiporter as a common triple-negative breast tumor therapeutic target." Cancer Cell **24**(4): 450-465.

Tompkins, V., J. Hagen, V. P. Zediak and D. E. Quelle (2006). "Identification of novel ARF binding proteins by two-hybrid screening." Cell Cycle **5**(6): 641-646.

Tomura, M., A. Sakaue-Sawano, Y. Mori, M. Takase-Utsugi, A. Hata, K. Ohtawa, O. Kanagawa and A. Miyawaki (2013). "Contrasting quiescent G0 phase with mitotic cell cycling in the mouse immune system." PLoS One **8**(9): e73801.

Torres, J., P. L. Regan, R. Edo, P. Leonhardt, E. I. Jeng, E. F. Rappaport, N. Ikegaki and X. X. Tang (2010). "Biological effects of induced MYCN hyper-expression in MYCN-amplified neuroblastomas." Int J Oncol **37**(4): 983-991.

Truong, L. N. and X. Wu (2011). "Prevention of DNA re-replication in eukaryotic cells." J Mol Cell Biol **3**(1): 13-22.

van Riggelen, J., A. Yetil and D. W. Felsher (2010). "MYC as a regulator of ribosome biogenesis and protein synthesis." Nat Rev Cancer **10**(4): 301-309.

Venezia, T. A., A. A. Merchant, C. A. Ramos, N. L. Whitehouse, A. S. Young, C. A. Shaw and M. A. Goodell (2004). "Molecular signatures of proliferation and quiescence in hematopoietic stem cells." PLoS Biol **2**(10): e301.

Vichai, V. and K. Kirtikara (2006). "Sulforhodamine B colorimetric assay for cytotoxicity screening." Nat Protoc **1**(3): 1112-1116.

Wang, K., S. J. Diskin, H. Zhang, E. F. Attiyeh, C. Winter, C. Hou, R. W. Schnepp, M. Diamond, K. Bosse, P. A. Mayes, J. Glessner, C. Kim, E. Frackelton, M. Garris, Q. Wang, W. Glaberson, R. Chiavacci, L. Nguyen, J. Jagannathan, N. Saeki, H. Sasaki, S. F. Grant, A. Iolascon, Y. P. Mosse, K. A. Cole, H. Li, M. Devoto, P. W. McGrady, W. B. London, M. Capasso, N. Rahman, H. Hakonarson and J. M. Maris (2011). "Integrative genomics identifies LMO1 as a neuroblastoma oncogene." Nature **469**(7329): 216-220.

Watanabe, I. and S. Okada (1967). "Effects of temperature on growth rate of cultured mammalian cells (L5178Y)." J Cell Biol **32**(2): 309-323.

Wirtz, M. and R. Hell (2007). "Dominant-negative modification reveals the regulatory function of the multimeric cysteine synthase protein complex in transgenic tobacco." Plant Cell **19**(2): 625-639.

Wise, D. R., R. J. DeBerardinis, A. Mancuso, N. Sayed, X. Y. Zhang, H. K. Pfeiffer, I. Nissim, E. Daikhin, M. Yudkoff, S. B. McMahon and C. B. Thompson (2008). "Myc regulates a transcriptional program that stimulates mitochondrial glutaminolysis and leads to glutamine addiction." Proc Natl Acad Sci U S A **105**(48): 18782-18787.

Wong, J. V., P. Dong, J. R. Nevins, B. Mathey-Prevot and L. You (2011). "Network calisthenics: control of E2F dynamics in cell cycle entry." Cell Cycle **10**(18): 3086-3094.

Wu, K. J., A. Polack and R. Dalla-Favera (1999). "Coordinated regulation of iron-controlling genes, H-ferritin and IRP2, by c-MYC." Science **283**(5402): 676-679.

Xie, Y., W. Hou, X. Song, Y. Yu, J. Huang, X. Sun, R. Kang and D. Tang (2016). "Ferroptosis: process and function." Cell Death Differ **23**(3): 369-379.

Yagoda, N., M. von Rechenberg, E. Zaganjor, A. J. Bauer, W. S. Yang, D. J. Fridman, A. J. Wolpaw, I. Smukste, J. M. Peltier, J. J. Boniface, R. Smith, S. L. Lessnick, S. Sahasrabudhe and B. R. Stockwell (2007). "RAS-RAF-MEK-dependent oxidative cell death involving voltage-dependent anion channels." Nature **447**(7146): 864-868.

Yang, W. S., R. SriRamaratnam, M. E. Welsch, K. Shimada, R. Skouta, V. S. Viswanathan, J. H. Cheah, P. A. Clemons, A. F. Shamji, C. B. Clish, L. M. Brown, A. W. Girotti, V. W. Cornish, S. L. Schreiber and B. R. Stockwell (2014). "Regulation of ferroptotic cancer cell death by GPX4." Cell **156**(1-2): 317-331.

Yang, Y., M. P. A, C. Hofler, G. Poschet, M. Wirtz, R. Hell and V. Sourjik (2015). "Relation between chemotaxis and consumption of amino acids in bacteria." Mol Microbiol **96**(6): 1272-1282.

Yao, G., T. J. Lee, S. Mori, J. R. Nevins and L. You (2008). "A bistable Rb-E2F switch underlies the restriction point." Nat Cell Biol **10**(4): 476-482.

Yao, G., C. Tan, M. West, J. R. Nevins and L. You (2011). "Origin of bistability underlying mammalian cell cycle entry." Mol Syst Biol **7**: 485.

Yuneva, M., N. Zamboni, P. Oefner, R. Sachidanandam and Y. Lazebnik (2007). "Deficiency in glutamine but not glucose induces MYC-dependent apoptosis in human cells." J Cell Biol **178**(1): 93-105.

Zirath, H., A. Frenzel, G. Oliynyk, L. Segerstrom, U. K. Westermark, K. Larsson, M. Munksgaard Persson, K. Hultenby, J. Lehtio, C. Einvik, S. Pahlman, P. Kogner, P. J. Jakobsson and M. A. Henriksson (2013). "MYC inhibition induces metabolic changes leading to accumulation of lipid droplets in tumor cells." Proc Natl Acad Sci U S A **110**(25): 10258-10263.

Zwang, Y., A. Sas-Chen, Y. Drier, T. Shay, R. Avraham, M. Lauriola, E. Shema, E. Lidor-Nili, J. Jacob-Hirsch, N. Amariglio, Y. Lu, G. B. Mills, G. Rechavi, M. Oren, E. Domany and Y. Yarden (2011). "Two phases of mitogenic signaling unveil roles for p53 and EGR1 in elimination of inconsistent growth signals." Mol Cell **42**(4): 524-535.